University of Cape Town

Department of Chemical Engineering
Rondebosch, Cape Town, South Africa

Masters Dissertation

The effect of different chemical classes on the swelling of NBR O-rings in blends with synthetic paraffinic kerosene

---

Author: Ross Burnham

Supervisor: Dr Chris Woolard
Co-supervisor: Prof Eric van Steen

January 2012

ACKNOWLEDGEMENTS

This research project has been made possible through the help and support of a number of people. Firstly the author wishes to thank his supervisor, Dr Chris Woolard, for his advice and valuable assistance throughout this project. He would also like to show his gratitude towards his co-supervisor, Prof Eric van Steen, and all of his work colleagues at the Sasol Advanced Fuels Laboratory for their assistance throughout this research.

The author would like to acknowledge Sasol Technology Fuels Research, under the leadership of Paul Morgan, who supplied much needed funding towards the research which was conducted. He also acknowledges the Faculty of Engineering and the Built Environment and the Department of Chemical Engineering at the University of Cape Town, for their support of the Sasol Advanced Fuels Laboratory.

Finally the author wishes to express his love and gratitude to his wife and family, for their understanding and support throughout the duration of his studies.

PLAGIARISM DECLARATION

1. I know that plagiarism is wrong. Plagiarism is using another's work and to pretend that it is one's own.

2. Each significant contribution to, and quotation in, this project from the work, or works of other people has been attributed and has cited and referenced.

3. This project is my own work.

4. I have not allowed, and will not allow, anyone to copy my work with the intention of passing it off as his or her own work.

5. I acknowledge that copying someone else's assignment or project, or part of it, is wrong, and declare that this is my own work.

Ross Burnham

SIGNATURE: Signed by candidate

DATE: 29 January 2012

ABSTRACT

Synthetic jet fuels provide a number of benefits over petroleum-derived fuels. They have thus been considered as alternative fuels. Compatibility issues, however, are of concern; specifically the interaction of synthetic fuels with polymeric materials which are commonly used to seal fuel systems. This is because of differences between the composition of synthetic fuels and petroleum-derived fuels. Synthetic fuel streams contain no or very low aromatics, unlike petroleum-derived fuels. This investigation was consequently initiated to gain a greater understanding of the factors affecting seal swell in the aviation industry. The study focussed interactions between fuel components from various fuel classes and nitrile rubber (NBR).

Currently fully and semi-synthetic jet fuels are required to contain a minimum of 8% aromatic components by volume in order to minimise any changes in polymeric swell when switching between synthetic jet fuels and petroleum-derived jet fuels.

In this study procedures were refined to allow seal swell to be assessed. ASTM D1414 and D471 were used as base methods together with the use of an elastomer compression rig that had been designed and built at the Sasol Advanced Fuel Laboratory (SAFL). A method was developed to remove plasticiser for the O-ring seals to provide samples that are more representative of O-rings in service. Experiments were conducted on both new and conditioned (deplasticised) NBR O-ring samples.

Materials tested in this investigation included petroleum-derived Jet A-1, Fischer Tropsch-derived synthetic paraffinic kerosene (SPK) and pure compounds including isomers of n-, iso- and cyclic paraffins, aromatics and oxygenates. The paraffins were tested as neat components. With the aromatics and oxygenates, 8% (v/v) blends with coal-to-liquid (CTL) SPK were prepared to simulate fully synthetic jet fuels that meet the minimum 8% aromatic specification. The data which were collected were primarily changes in mass and volume of the O-rings which underwent

fuel exposure. An assessment was made of both the kinetics of fuel uptake and the extent of swell achieved at equilibrium.

Initial experiments focussed on method refinement. This included the measurement techniques (gravimetric, volumetric and seal swell rig), O-ring conditioning (*i.e.* plasticiser removal), the effects of temperature and the solvent to polymer ratio used. The greatest level of repeatability was achieved with gravimetric measurements. Similar swelling trends were observed with volumetric measurements, although with lower repeatability.

Solubility parameters and molar volume were shown to be key determinants of seal swell. It was demonstrated that the extent of swell was not significantly different between n- and iso- isomers of octane and dodecane. What was different was that n-paraffins initially swell faster than their iso-equivalents. A significant difference was observed with cycloalkane isomers which swell to a much greater extent. It is suggested that this difference is the result of a combination of molar volume and solubility parameter differences.

A study on a series of n-alkanes showed that although solubility parameters increase with increasing carbon number, seal swell decreases. Molar volume, by contrast, decreases. Thus for n-alkanes molar volume is the key determinant. A statistically significant correlation between the density of n-alkanes and the extent of swell was observed.

Investigations into blends of coal-to-liquid (CTL) SPK showed that the seal swell was highly dependent on the hydrocarbon aromatic used. Some blends swelled more than petroleum-derived Jet A-1 and some less than Jet A-1. Again molar volume was demonstrated to be important but also the ability of aromatics to form hydrogen-bond like interactions with NBR. Lower molar volumes and higher δ_h values produced more favourable swelling. The importance of the presence of multiple rings was also demonstrated by the increased swelling of the C10, tetralin, over other C10 aromatics such as n-butylbenzene.

Aromatic ethers caused significantly more swell than hydrocarbon aromatics. Some of these aromatic oxygenates swelled even more than petroleum-derived Jet A-1 even when used at the minimum 8% aromatic level. This was explained in terms of their even stronger polar and hydrogen bond interactions.

The effects of temperature were an increase in the rate of swelling, as expected, and a slight decrease in the extent of swelling at elevated temperatures. However, the influence of temperature on the aromatic oxygenate, benzyl alcohol, which has previously been reported as producing large swell even when added at concentrations as low as 0.5%, was significant. It is suggested that this is because of the very strong hydrogen bond between benzyl alcohol and NBR. Because of the exothermic nature of hydrogen bonding, the equilibrium constant for this interaction decreases at elevated temperatures leading to less swell.

The results from this study suggest that lighter (lower carbon number) SPKs and SPKs containing cycloparaffins would promote swelling. The addition of lighter, higher δ_h and/or multi-ring aromatics to SPK would produce the most swell of the aromatic species added. This could be even more enhanced by the presence of aromatic oxygenates. Such compounds could be targeted for blending with synthetic paraffins to produce fully synthetic jet fuels but their impact on other properties such as flash point and distillation behaviour cannot be ignored.

TABLE OF CONTENTS

ACKNOWLEDGEMENTS ii
ABSTRACT iii
LIST OF ILLUSTRATIONS ix
LIST OF TABLES xii
LIST OF ACRONYMS xiii

1. INTRODUCTION 1
   1.1. Motivation for This Study 1
   1.2. Objectives 3
   1.3. Scope of the Study 3

2. LITERATURE REVIEW 5
   2.1. Petroleum-Derived Fuels 5
   2.2. Synthetic Fuels 6
      2.2.1. Fischer-Tropsch Processes 7
         2.2.1.1. High Temperature Fischer-Tropsch (HTFT) Processes 8
         2.2.1.2. Low Temperature Fischer-Tropsch (LTFT) Processes 9
         2.2.1.3. A comparison of LTFT versus HTFT processes 9
   2.3. Civil Aviation Jet Fuels 11
      2.3.1. Petroleum-Derived Jet Fuels 11
      2.3.2. Semi and Fully Synthetic Jet Fuels 13
      2.3.3. Synthetic vs. petroleum-derived jet fuels 15
   2.4. Elastomeric Materials 16
      2.4.1. Nitrile Rubber 17
      2.4.2. Polymeric Additives 18
      2.4.3. Polymer Ageing 19
   2.5. Factors Affecting Transport Phenomena and Degree of Swell 20
      2.5.1. Solubility Parameters 23
         2.5.1.1. Hildebrand Solubility Parameters 23
         2.5.1.2. Hildebrand Solubility Parameters for Solvent Mixtures 25
         2.5.1.3. Hansen Solubility Parameters 26
         2.5.1.4. Uncertainties Associated with Solubility Parameters 28
      2.5.2. Flory-Rehner Theory 29
      2.5.3. The Effect of Molar Volume and Shape of Solvent on Swelling 32
      2.5.4. The Effect of Crosslink Density on Swelling 33
      2.5.5. Effect of Temperature on Swelling 33
      2.5.6. Effect of Plasticisers on Seal Swell 35
   2.6. Previous Investigations into the Effect of Blending Low Level Components into SPK on Seal Swell 36

3. EXPERIMENTAL PROCEDURES 41
   3.1. Materials Used 41
   3.2. Equipment Used 43
      3.2.1. Mass measurements 43
      3.2.2. Dilatometric measurements 43
      3.2.3. SAFL Elastomer Compression Rig 43
      3.2.4. Thermogravimetric Analyser 44

3.3. Experimental Methods 44
3.3.1. O-ring Conditioning Procedure 44
3.3.2. Static Exposure Treatments 45
3.3.2.1. Gravimetric Method 45
3.3.2.2. Optical Dilatometric Method 46
3.3.3. Dynamic Experiments Using the Elastomer Compression Rig 48
3.3.4. Method Refinement 49
3.3.4.1. Degree of Repeatability 49
3.3.4.2. Solvent to Polymer Ratio Effects 50
3.3.4.3. The Effect of Temperature 50
3.3.4.4. The Effect of Plasticiser Extraction 50
3.3.5. Investigation into the Effect of Chemical Class and Structure 51
3.3.5.1. Blends with SPK 51
3.3.5.2. Switch-load Testing 51
3.3.6. Density Determination 52
3.3.7. Thermogravimetric Analysis 53

4. METHOD REFINEMENT 54
4.1. Static Solution Exposure Investigation 54
4.1.1. Static Gravimetric Experiments 55
4.1.1.1. Solvent to Polymer Ratio 55
4.1.1.2. Repeatability of Gravimetric Measurements 56
4.1.1.3. The Effect of Temperature on Seal Swell 59
4.1.2. O-ring Conditioning Procedure 60
4.1.3. Determination of the Density of NBR Samples Before and After Plasticiser Extraction 63
4.1.4. Effect of Plasticiser Extraction on Seal Swell 64
4.1.5. Volumetric Measurements 65
4.1.5.1. Optical Dilatometry 66
4.1.5.2. Elastomer Compression Rig 67
4.2. Discussion 70
4.2.1. Measurement Approach 70
4.2.2. Duration of Solvent Exposure 75
4.2.3. Effect of Temperature on Seal Swell 75
4.2.4. Plasticiser Effects 77
4.2.5. O-ring Conditioning 77

5. EFFECT OF DIFFERENT CHEMICAL CLASSES ON SEAL SWELL 80
5.1. Investigations using Pure Components 80
5.1.1. Paraffinic Isomers 80
5.1.1.1. Pure Paraffin Isomers (Octane and Dodecane) 80
5.1.1.2. CTL and GTL SPK 84
5.1.2. Effects of Carbon Chain Length on Seal Swell 85
5.1.3. Pure Aromatic Hydrocarbon Solvents 86
5.1.4. Pure Oxygenated Aromatic Solvents 87
5.2. Blends of SPK with low level components 90
5.2.1. Blends of SPK with petroleum-derived Jet A-1 90
5.2.2. Blends of SPK and Aromatic Hydrocarbons 91
5.2.3. Blends of SPK and Aromatic Oxygenates 92
5.2.4. Effect of Temperature on the Swelling of SPK Blends 95
5.3. Switch Loading 97

5.4. Blend levels at which the density specification is met 101
5.5. Discussion 102
5.5.1. Paraffinic Isomers 102
5.5.1.1. Paraffinic Structure 102
5.5.1.2. The Influence of Molar Volume 103
5.5.2. Blends of SPK and petroleum-derived Jet A-1 105
5.5.3. Blends of SPK and Aromatic Hydrocarbons 105
5.5.4. Blends of SPK and Aromatic Oxygenates 108
5.5.5. Effect of Temperature on the Swelling of NBR O-rings 110
5.5.6. Switch Loading 113

6. CONCLUSIONS 115
6.1. Method Development 115
6.2. Effect of Different Chemical Classes on Seal Swell 116

7. RECOMMENDATIONS FOR FUTURE WORK 119
7.1. Equipment Improvements 119
7.1.1. Continuous Mechanical Measurements of Dilation 119
7.1.2. Optical Measurements 120
7.2. Future Experimental Work 121
7.2.1. Leakage 121
7.2.2. Seal Swell of Real Jet Fuel 121
7.2.3. Temperature Effects on Seal Swell 121
7.2.4. Concentration of Aromatics in NBR 122
7.2.5. Polymer Selection 122
7.2.6. The Stability of Blends of Aromatic Oxygenates 122

8. REFERENCES 123

9. APPENDICES 132
9.1. Appendix A - Risk Assessments 132
9.2. Appendix B - SAFL Elastomer Compression Rig Operation and Construction 134
9.3. Appendix C – Density determinations 137
9.4. Appendix D – Calculation of volume changes from mass changes 138
9.5. Appendix E – Volume % changes for 4% blends in SPK 140

LIST OF ILLUSTRATIONS

Figure 2.1: Production costs and total greenhouse gas emissions for the production of liquid transportation fuel from different hydrocarbon feedstock 7
Figure 2.2: Simplified schematic of Sasol's HTFT process 8
Figure 2.3: Simplified schematic of Sasol's LTFT process 9
Figure 2.4: Hydrocarbon distribution in straight run Merox kerosene 12
Figure 2.5: Sasol's production scheme for semi-synthetic jet fuel 13
Figure 2.6: Carbon number distribution of paraffins in a typical HTFT SPK 14
Figure 2.7: Various seal types found in aviation systems 17
Figure 2.8: Monomeric unit representation of the molecular structure of NBR 18
Figure 2.9: The molecular structure of typical plasticiser molecules dioctyl adipate and dibutyl phthalate used in NBR vulcanisates 19
Figure 2.10: The change in mass of NBR O-rings exposed to Jet A-1 and SPK at 50°C 21
Figure 2.11: Effect of switching the fuel to which an O-ring is exposed 22
Figure 2.12: Degree of swelling of a linseed oil film for a number of solvents 26
Figure 2.13: Predicted Molar volume effects on volume swell of NBR at 25°C 32
Figure 2.14: Percentage mass uptake as crosslink density is increased, for a HNBR immersed in toluene 33
Figure 2.15: Effect of temperature on sorption of p-xylene into NBR/EVA blends 34
Figure 2.16: Effects of plasticisers on the swelling of Nylon 11 exposed to methanol 35
Figure 3.1: Microscope image of a magnified O-ring indicating the selection of the three points required to obtain the inner (i.d.) or outer (o.d.) diameter 46
Figure 3.2: Illustration of the determination of projected area of an O-ring 47
Figure 4.1: Comparison of "as received" O-rings exposed to Jet A-1 and SPK at 50°C 54
Figure 4.2: Solvent ratio effects on the swelling of "as received" O-rings treated in Jet A-1 at 50°C 56
Figure 4.3: Repeatability of "as received" O-ring samples treated in toluene at 50°C 57
Figure 4.4: Repeatability of "as received" O-ring samples treated in Jet A-1 at 50°C 58
Figure 4.5: Repeatability of "as received" O-ring samples treated in n-dodecane at 50°C 58
Figure 4.6: Effect of temperature on the swelling of "as received" O-rings treated in Jet A-1 at 23°C and 50°C 59
Figure 4.7: Effect of temperature on the swelling of "as received" O-rings treated in o-xylene at 23°C and 50°C 60
Figure 4.8: Extraction of Jet A-1 and CH_2Cl_2 from O-rings under vacuum 62
Figure 4.9: Thermogram of an "as received" NBR O-ring heated at 5°C/min. 62
Figure 4.10: Thermogram of a deplasticised NBR O-ring heated at 5°C/min. 63
Figure 4.11: Comparison between the average of three "as received" and deplasticised O-rings exposed to n-dodecane at 50°C 64
Figure 4.12: Comparison between the average of three "as received" and deplasticised O-rings exposed to Jet A-1 at 50°C 65
Figure 4.13: Volume swelling ratio versus exposure time for deplasticised O-rings exposed to Jet A-1 and SPK at 50°C 67

Figure 4.14:	Repeatability of compression rig swelling experiments for 10 "as received" O-rings exposed to Jet A-1 at 50°C, with optical measurements for reference	68
Figure 4.15:	Compression rig swelling experiments with no fuel at room temperature for experimental cylinders 2 and 6	69
Figure 4.16:	Elastomer compression rig dilation of "as received" O-rings exposed to Jet A-1 and SPK at 50°C	71
Figure 4.17:	Comparisons of optical versus gravimetric measurements for deplasticised O-rings in Jet A-1 and SPK at 50°C	72
Figure 4.18:	Comparison of calculated and measured volume swelling for deplasticised O-rings exposed to Jet A-1 at 50°C	73
Figure 4.19:	Comparison of calculated and measured volume swelling for deplasticised O-rings exposed to SPK 50°C	74
Figure 4.20:	Plasticiser extraction from "as received" O-rings exposed to Jet A-1.	79
Figure 5.1:	Comparison of the mass uptake for "as received" O-rings exposed to various octane isomers at 50°C	81
Figure 5.2:	Comparison of the mass uptake for deplasticised O-rings exposed to the isomers of octane and dodecane at 50°C	82
Figure 5.3:	Comparison of the volume increase for deplasticised O-rings exposed to isomers of octane at 50°C	83
Figure 5.4:	Comparison of the mass swelling ratio for "as received" O-rings exposed to CTL SPK and GTL SPK at 50°C	84
Figure 5.5:	Chemical structure of aromatic compounds investigated	86
Figure 5.6:	Chemical structure of oxygenates investigated	88
Figure 5.7:	Comparison of swelling (measured by mass) ratio for "as received" O-rings exposed to pure anisole, BzOH, dibenzyl ether and toluene at 50°C	89
Figure 5.8:	Calculated volume swell for deplasticised samples in various concentration of dibenzyl ether in SPK. The red line indicates the swell induced by Jet A-1	94
Figure 5.9:	The effect of temperature on the swelling of "as received" O-rings in SPK + 0.5% BzOH at 23°C and 50°C. The dashed red and blue lines indicate the extent of swell of samples treated in Jet A-1 at 50°C and 23°C respectively for 300 days.	96
Figure 5.10:	Effect of temperature effects on the swelling of deplasticised O-rings in SPK + 8% dibenzyl ether	97
Figure 5.11:	Switch loading experiment between Jet A-1 and SPK conducted on "as received" samples. The swelling curves for neat Jet A-1 and SPK are included for comparison.	98
Figure 5.12:	Switch loading experiment between Jet A-1 and SPK conducted on deplasticised O-rings. The swelling curves for neat Jet A-1 and SPK are included for comparison.	99
Figure 5.13:	Switch loading experiment conducted on deplasticised samples with graphs of O-rings exposed to Jet A-1 and SPK + 8% toluene provided for reference	100
Figure 5.14:	Switch loading experiment conducted on deplasticised samples with graphs of O-rings exposed to Jet A-1 and SPK + 4% benzyl ether provided as reference	100
Figure 5.15:	Correlation between volume change and the inverse of density caused by the exposure of "as received" O-rings to pure n-paraffins at 50°C	104

Figure 5.16:	The relationship between change in swell at equilibrium and Jet A-1 content in CTL SPK : Jet A-1 blends	105
Figure 5.17:	Percentage mass change for NBR O-rings exposed to Jet A-1, SPK, SPK + 8% Toluene and SPK + 0.5% BzOH for 48 hours at 23°C	111
Figure 5.18:	Switch loading experiments conducted using the elastomer compression rig at 50°C	112
Figure 5.19:	Switch loading investigation, switching between Jet A-1 and SPK	115
Figure 9.1:	Basic compression rig module construction	135
Figure 9.2:	Compression rig operation schematic	136
Figure 9.3:	Sample compression rig hysteresis curve, indicating data capture points	136

LIST OF TABLES

Table 2.1:	Commercial products produced from crude oil, indicating carbon chain range and boiling point	5
Table 2.2:	Comparison of LTFT and HTFT processes	10
Table 2.3:	Product selectivity for LTFT and HTFT processes	10
Table 2.4:	Chemical composition and selected properties of a petroleum-derived Jet A-1 compared with a number of SPKs	16
Table 2.5:	Hildebrand solubility parameters for selected solvents	24
Table 2.6:	Hansen solubility parameters for nitrile rubber and its components)	27
Table 2.7:	Hansen solubility parameters for selected fuels	28
Table 2.8:	Average mass change after 43 days at 40°C for N0674-70 NBR coupons and N0674-70 O-rings exposed to a number of fuels	37
Table 2.9:	Swelling of NBR O-rings in S-5 blended with a number of additives	38
Table 3.1:	Solvents used in study with indication of grade, solubility parameter and molar volume	42
Table 3.2:	Sample number and solvents used to determine the degree of repeatability for the various experimental methods	50
Table 4.1:	Repeatability of mass measurements of samples exposed to various solvents across a range of solubility parameters	57
Table 4.2:	Gravimetric measurements on "as received" O-rings swollen in Jet A-1 and CH_2Cl_2	61
Table 4.3:	Density of "as received" and deplasticised O-rings	63
Table 4.4:	Volumes changes of "as received" O-rings exposed to varying solvents at 50°C	66
Table 4.5:	Thermal expansion coefficient an densities of Jet A-1 and SPK	72
Table 4.6:	Mass swelling ratio at 48 h for varying concentration of carbon black filled NBR moulded disks exposed to motor oil	76
Table 5.1:	Solvent properties and volumetric swell changes for isomers of octane and dodecane on deplasticised O-rings at 50°C	83
Table 5.2:	Solvent properties and experimental summary for "as received" O-rings exposed to different n-paraffins on at 50°C	85
Table 5.3:	Solvent properties and experimental summary for the exposure of "as received" O-rings to pure aromatics at 50°C	87
Table 5.4:	Solvent properties and experimental summary for the exposure of "as received" O-rings to selected oxygenated aromatic solvents at 50°C	89
Table 5.5:	Swelling of deplasticised O-rings exposed to blends of petroleum-derived Jet A-1 and SPK at 50°C	90
Table 5.6:	Solvent properties and experimental summary for the exposure of deplasticised O-rings to blends of aromatic hydrocarbons and SPK	91
Table 5.7:	Solvent properties and experimental summary for the exposure of deplasticised O-rings to blends of aromatic oxygenates and SPK at 50°C	93
Table 5.8:	Mass uptake and calculated volume change for deplasticised O-rings in blends of dibenzyl ether with SPK at 50°C	94
Table 5.9:	Solvent blend percentage required in order to obtain minimum jet fuel density specification of 0.771 g/cm^3	102
Table 5.10	Concentration factors of aromatic compounds during swelling	109
Table 9.1:	Solvent properties and experimental summary for the exposure of deplasticised O-rings to blends of aromatic species and SPK at 50°C	140
Table 9.2:	Concentration factors of aromatic compounds during swelling	140

LIST OF ACRONYMS

ASTM	ASTM International (formerly American Society for Testing and Materials)
BzOH	Benzyl alcohol
CTL	Coal-to-liquid
CV	Coefficient of variation
DiEGME	Diethylene glycol monomethyl ether
EVA	Ethylene-vinyl acetate polymer
FSJF	Fully synthetic jet fuel
FT	Fischer-Tropsch
GHG	Greenhouse gas
GTL	Gas-to-liquid
HNBR	Hydrogenated nitrile rubber
HTFT	High temperature Fischer-Tropsch
i.d.	Inner diameter
Jet A-1	Commercial DEF STAN 91-91 petroleum-derived jet fuel
JFTOT	Jet fuel thermal oxidation tester
JP-5	US navy's petroleum-derived jet fuel
LTFT	Low temperature Fischer-Tropsch
NBR	Nitrile rubber
o.d.	Outer diameter
ORTIA	Oliver R. Tambo International Airport
PM	Particulate matter
Q%	Mass swelling ratio
R%	Volume swelling ratio
S-5	Synthetically derived kerosene produced by Syntroleum
S-8	Synthetically derived kerosene produced by Syntroleum
SAFL	Sasol Advanced Fuels Laboratory
SAS	Sasol Advanced Synthol
SDA	Static dissipater additive
SPK	Synthesised paraffinic kerosene
SSJF	Semi-synthetic jet fuel
TGA	Thermal gravimetric analysis
VTDR	Video tube deposit rater
WSD	Wear scar diameter

CHAPTER 1

1. INTRODUCTION

1.1. Motivation for This Study

The development of alternative fuels has been driven by concerns about the use of petroleum-derived fuels, such as particulate matter (PM) and sulphur dioxide emissions, expected escalations in the oil price and supply constraints (1) (2). The use of alternative fuels, however, comes with its own set of challenges. Alternative fuels need to be fully fungible with existing fuels, requiring no engine modification and must be compatible with materials used in aircraft fuel systems. Synthetic fuels produced by Fischer Tropsch (FT) processes utilising coal and natural gas best meet these requirements yet may still require the addition of low level blending components to meet current specifications (3).

The first use of synthetic fuels in commercial aviation applications was in early in 1999 at OR Tambo International Airport (ORTIA) in Johannesburg, South Africa, when semi synthetic jet fuel (SSJF) was introduced. This SSJF, a blend of FT synthetic jet fuel with petroleum-derived Jet A-1, addressed potential complications associated with synthetic fuel (4). A number of additional specifications were incorporated into Def Stan 91-91 (5) and ASTM D7566 (6) to allow the use of SSJF as a commercial jet fuel. These included setting a minimum volume aromatic content of 8% in order to limit volumetric changes of polymeric seals in the fuel system (6).

Following the success of SSJF, a fully synthetic jet fuel (FSJF) was approved in July 2008. A minimum 8% aromatic content by volume was still required but this could be achieved using synthetic aromatic compounds (7). Blending a synthetic fuel with aromatics, however, raises processing complexity (3). The 8% minimum aromatic specification is under investigation as it appears to be based on a historical value that has shown adequate seal swell performance in the past and is not necessarily the polymeric failure limit (3) (8) (9).

INTRODUCTION

Currently an approved synthetic jet fuel component, synthetic paraffinic kerosene (SPK), used in semi synthetic jet fuel is produced from components obtained via High Temperature Fischer Tropsch (HTFT) processes. The product produced is mainly iso-paraffinic in nature (10). Future interest in using the Low Temperature Fischer Tropsch (LTFT) processes to target diesel and jet fuel range products is under investigation (11). This, however, would alter the product chemistry by producing more n-paraffinic molecules (12). The change in the paraffinic isomers, moving from iso- to n-paraffins results in a slight increase of fuel density, an increase in freezing point and may further affect the degree of polymeric swell.

The purpose of this study was to look into the effects that various chemical classes have on the compatibility of polymeric materials in fuel systems. This study specifically focused on nitrile rubber (NBR) because this rubber has shown to be more sensitive to changes in fuel chemistry than other polymers typically found in aviation fuel systems (2) (13). In particular the study investigated what structural properties of aromatic compounds would produce the most swell.

Considerably less seal swell has been observed when seals are exposed to synthetic paraffinic kerosenes (SPK) which do not contain aromatic species than when they are exposed to petroleum-derived Jet A-1. As a consequence O-rings, which have swollen due to the effect of petroleum-derived fuels in service, may shrink, harden and fail when exposed to synthetic fuels with no or very little aromatic content (14).

The effects that fuels have on polymeric materials is of great interest since seals, gaskets and hoses are used in a number of key areas in fuel systems where seal failure resulting in fuel leaks may lead to devastating consequences. Therefore, a conversion to pure synthetic fuels cannot be made without considering changes in sealing properties of the polymer.

The aromatic content is not the only factor which may affect the chemical composition of a synthetic fuel. The fuel may vary significantly because of the feedstock and the method of production. Since HTFT and LTFT products are notably

different in their iso- and n-paraffinic nature, these effects may also impact on the seal swell caused by synthetic jet fuels (4).

1.2. Objectives

The objectives of this study were therefore to:

- identify appropriate experimental procedures in order to investigate seal swell repeatability,
- identify a suitable method for the extraction of plasticisers in "as received" O-ring samples to produced O-rings similar to O-rings used in service,
- gain a greater understanding into the effect that fuels and solvents have on seal swell, by investigating the effect of different structural characteristics, e.g. branching, cyclisation and molecular size on seal swell,
- assess the impact of low level blending components, such as aromatics and oxygenates with SPK on seal swell in comparison with Jet A-1, and
- understand the influence of different structural characteristics of aromatic compounds on seal swell.

1.3. Scope of the Study

The primary focus of this investigation was on the effects that various chemical classes have on the swelling of NBR O-rings, using methods based on ASTM static exposure technique D1414 (15) (Standard test methods for rubber O-rings) and D471 (16) (Standard test methods for rubber properties – Effect of liquids)) and using an elastomer compression rig built at the Sasol Advanced Fuels Laboratory (SAFL) (17).

Other indirect methods of observing seal swell such as the use of an Elastocon (18) were not investigated. Furthermore other test methods which assess changes in the properties of O-rings such stress relaxation and tensile tests which have been used by other research groups were not investigated in this study (3) (4).

Only NBR O-rings were investigated as these have been shown to be most sensitive to changes in fuel composition. Fluorosilicone and Viton O-rings were consequently not investigated even though such elastomers are also used in aviation fuel systems.

The in-service effects on O-rings were restricted to plasticiser extraction. Effects such as hardening as a result of heat induced crosslinking were not addressed. Nor were the effects of the exposure of O-rings to fuel derived peroxides investigated.

CHAPTER 2

2. LITERATURE REVIEW

2.1. Petroleum-Derived Fuels

Petroleum-derived fuels are produced by the refining of crude oil which primarily contains hydrocarbon molecules. These include paraffins (alkanes), naphthenes (cycloalkanes) and aromatic hydrocarbons. Other elements are, however, present. Along with nitrogen, oxygen and sulfur, crude oil also contains trace elements of metals such as iron, nickel, vanadium and copper. Depending on the processes used to upgrade crude oil, these polar compounds may or may not be found in the final product, which may alter fuel properties (19).

Since the paraffins that are present in crude oil generally have between 5 and 70 carbon atoms per molecule, fractional distillation is required in order to separate these components into the required carbon number range for a particular fuel application.

Table 2.1 indicates the typical carbon number and boiling point ranges for each product produced.

Table 2.1: Commercial products produced from crude oil, indicating carbon chain range and boiling point (20)

Carbon chain range	Product produced	Boiling point range (°C)
C_3 to C_4	LPG	< 45
C_5 to C_{10}	Gasoline	45 – 155
C_9 to C_{13}	Kerosene	165 – 260
C_{10} to C_{24}	Diesel fuels	240 – 360
C_{13} to C_{40}	Fuel oil	> 360

Relatively high concentrations of aromatic and sulfur compounds may still be present in the final fuel. The aromatic compounds increase particulate matter emissions, an

environmental concern (3). Aromatic compounds, however, boost density (4). There exists thus a delicate balance between environmental concerns and the required properties of the fuel.

2.2. Synthetic Fuels

Unlike petroleum-derived fuels, synthetic fuels can be produced from a number of different raw materials, such as coal, natural gas and biomass. Currently coal and natural gas are commercially converted into liquid hydrocarbons by Coal-To-Liquid (CTL) and Gas-To-Liquid (GTL) Fischer-Tropsch (FT) processes (21). The final syncrude produced from High Temperature Fischer Tropsch (HTFT) or Low Temperature Fischer Tropsch (LTFT) processes can differ significantly. The decision whether to use HTFT or LTFT is based strongly on the product stream being targeted and on the available feedstock (22). There are, however, cost and environmental considerations which also impact on the decision about which process to use.

Due to the nature of processing and handling of coal, CTL synfuels are more costly than GTL synfuels, in addition to having higher greenhouse gas (GHG) emissions because of the higher carbon to hydrogen ratio in coal compared to natural gas (21) and the energy requirements of the processing steps involved. Figure 2.1 shows both the production costs and total GHG emission of producing liquid transportation fuel (including gasoline, kerosene and diesel) from a number of different feedstocks.

The dark segments in Figure 2.1 shows a conservative estimate of the amount of that resource available, while the lighter portion represents a less certain estimate (21). Given that the availability of oil is expected to decrease, the interest in using synthetic fuels is likely to grow, with specific focus on GTL technology as cost and GHG emissions are more favourable (21).

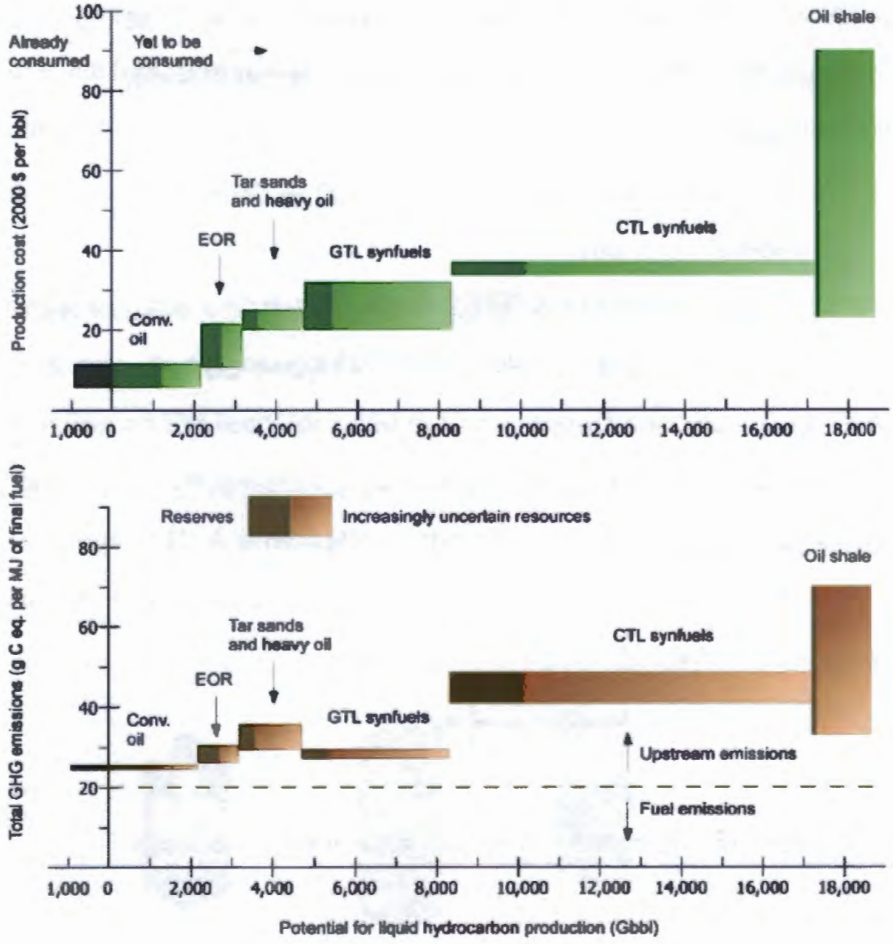

Figure 2.1: Production costs and total greenhouse gas emissions for the production of liquid transportation fuel from different hydrocarbon feedstock (reproduced from Brandt and Farell (21))

2.2.1. Fischer-Tropsch Processes

Fischer-Tropsch (FT) processes are used for the conversion of raw carbon-based feedstocks into synthetic fuels, ultimately changing carbon rich raw materials into fuels that are compatible with existing engines. The fuels produced by FT processes may be tailored to the required products by varying operational conditions such as reactor temperature, pressure and feed ratio of the reactants.

The general production process utilising FT technology can be divided into four basic processing stages (22) (23) (24):

- Feedstock is converted into carbon monoxide and hydrogen gas (syngas) and a small quantity of other compounds such as carbon dioxide.

  From coal

  Steam gasification $C + H_2O \rightarrow CO + H_2$

  From natural gas

  Autothermal reforming $2CH_4 + O_2 + CO_2 \rightarrow 3CO + H_2O + 3H_2$

  or Steam reforming $CH_4 + H_2O \rightarrow CO + 3H_2$

- Purification, which removes substances such as sulfur, therefore preventing poisoning of the FT catalyst.

- FT synthesis of the syngas into hydrocarbons.

  $CO + 2H_2 \rightarrow -(CH_2)_n- + H_2O$

- Finally the refining of the FT product into commercial fuels.

2.2.1.1. High Temperature Fischer-Tropsch (HTFT) Processes

Modern HTFT processes are carried out at temperatures near 340°C, using iron based catalysts (25). Figure 2.2 is a summarised flow diagram of the Sasol HTFT process.

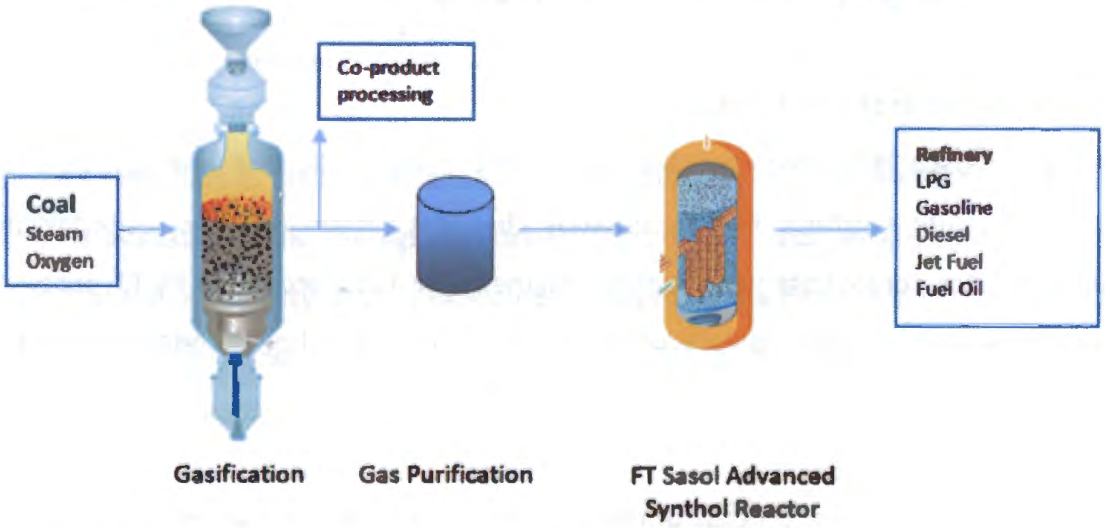

Figure 2.2: Simplified schematic of Sasol's HTFT process (reproduced from Sasol Refinery Schematic (26))

Gasoline-range compounds are the primary products from Sasol Advanced Synthol (SAS) reactors. Jet fuel, diesel and fuel oil components are produced to a lesser extent (25). Upgrading of SAS reactor products may be used to increase the range of jet fuel components (13).

2.2.1.2. Low Temperature Fischer-Tropsch (LTFT) Processes

LTFT processes, operated between 210°C and 260°C, utilise either iron or cobalt based catalyst depending on the feedstock and desired product spectrum (11). They typically produced high molecular weight n-paraffinic waxes which may be cracked into the required fuel range (11). A schematic of the Sasol LTFT process using a slurry phase reactor can be seen in Figure 2.3 (26).

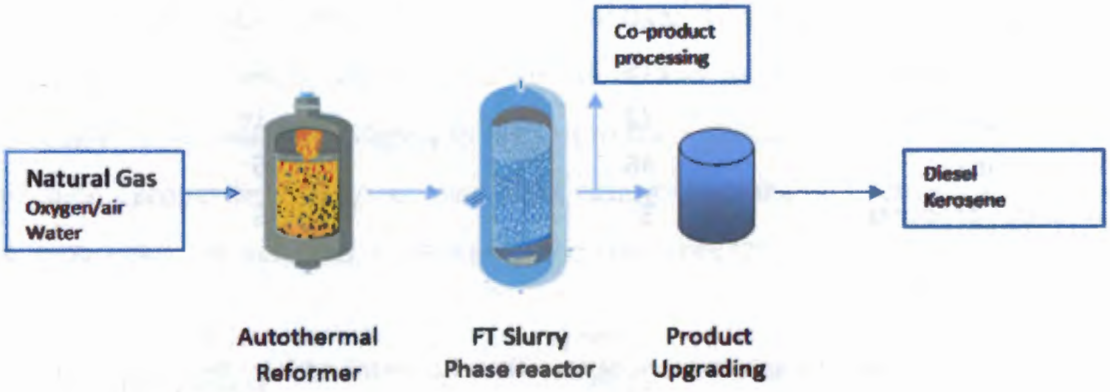

Figure 2.3: Simplified schematic of Sasol's LTFT process (reproduced from Sasol Refinery Schematic (26))

2.2.1.3. A comparison of LTFT versus HTFT processes

The differences between the product slates produced by HTFT and LTFT processes determine the refinery operations. Table 2.2 summarises the two FT processes while Table 2.3 indicating the selectivity of the products produced.

Table 2.2: Comparison of LTFT and HTFT processes (11) (24)

	LTFT	HTFT
Temperature (°C)	210 – 260	310 – 340
Modern reactor type	Fixed slurry bed	Fixed (Sasol advanced synthol) fluidised bed
Main products	n-Paraffinic waxes	Gasoline range, alpha olefins and oxygenates

Table 2.3: Product selectivity for LTFT and HTFT processes (12)

Products	LTFT Arge (weight %)	HTFT Synthol (weight %)
Carbon number distribution		
$C_3 - C_4$, LPG	10	30
$C_5 - C_{10}$, naphtha	19	40
$C_{11} - C_{22}$, distillate	22	16
C_{22} and heavier	46	6
Aqueous products	3	8
Compound classes		
Paraffins	Major product	>10%
Olefins	>10%	Major product
Aromatics	<1%	5-10%
Oxygenates	5-15%	5-15%
S- and N-species	None	None
Water	Major by-product	Major by-product

It can be seen in Table 2.3 that HTFT processes favour the production of straight run gasoline. The LTFT process predominantly produces heavy oils and waxes which may be cracked down into the middle distillate range. This results in the synthetic fuel requiring blending or processing in order to produce a suitable fuel for commercial applications (27). For example the LTFT product must undergo isomerisation in order to meet jet fuel freezing point specifications as well as requiring the addition of aromatics to boost density.

As FT products are dependent on manufacturing conditions and the final refinery processes, the chemical composition may vary depending on the process.

2.3. Civil Aviation Jet Fuels

2.3.1. Petroleum-Derived Jet Fuels

Several grades of petroleum-derived kerosenes are approved to be used in commercial gas turbine engines. These include, but are not limited to, fuels such as Jet A-1, Jet A, and Jet B. Jet A-1 is an international jet fuel suitable for most turbine engines and has a freezing point of -47°C. Jet A is used only within the continental United States of America, it has a higher freezing point specification of -40°C. Jet B is predominantly used in very cold climates where cold weather performance is essential, such as Northern Canada and Alaska. This fuel comprises a greater distillation cut including naphtha and kerosene, and has a freezing point of -51°C. Although these fuels differ slightly in respect to their distillation cut and some of their specified properties, they contain the same hydrocarbon chemical species, *i.e.* n-paraffins, iso-paraffins, naphthenes and aromatics (28).

Jet fuels are produced to internationally standardised sets of specifications such as ASTM D1655 (29) and Def Stan 91-91 (5). A number of specified properties target legacy issues. Aircraft have long service lives. Consequently fuels need to be able to be used in old aircraft (> 20 years) as well as newer aircraft. Furthermore they need to be available worldwide. This consequently limits the nature of alternative fuels that can be developed to be used interchangeably with petroleum-derived Jet A-1.

Figure 2.4 below shows the carbon number distribution for a Merox treated Jet A-1 (30).

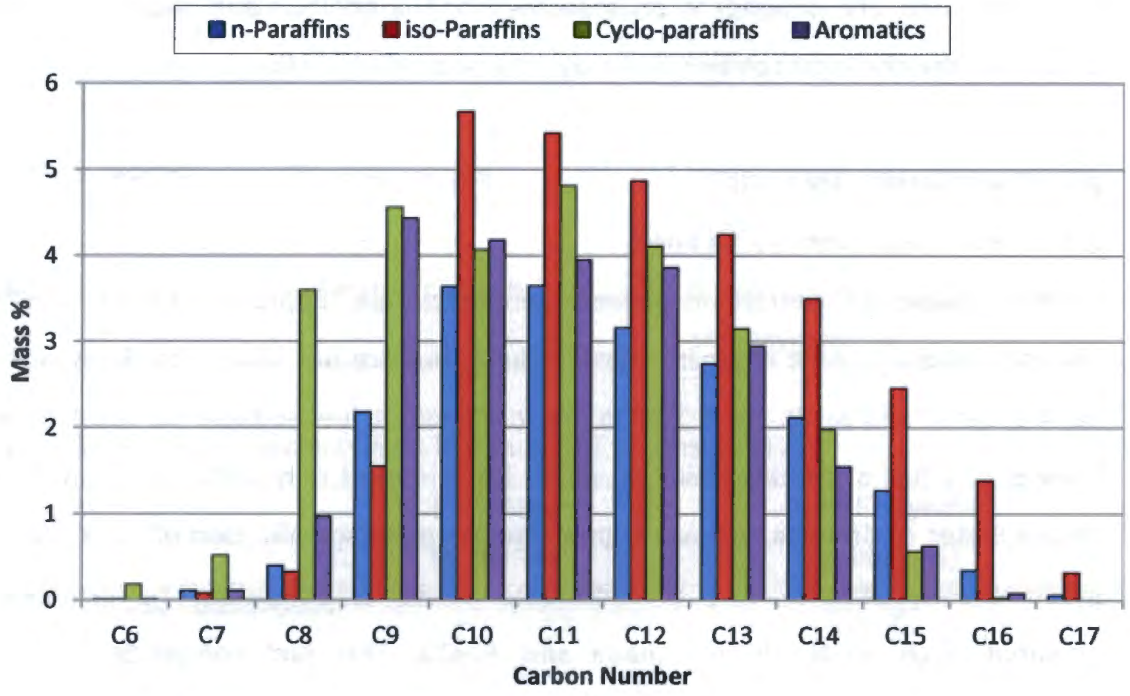

Figure 2.4: Hydrocarbon distribution in straight run Merox kerosene (adapted from van der Westhuizen *et al.* (30)).

It can be seen that the bulk of the species have carbon numbers between 8 and 16, peaking in the range 10 to 12 depending on the species concerned (30). As the separation of the kerosene cut from the crude oil is based on a boiling point range, the carbon number distribution can be affected by the size of the central distillation unit in the processing of crude oil. Therefore, different processing plants may produce a kerosene cut that can be slightly different in composition (17). A survey of US Airforce JP-8 samples revealed that 95% of these fuels had aromatic contents between 10 and 25% (2). Note that 25% is the maximum allowed aromatic content in Jet A-1 and JP-8 (29).

The figure illustrates that for a typical petroleum-derived jet fuel the amount of iso-paraffins is usually greater than that of n-paraffins. This allows Jet A-1 to meet the freezing specification (4). The aromatic species also lower freezing point and increase the fuel's density.

2.3.2. Semi and Fully Synthetic Jet Fuels

Because jet engines have historically been designed for petroleum-derived jet fuels, any synthetic fuels develop have to be fully fungible. This may require the blending of low level components. As an example, one might add aromatic compounds to paraffinic synthetic components which improve fuel density and seal swell. However, this adds cost and increases soot precursors (3). The addition of blending components would ideally be added in the lowest possible concentrations that would satisfy the application/specification (31).

In December 1998 Sasol was granted approval by the UK Ministry of Defence to use up to 50% SPK produced by the HTFT process in Secunda as a blend component with petroleum-derived jet fuel (4). This allowed Sasol in 1999 to be the first company to produce a commercial semi-synthetic jet fuel (SSJF) for local and international airline operation from O.R. Tambo International Airport (ORTIA) in Johannesburg, South Africa (4). The SSJF addressed issues of low lubricity, low fuel density and aromatics and needed to meet the requirements in the ASTM D7566 (6) and DEF STAN 91-91 (5) for Jet A-1 (13). A schematic diagram of the production of this SSJF can be seen in Figure 2.5.

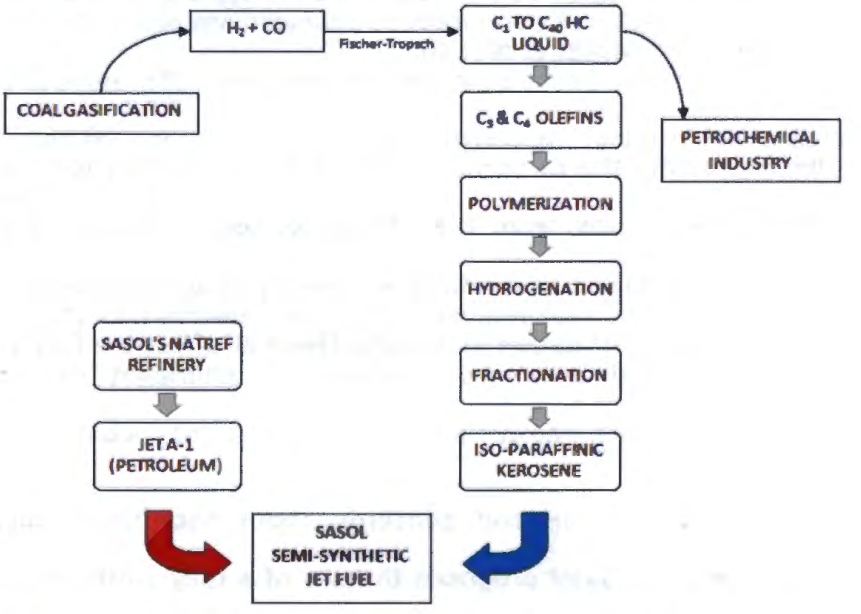

Figure 2.5: Sasol's production scheme for semi-synthetic jet fuel (reproduced from Moses *et al.* (13)).

The SPK components produced via HTFT and further refining are primarily iso-paraffins with small amounts of cyclic paraffins and very small amounts of n-paraffins.

Figure 2.6 shows the mass hydrocarbon distribution of SPK which can be seen to lie between C_8 and C_{13} (13).

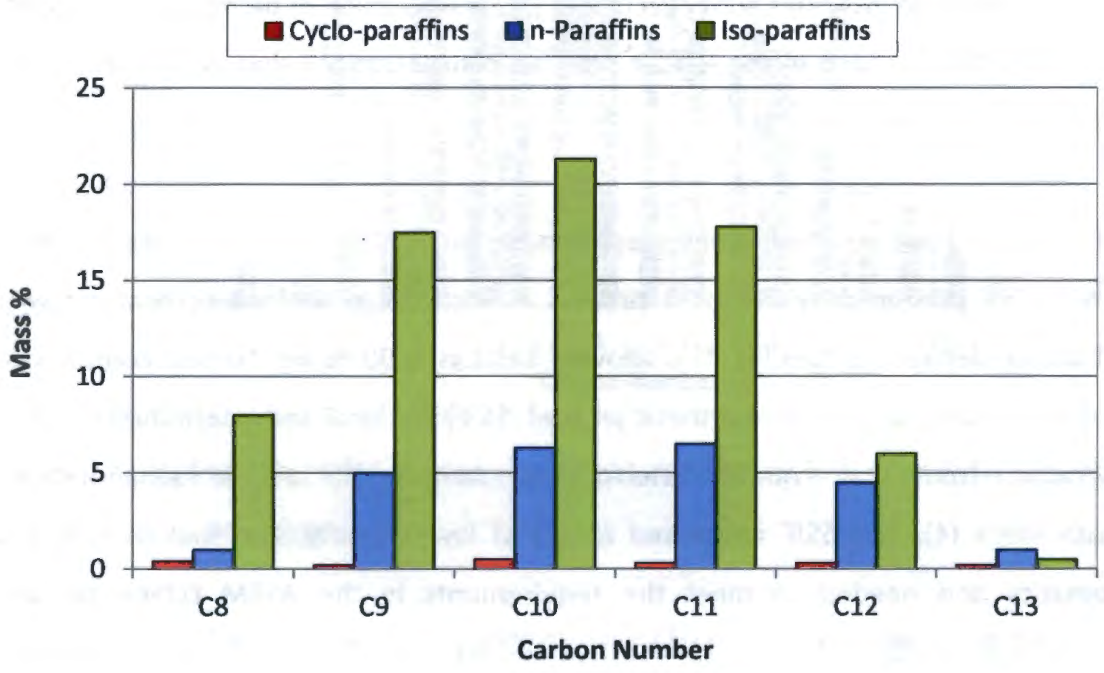

Figure 2.6: Carbon number distribution of paraffins in a typical HTFT SPK (adapted from Moses *et al* (13)).

Comparing this figure with the carbon distribution of a typical Jet A-1 seen in Figure 2.4, distinct differences can be seen. The differences seen between Jet A-1 and SPK include a significantly higher iso to n ratio, the absence of aromatic compounds and a narrower carbon number distribution in the SPK. These all affect the final properties of the fuel.

Based on the success of SSJF and concerns about the future supply of the petroleum-derived jet fuel, Sasol proposed the use of a fully synthetic jet fuel (FSJF) produced by the HTFT process. In December 2003 Sasol's FSJF was submitted for approval for commercial use. This approval was granted in April 2008 for a FSJF produced from blends of light distillate, heavy naphtha and the iso-paraffinic streams

from Sasol's Secunda refinery (5) (7). The world's first commercial passenger flight using FSJF took place on the 21 September 2010 from Lanseria Airport in Johannesburg to Ysterplaat Air Force base in Cape Town during the Africa Aerospace and Defence 2010 exhibition.

In order to produce a jet fuel from HTFT products produced from coal the preferred upgrading process to produce FT kerosene involves oligomerisation and subsequent hydrogenation. The key feedstocks are C_3 and C_4 olefins produced during the HTFT step. By contrast LTFT products produced from gas would be waxes which would require hydrocracking, hydrotreating and fractionation (4).

2.3.3. Synthetic vs. petroleum-derived jet fuels

Differences in the composition of petroleum-derived Jet A-1 and the various synthetic fuel components are compared in Table 2.4 (4). The table shows that there are significant differences in density and the aromatic content between synthetic jet fuel components compared to petroleum-derived Jet A-1.

In order to meet the density specification additional components need to be added to the SPKs. Typically these are aromatic compounds since they have higher densities. It can be seen that the GTL SPKs contain more n-paraffins than the CTL SPK in the table. The Jet A-1 used for comparison contains a significant faction of cycloparaffins. These too increase the density of Jet A-1.

The compatibility of synthetic fuels with aviation fuel systems is a particular issue. Strict regulations regarding the levels of aromatics in synthetic jet fuels were introduced in order to prevent potential problems arising from seal swell differences (5).

Table 2.4: Chemical composition and selected properties of a petroleum-derived Jet A-1 compared with a number of SPKs (4)

Property	Limits	Jet A-1	Sasol CTL	Isomerised Sasol GTL	Shell GTL	Syntroleum S-8
Composition						
Aromatics, v%	8.0*-25**	19	1	0	0.2	0
n-Paraffins, m%	--	20	2	23	41	17
iso-Paraffins, m%	--	26	87	76	58	82
cyclic-Paraffins, m%	< 15#	31	10	1	1	1
Volatility						
Density @ 15°C, kg/m^3	771-836	800	765	735	736	756
Thermal Stability						
Filter pressure drop, mm Hg	25 (max)	0	0	0	0	0
Tube deposit rating	<3 $	<1(275°C)	<1(325°C)	<1(325°C)	1(325°C)	1(325°C)

*	Minimum specification applicable to SSJF and FSJF. There is no minimum specification for petroleum-derived Jet A-1
**	Maximum specification for Jet A-1, SSJF and FSJF
#	Maximum specification applicable to FSJF. There is no maximum specification for petroleum-derived Jet A-1
$	Temperature of tube deposit rating dependent on fuel, 275°C for petroleum-derived, 325°C for synthetically derived
Sasol CTL	Coal derived kerosene approved for semi and fully synthetic jet fuel blends
Sasol GTL	Isomerised product of a GTL stream
Shell GTL	Natural gas derived kerosene produced by Shell
S-8	Natural gas derived kerosene produced by Syntroleum

2.4. Elastomeric Materials

Polymers consist of a number of repeating units which are typically covalently bonded together (32). A subset of these is the elastomers. Elastomers are amorphous polymers that are capable of being stretched or compressed and return to their original shape without permanent deformation. The materials typically have a low Young's modulus with a high yield strain and a glass transition temperature below room temperature (33).

Elastomers are used above their glass transition temperature. This allows for a considerable amount of chain mobility. They are characteristically only lightly crosslinked, which allows elastomers to be stretched without permanent deformation. They are thus commonly used in static and dynamic seals (32). The elastomeric materials most commonly used as O-rings, gaskets, diaphragms and bladders in aircraft fuel systems are nitrile rubber (NBR), Viton and fluorosilicone (34). These

components are used in a number of key areas in fuel systems, where failure may have devastating consequences. Of interest are the NBR compounds which are more sensitive to the fuel chemistry compared to the other polymers typically found in the aviation fuel system (2) (13).

Figure 2.7 shows various seal types that can be found in aviation systems.

Figure 2.7: Various seal types found in aviation systems (supplied courtesy of SAA Technical)

2.4.1. Nitrile Rubber

Nitrile rubber (NBR) is an unsaturated copolymer synthesised by emulsion polymerisation of butadiene and acrylonitrile and is widely used in fuel exposed systems due to its resistance to oils and fuels (35) (36). Figure 2.8 illustrates the monomers of butadiene and acrylonitrile together with a monomeric unit representation of NBR.

NBR has good mechanical properties and is resistant to most fuels and oils (32). It also has a wide operational temperature range from -40°C to 125°C (37). NBR is consequently widely used in fuel systems where varying operational temperature are common, for example in the aviation industry.

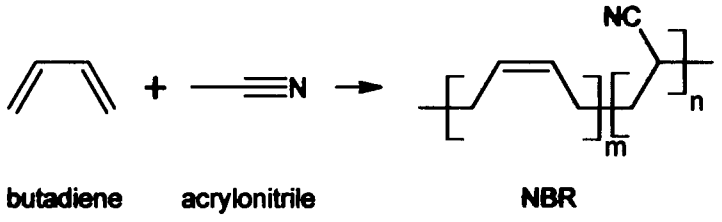

Figure 2.8: Monomeric unit representation of the molecular structure of NBR

Fuel seals are one of most common applications for NBR components and are typically O-rings in the shape of a torus with a circular cross-section. Depending on the application, the polymeric component can be tailored to meet the required properties needed in service. These properties can be altered by varying the polymeric matrix or by the addition of additives that promote the desired properties.

2.4.2. Polymer Additives

Polymer additives are used to modify polymeric properties and to aid in processing so as to produce articles fit for service. These additives include crosslinking agents, plasticisers, stabilisers (which prevent polymer degradation) and reinforcing fillers (38).

Plasticisers play an important role in determining the degree of seal swell caused by solvent interactions and are thus particularly examined in this report. They are added to polymers to lower the glass transition temperature which results in the increase of flexibility. As a result the ease of processing and degree of seal swell is affected.

Two typical plasticisers, dibutyl phthalate ($C_{16}H_{22}O_4$) and dioctyladipate ($C_{22}H_{42}O_4$), used in NBR vulcanisates, are shown in Figure 2.9 (39). These molecules are able to embed between the polymeric chains, resulting in the chains being spaced further apart, thus increasing the free volume (38).

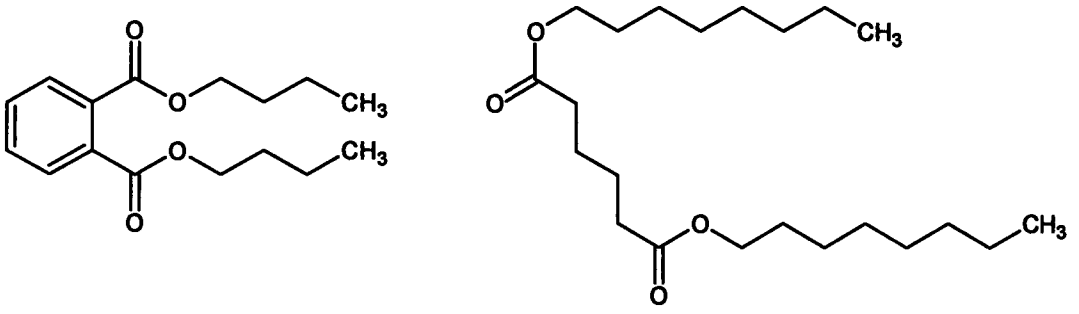

dibutyl phthalate dioctyl adipate

Figure 2.9: The molecular structure of typical plasticiser molecules dioctyl adipate and dibutyl phthalate used in NBR vulcanisates (39)

Different hardness polymers may be produced by altering the amount of plasticisers present but also by changing the degree of vulcanisation and filler loading. The extraction of plasticiser in service from the component is a common problem associated with the use of polymeric components. This may result in changes in physical properties and dimensions of the polymeric article.

2.4.3. Polymer Ageing

The ageing of polymeric materials is a complex chemical process which results in the deterioration of the polymer. This may be via chain scission, an increase in chain crosslinking and the removal of additives such as plasticisers and stabilisers (40).

The ageing process may be accelerated by the environmental conditions to which the O-rings are exposed, *e.g.* high temperatures, mechanical stress, and exposure to solvents, ozone and oxygen. The conditions that the polymeric component will be exposed to in service needs to be assessed in order to determine the impact of ageing (40). Commonly NBR components used in the aviation industry are subjected to varying temperatures and exposure to fuels and lubricants in service.

Thermal ageing results because at elevated temperatures the rate of oxygen diffusion into a polymeric material is accelerated which leads to oxidative degradation by

excessive crosslinking and molecular scission. As temperature increases the rate of polymeric deterioration caused by oxidation increases (40) (41).

The effects on polymeric materials due to the exposure to fluids can be determined by carrying out tests in known fluids for specific immersion periods. Certain fuels and solvents diffuse into the polymer and may result in additives, such as plasticisers leaching out. Factors affecting the rate of molecular transport of solvent into the polymer are discussed in the following sections.

2.5. Factors Affecting Transport Phenomena and Degree of Swell

A dynamic environment is created when polymeric materials are exposed to solvents. These solvents are able to migrate into the polymeric matrix, thereby forcing the polymeric chains apart (14). This results in a subsequent increase in volume and a decrease in hardness of the polymeric component. More complex swelling behaviour is seen with polymeric materials that contain plasticisers and processing oils. In this case the overall volume change is a combination of competing processes: the diffusion of solvent into the polymer, causing swelling, and the extraction of removal of plasticisers, causing shrinkage. The level of swell is highly dependent on the relative dominance of each process.

The transport of molecules through a polymer takes place due to random molecular motion of individual molecules (42). This process is driven by the chemical potential difference between the bulk solvent and the solvent in the polymer, and involves sorption, diffusion and permeation (42). As the chemical potential begins to equalise the transport phenomena begin to slow (43). This may be observed in Figure 2.10 which shows how the rate of molecular transport decreases with time (44).

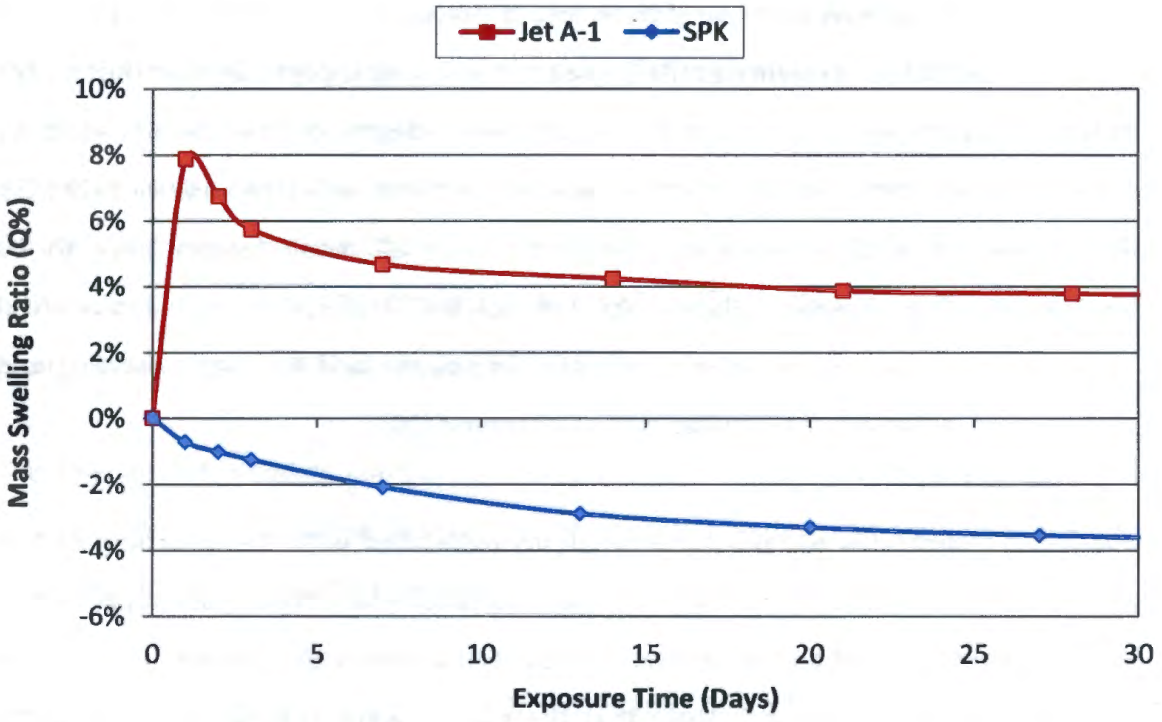

Figure 2.10: The change in mass of NBR O-rings exposed to Jet A-1 and SPK at 50°C (44)

When NBR O-rings are exposed to Jet A-1, the rate of absorption of fuel is greater than that of plasticiser extraction during the initial phase. Later the latter process is dominant till finally both become slow and equilibrium is approached. By contrast O-rings exposed to SPK display behaviour where the rate of plasticiser extraction is greater than that of solvent entering. This results in an overall decrease in the sample's mass.

Polymeric properties such as the degree of unsaturation, crosslinking and crystallinity as well as the nature of any fillers present all affect the transport rate. These properties have the result of affecting the amount of free volume in the polymeric material which is associated with chain segmental mobility. This is significant as greater free volume is associated with a fast transport rate due to the unimpeded motion of molecules (42).

The amount of solvent that can diffuse into a polymeric sample and the extent of plasticiser extraction, determines the degree of swell. This is dependent on differences in solubility parameters and molar volume of solvent, degree of free volume, additives (such as plasticisers), crosslink density, quantity of fillers and temperature (42) (43). The degree of swell is a complex property since all these factors have to be considered. The general relationship for solvent interacting with polar NBR components is that as the solvent increases in polarity and hydrogen bonding and decreases in molar volume, greater swell is observed (10).

Figure 2.11 illustrates the potential problems associated with the switching of fuel types when the extraction of the plasticiser has taken place. The figure represents a cross-sectional view of an O-ring inside a groove, illustrating the change in O-ring size as fuel chemistry is changed. Note that the gap between the two surfaces which require sealing is exaggerated.

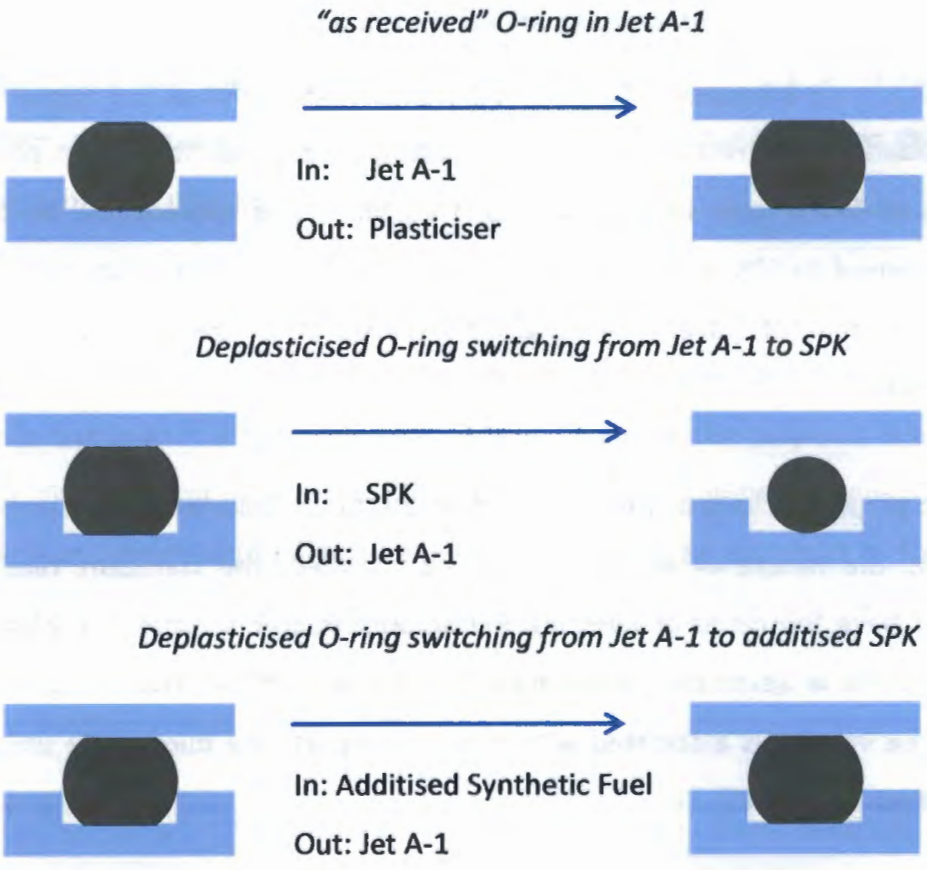

Figure 2.11: Effect of switching the fuel to which an O-ring is exposed

An O-ring exposed to Jet A-1 displays an overall volume increase; this being the sum of the fuel absorbed and plasticiser extraction. If the deplasticised sample was then switched to an SPK, an overall volume decrease would be observed once the extraction of the Jet A-1 had taken place. The best outcome of switching fuel types can be observed in the last illustration which shows no volume change effect. This can be brought about by using SPK with the addition of low level blending components such as aromatic compounds that can promote swell.

The selection of blending components is based on the desired behaviour in the final product. For example, when seal swell is of priority, blending components that show seal swell potential should be selected.

The theoretical degree of swell can be estimated by taking solubility parameters, molar volume and solvent shape into account.

2.5.1. Solubility Parameters

The relationship between the polymer and solvent may be further understood by considering solubility parameters. Solubility parameters assist in determining the degree to which a polymer may swell when in contact with a solvent. The principle behind this is the concept that "like dissolves like". Thus if the solvent solubility parameter is similar to that of the polymer, the two are likely to be miscible or in the case of crosslinked polymers, significant swelling will occur. Of interest are the Hildebrand and Hansen solubility parameters.

2.5.1.1. Hildebrand Solubility Parameters

The Hildebrand solubility parameter for a solvent is defined as the square root of the cohesive energy density. This may be calculated from the heat of vaporisation and the molar volume as seen in Equation 2.1 (45).

$$\delta = \sqrt{\frac{\Delta H_v - RT}{V_m}} \qquad (2.1)$$

where:

ΔH_v = heat of vaporisation

R = molar gas constant

T = boiling point in kelvin

V_m = molar volume

The Hildebrand solubility parameter is a numerical value that is essentially a measure of the energy of vaporisation (46). Molar volume is an integral part of Hildebrand's equation. Smaller molar volumes favour lower cohesive energy densities.

Since vaporisation and solubility both rely on overcoming the intermolecular van der Waals forces holding the molecules together, the Hildebrand solubility parameter allows the solubility behaviour of a solution to be predicted using a single term component. Table 2.5 indicates the Hildebrand solubility parameters for a selected number of solvents.

Table 2.5: Hildebrand solubility parameters for selected solvents (47)

Compound type	Solvent	Carbon number	Molar volume (cm^3/mol)	δ ($(MPa)^{1/2}$)
n-Paraffins	n-Hexane	C_6	131.6	14.9
	n-Heptane	C_7	147.4	15.3
	n-Octane	C_8	163.5	15.5
i-Paraffin	2,2,4-Trimethylpentane	C_8	166.1	14.1
Cyclic-Paraffins	Cyclohexane	C_6	108.7	16.8
	Methylcyclohexane	C_7	128.3	16.0
Aromatics				
	Toluene	C_7	106.8	18.2
	o-Xylene	C_8	121.2	18.1
Alcohols	n-Hexanol	C_6	124.9	21.0
	n-Heptanol	C_7	141.4	20.5
	n-Octanol	C_8	157.7	20.6

The table shows that as the chain length of n-paraffins increases, the solubility parameter increases. This is due to greater forces of attraction between larger molecules because of more molecular contacts. The surface area of molecules is the major factor that affects the degree of induced temporary polarity. Large molecules are found to have a greater number of temporary dipoles and as a result have greater intermolecular attractions (46).

It is also apparent that cyclic-paraffins and aromatics have noticeably higher values than n- and iso-paraffins. Furthermore iso-paraffins have lower solubility parameters than n-paraffins.

The aromatics have greater solubility parameters because of the charge distribution around aromatic rings. Aromatic rings typically have a δ^+ on the hydrogens and a δ^- at the centre of the rings. This leads to dipole-dipole interactions. In the table the alcohols show the highest solubility parameters because of the possibility of hydrogen bonding. This has the effect of increasing the enthalpy of vaporisation which exceeds the relative increase in boiling point.

2.5.1.2. Hildebrand Solubility Parameters for Solvent Mixtures

The Hildebrand solubility parameter for a mixture of two or more solvents can be estimated by averaging the Hildebrand values of the individual solvent by volume, (Equation 2.2). Using this principle, the behaviour of jet fuel surrogates based on seal swell can be predicted (46).

$$\delta_{blend} = \sum \phi_i \delta_i \qquad (2.2)$$

where:

ϕ_i = volume fraction

δ_i = solubility parameter of component

As the Hildebrand values rely mostly on the total attraction between molecules and do not distinguish between the different forces present, certain inconsistencies may arise. This can be observed in Figure 2.12 which shows the degree of swelling of a dry linseed oil film exposed to a number of solvents. The general observation seen is that as the solubility parameter of the solvent approaches that of the polymer the degree of swelling increases. The degree of swelling, however, for methyl ethyl ketone and acetone does not follow this behaviour (48).

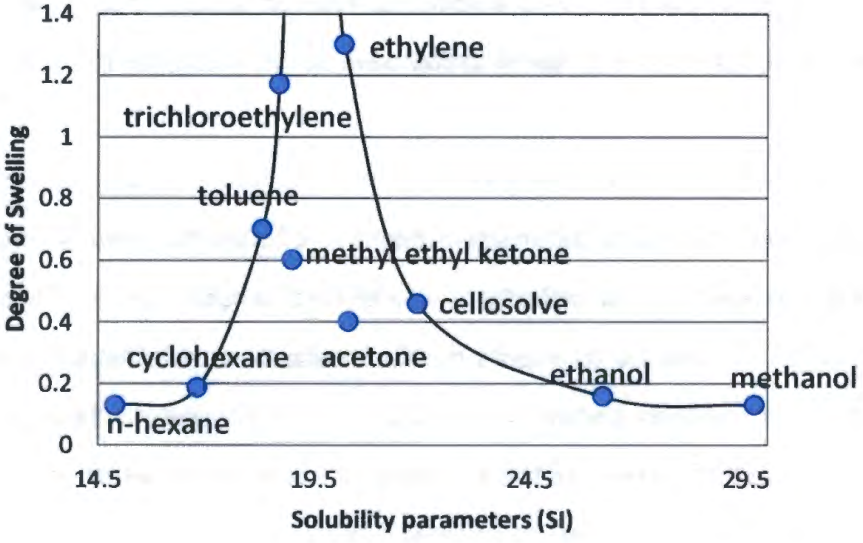

Figure 2.12: Degree of swelling of a linseed oil film for a number of solvents (adapted from Feller *et al.* (48))

The inconsistency may be explained by noting that the total cohesive energy is a sum of a number of different forces. In order to address these issues, the types of polar contributors must be differentiated into the various components: dispersion forces, polar forces and hydrogen bonding forces. This separation of intermolecular forces is taken into account using Hansen solubility parameters.

2.5.1.3. Hansen Solubility Parameters

Hansen solubility parameters are an extension of the Hildebrand solubility parameter concept. Here the solubility parameter is split into three components: that due to dispersion, polar and hydrogen bonding interactions as seen in Equation 2.3 (45).

$$\delta^2 = \delta^2_d + \delta^2_p + \delta^2_h \quad (2.3)$$

where:

δ^2_d = dispersion component

δ^2_p = polar component

δ^2_h = hydrogen bonding component

The observed dispersion forces in aliphatic hydrocarbons are a result of induced polarity fluctuations around the molecular surface caused by the proximity of other molecules. These induced attractions caused by changes in the molecules polarity are known as London dispersion forces (46).

The cohesive energy due to the interaction between permanent dipoles is termed the polar solubility parameter. The dipole moment of these molecules is the primary parameter used to calculate these interactions (47). The final cohesive energy contributor is the hydrogen bonding component. This term not only includes the hydrogen bonding interaction between molecules, but also any residual interactions that contribute to the total cohesive energy that are not accounted for by the dispersion and polar components (47).

Table 2.6 shows Hansen solubility parameters for NBR as well as the determined values for the co-polymer based on 30% poly(acrylonitrile) which is typically used for fuel exposed O-rings (49). Table 2.7 shows Hansen solubility parameters for a synthetic jet fuel (S-5), petroleum-derived fuel (JP-5), n-octane, iso-octane, toluene and benzyl alcohol.

Table 2.6: Hansen solubility parameters for nitrile rubber and its components (49)

Polymer	Solubility parameter $((MPa)^{1/2})$			
	δ_{total}	δ_d	δ_p	δ_h
Poly(acrylonitrile)	25.3	18.2	16.2	6.8
Poly(butadiene)	18.0	17.0	0.0	1.0
Nitrile rubber (30% acrylonitrile)	18.3	17.4	4.9	2.7

The solubility parameters shown in Table 2.7 may be used to predict which solvent would potentially show the greatest interaction with a specific polymer. Comparing the data in Table 2.7 with the values for NBR in Table 2.6, it is expected that toluene and benzyl alcohol would show a stronger interaction and lead to a high degree of swell. The table further shows how solvents such as n-octane only have a dispersion component in contrast to the benzyl alcohol which shows strong hydrogen bonding and polar interactions.

Table 2.7: Hansen solubility parameters for selected fuels

Solvents		Solubility parameter $((MPa)^{1/2})$			
		δ_{total}	δ_d	δ_p	δ_h
S-5*	(Synthetically derived)	16.0	16.0	0.0	0.0
JP-5*	(Petroleum-derived)	16.5	16.5	0.2	0.5
n-Octane**		15.5	15.5	0.0	0.0
iso-Octane#		14.1	14.1	0.0	0.0
Toluene**		18.2	18.0	1.4	2.0
Benzyl alcohol**		23.8	18.4	6.3	13.7

* Ref (49) ** Ref (47) # Ref (50)

2.5.1.4. Uncertainties Associated with Solubility Parameters

The total values obtained using either the Hildebrand or Hansen solubility parameters are expected to be equal. Differences do, however, occur. These are the result of experimental difficulties in determining heats of vaporisation, particularly for substances with high boiling points. Additionally uncertainties in determining both the polar and hydrogen bonding solubility parameters arise.

Hansen and Skaarup derived an equation to determine the polar solubility parameter. This equation requires the use of molar volume, the dipole moment, the refractive index, and the dielectric constant (51) (47). These values, however, are not available for many compounds. Thus estimations of these values were required which may lead to inaccurate values. The hydrogen bonding parameter is frequently determined by subtracting the polar and dispersion parameters from the total energy of vaporisation.

This method is reasonable should accurate and reliable data be available for the latent heat and the dipole moment.

Should this data not be available, group contributions are used which may result in some error (47). The most widely used method for estimating group contributions of δ_d, δ_p and δ_h is that presented by Hansen himself (52) .

Since solubility parameters best describe the interactions of pure molecules, uncertainties rise when considering mixtures of solvents and co-polymers. For example volume additivity rules are used to estimate the Hansen solubility parameters for the NBR co-polymer (45) (49).

The solubility parameter concept generally aids in determining the degree of swell. There are, however, exceptions to the rule that have to be further investigated. Factors such as molecular volume and molecular shape may further affect the swell (3) (14). The use of the Flory-Rehner theory helps in understanding some of these effects.

2.5.2. Flory-Rehner Theory

Flory and Rehner developed a theory for the extent of swell at equilibrium for a crosslinked polymer exposed to solvents (53) (54). Their theory accounts for the ability of elastomers to absorb large amounts of solvent without dissolving and their being able to deform extensively with correspondingly small stresses (55).

The hypothesis is based on the free energy change of swelling consisting of the free energy of mixing and the free energy of elastic deformation (55).

$$\Delta G = \Delta G_m + \Delta G_{el} \qquad (2.4)$$

where:

ΔG_m = free energy of mixing

ΔG_{el} = free energy change due to elastic deformation

Swelling increases the entropy which results in a decrease in free energy. The enthalpy of mixing slightly offsets this effect since for most mixing processes this is endothermic.

The enthalpy for swelling is represented by Equation 2.5 (33). The smaller this value the greater the degree of swell.

$$\Delta H_m = n_1 RT\chi\phi_p\phi_s \tag{2.5}$$

where:

n_1	=	number of moles of solvent
R	=	molar gas constant
T	=	temperature in kelvin
χ	=	polymer-solvent interaction parameter
ϕ_p	=	volume fraction of the polymer
ϕ_s	=	volume fraction of the solvent

This can then be used to arrive at a relationship between the crosslink density of the polymer and the degree of swelling.

$$\text{Crosslink density} = \frac{\rho_r}{2M_c} = \frac{-\left[\ln(1-\phi)+\phi+\chi\phi^2\right]}{2V_s\left(A\phi^{1/3}-B\phi\right)} \tag{2.6}$$

where:

ρ_r	=	density of rubber
M_c	=	the average molar mass of polymer segments between crosslink
ϕ	=	volume fraction of rubber at equilibrium
χ	=	polymer-solvent interaction
V_s	=	molar volume of solvent
A	=	theoretical constant
B	=	theoretical constant

The theoretical constants "A" and "B" are dependent on treatment of the free energy of expansion. The most widely used values for constants "A" and "B" are 1 and 0.5 respectively (56).

The Flory-Rehner equation uses the polymer-solvent interaction parameter, χ, which is determined with the use of the solubility parameters. In newer theories, χ has been replaced by the χ_{12} parameter.

The calculation of the χ_{12} parameter is as follows (47).

$$\chi_{12} = \beta + \frac{V}{RT}(\delta_1 - \delta_2)^2 \qquad (2.7)$$

where:

β	=	entropic contribution to the interaction parameter
V	=	molar volume of solvent
R	=	molar gas constant
T	=	temperature in kelvin
δ_1	=	solubility parameter of solvent
δ_2	=	solubility parameter of polymer

The equation shows that when the solubility parameters of the polymer and solvent are similar the polymer-solvent interaction parameter will be minimised. Equation 2.6 predicts increased swell under these conditions.

Hansen accounts for the empirical β term by replacing χ_{12}.

$$\chi_{12} = \frac{VA_{12}}{RT} \qquad (2.8)$$

A_{12} is given by

$$A_{12} = [(\delta_{d2} - \delta_{d1})^2 + 0.25(\delta_{p2} - \delta_{p1})^2 + 0.25(\delta_{h2} - \delta_{h1})^2] \quad (2.9)$$

Note, however, that the 0.25 in A_{12} is still an empirical constant.

2.5.3. The Effect of Molar Volume and Shape of Solvent on Swelling

It should be further understood that molecules with smaller molar volumes will pack more closely when absorbed into a polymer, resulting in a greater molecular uptake of the solvent. Molar volume is defined as the volume of one mole of a substance. Not only does this affect the solubility parameters (Equation 2.1) and indirectly influences swell but it also does so directly (Equation 2.6)

Since the size and shape of a penetrant influence how easily a molecule may enter a polymeric matrix and thus pry chains apart, it can be understood that as molar volume decreases it is observed that seal swell increases (14). Figure 2.13 shows how the Flory-Rehner equation predicts that as molar volume decreases swelling increases.

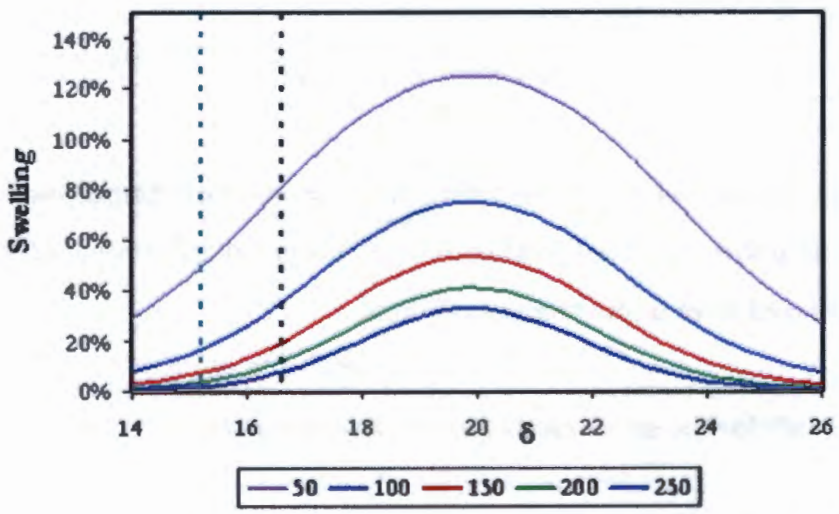

Figure 2.13: Predicted Molar volume effects on volume swell of NBR at 25°C (reproduced from Visram (17)). The values in the legend are molar volumes in cm^3/g.

2.5.4. The Effect of Crosslink Density on Swelling

Crosslinking of polymer chains restricts the extensibility of a polymer. Therefore an increased crosslink density results in a reduction of seal swell (43).

The crosslink density may be controlled by varying the temperature of production or the amount and type of vulcanising agents. In service, however, if a component is subjected to high temperature for extended periods of time additional crosslinking may occur. This may result in the hardening of the component which may lead to O-ring failure.

Figure 2.14 shows the effect of increasing the crosslink density on the swelling of hydrogenated nitrile rubber (HNBR) immersed in toluene. The increase in crosslinking can be seen to decrease the percentage mass uptake with time (57).

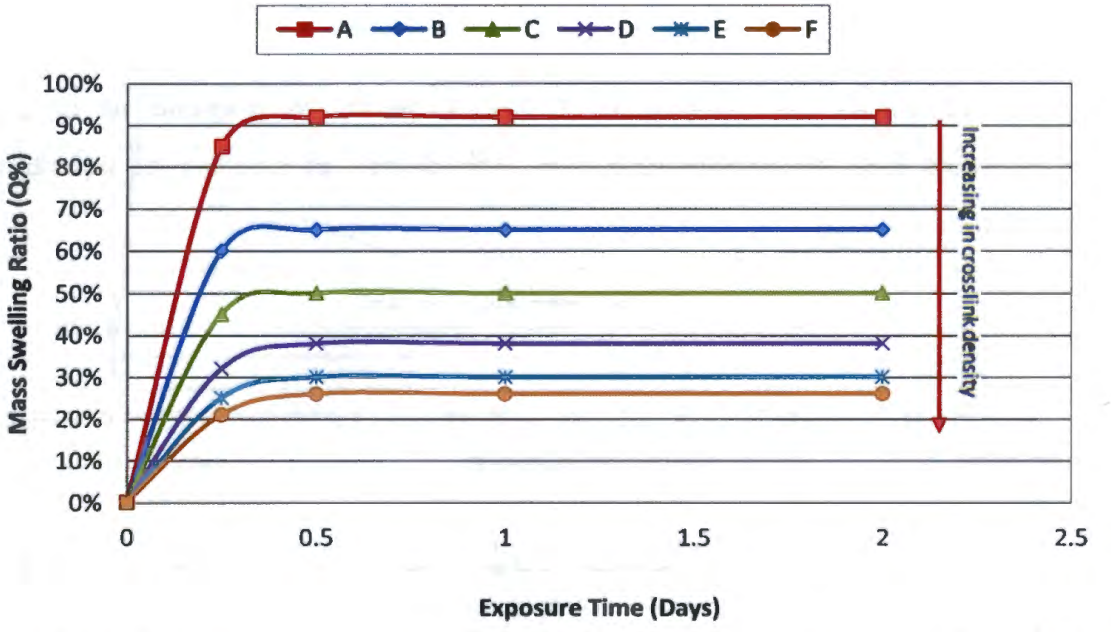

Figure 2.14: Percentage mass uptake as crosslink density is increased, for a HNBR immersed in toluene (adapted from Campion *et al.* (57))

2.5.5. Effect of Temperature on Swelling

Temperature also has an effect on seal swell. Due to the viscoelastic behaviour of rubbers, an increase in temperature will increase the mobility of the polymeric chains. This may result in softening and an increase in the rate of seal swell (43). The

temperature further affects the sorption coefficient of the solvent into the polymer as seen in Equation 2.8, which shows the Van't Hoff equation relating equilibrium constants for sorption processes to temperature (58). Because mixing is usually endothermic, it is expected that as temperature increases the sorption coefficient will increase leading to more swell.

$$\ln K_S = \frac{\Delta S}{R} - \frac{\Delta H}{RT} \qquad (2.10)$$

where:

ΔS	=	entropy of sorption
R	=	molar gas constant
ΔH	=	enthalpy of sorption
T	=	temperature in kelvin

Figure 2.15 shows the swelling of NBR/EVA blends in p-xylene at different temperatures (58). As temperature rises, the degree of swelling at equilibrium increases.

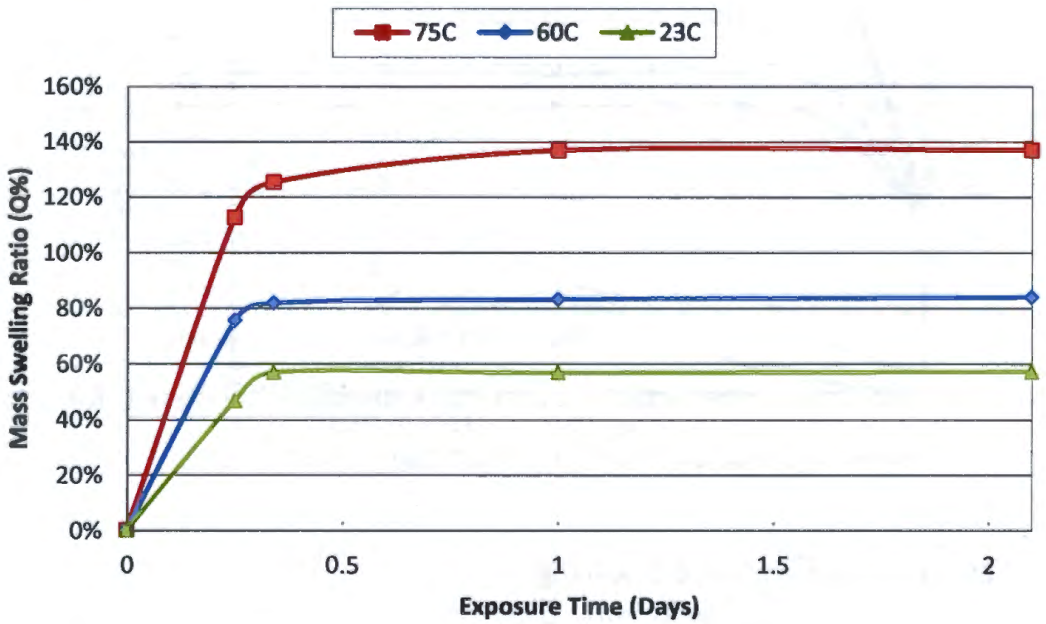

Figure 2.15: Effect of temperature on sorption of p-xylene into NBR/EVA blends (adapted from Joseph *et al.* (58))

2.5.6. Effect of Plasticisers on Seal Swell

Plasticisers have the effect of increasing segmental mobility, which results in an increase in solvent transport (42). Plasticisers, however, may also leach out of the polymer which may result in a decrease in the percentage mass uptake. Figure 2.16 shows how the presence of plasticisers in nylon 11 exposed to methanol affects the percentage mass uptake with time (57). The deplasticised sample shows a far greater nett percentage mass uptake compared to the plasticised sample. This is due to the extraction of plasticisers from the polymer, counteracting the increase in mass because of solvent uptake.

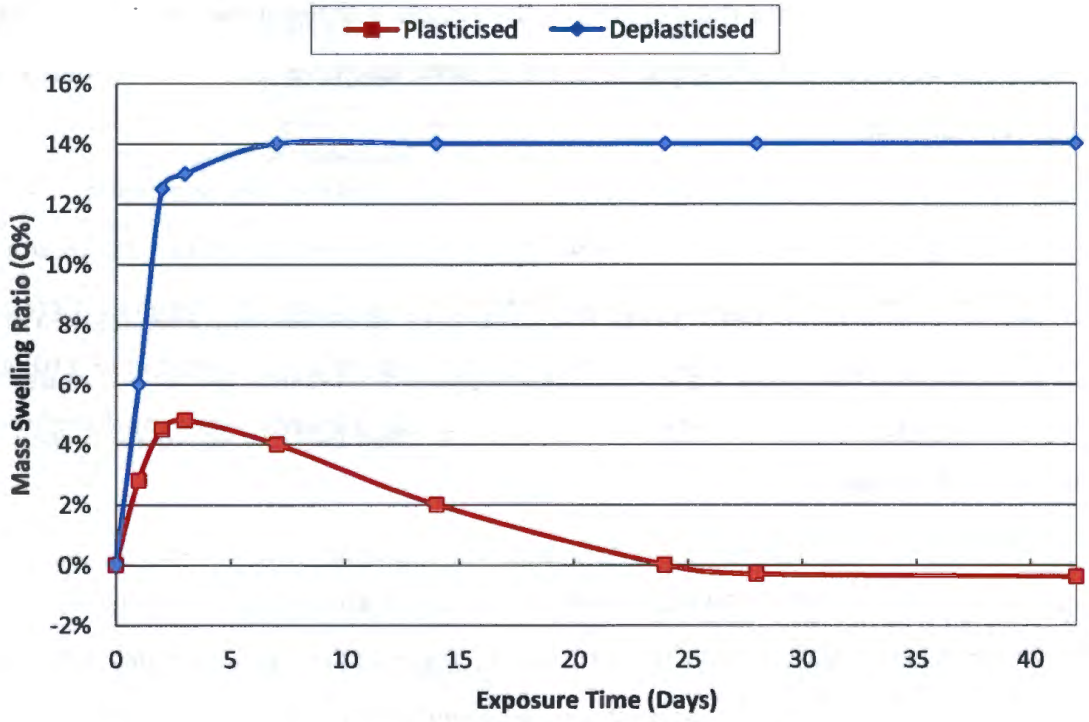

Figure 2.16: Effects of plasticisers on the swelling of Nylon 11 exposed to methanol (adapted from Campion *et al.* (57))

The presence of plasticisers results in the mass swelling ratio observed to be a consequence of two processes: the extraction of plasticisers from the sample and the absorption of solvent (57) . The driving force behind plasticiser extraction is the concentration gradient of plasticiser between the polymer and the surrounding solution. The extraction rate is dependent on temperature, the chemical nature of the plasticiser and plasticiser concentration. It has been found that in most instances the

interfacial mass transport of the plasticiser to the external solvent is the rate controlling step rather than the diffusion of the plasticiser in the polymeric matrix to the surface (59).

2.6. Previous Investigations into the Effect of Blending Low Level Components into SPK on Seal Swell

A number of previous studies have been performed on the effect of SPK:aromatic blends on seal swell. Many of the reported studies, however, do not indicate experimental parameters such as samples size, temperature, conditioning procedure and the sample to solvent ratio, replicating the results is challenging. This makes direct comparison between experiments, where the same low level blend components are used, very difficult.

Most swelling studies have been carried out on "as received" samples. This results in having to take the rate of plasticiser extraction into account and requires a greater time for the experiments to reach equilibrium. Work done by Corporan *et al.* (10) and Graham *et al.* (2) are of the few studies where experiments were performed on deplasticised samples.

The specifications for SSJF and FSJF require a minimum aromatic content by volume of 8% (29). It is uncertain whether this represents the true limit of aromatics needed to produce adequate behaviour. As cost and environmental aspects are affected by the addition of blending components, this needs to be further investigated (3). Blends of various aromatic compounds in synthetic fuels have in previous studies caused different degrees of seal swell. Therefore, it is expected that when aromatic compounds are added to meet the minimum 8% level, this would result in varying degrees on swell, depending on the aromatic used (3) (17).

Muzzell *et al.* observed different mass swell changes when N0674-70 coupons and N0674-70 O-rings where treated with a number of fuels (34) (see Table 2.8). What was observed is that far less fuel was taken up by a synthetic fuel (S-5) than petroleum-derived JP-5. The addition of an aromatic solvent which contained $C_9 - C_{11}$

hydrocarbons was seen to increase swell. The degree of swell lay midway between the SPK and the JP-5 because only 10% aromatic solvent was added. Petroleum-derived jet fuels have aromatic contents closer to 20% (5).

Table 2.8: Average mass change after 43 days at 40°C for N0674-70 NBR coupons and N0674-70 O-rings exposed to a number of fuels (34)

Fuel	Mass Swelling Ratio (Q%)	
	N0674-70 Coupons	N674-70 O-rings
S-5	0.97 ± 0.1	-0.28 ± 0.1
S-5 + 10%A150	3.71 ± 0.1	0.55 ± 0.1
JP-5	5.80 ± 0.1	1.20 ± 0.1
ECD-1	5.72 ± 0.1	1.25 ± 0.1

S-5	synthetic GTL kerosene from Syntroleum Corporation
A150	mixture of $C_9 - C_{11}$ hydrocarbons with >99% aromatics
JP-5	petroleum-derived US Navy jet fuel (28)
ECD-1	ultra-low sulfur diesel

It is unclear why Muzzell *et al.* (34) observed lower swell for O-rings than coupons although the rubber compounds were the same. It is possible the coupons were thick and so not all plasticizer had been leached out.

Thus investigations into blending components using a number of aromatics and oxygenates have been performed (17) (19). Research has further shown that oxygenated compounds, such as benzyl alcohol added in concentration of only 0.5% can produce similar swell to that of petroleum-derived jet fuel at 23°C (17). This result is significant as it shows that depending on the additive used in the fuel blend, significantly different properties can be obtained.

Link *et al.* investigated the swelling effects on a number of synthetic fuel blends. Nitrile rubber O-rings were used in this study. They followed the ASTM D1414 (15) and D471 (16) methods for obtaining volume swell data. The results for the various blends are shown in Table 2.9.

Table 2.9: Swelling of NBR O-rings in S-5 blended with a number of additives (27)

Additive	Blending level (%)	Volume swell after 48 h (%)
Conventional jet fuel (JP-5)	-	16.2±1.0
Hydrocarbons		
Cycloparaffins		
Decalin	1	0.8±0.1
Aromatics		
Tetralin	1	0.9±0.1
Naphthalene	1	1.2±0.5
Oxygenates		
n-Paraffinic alcohols		
1-Octanol		2.5±0.3
Aromatics		
Phenol	1	15.4±1.0
2,4-Dimethylphenol	1	12.8±0.4
2-Ethylphenol	1	13.5±0.5
2-Proplyphenol	1	12.0±0.2
Benzyl alcohol	1	17.5±0.4
Benzyl alcohol	0.75	13.0±0.0
Benzyl alcohol	0.5	6.8 ±0.1
1-Naphthol	0.2	3.3 ±0.1

They concluded that it was possible to match the degree of swell of nitrile O-rings swollen in petroleum-derived jet fuel with synthetic fuels blended with certain additives. The additives which showed the most promise were aromatic hydroxy compounds such as the phenols, naphthols and benzyl alcohol (27).

Link *et al.* (27) felt that an ideal fuel additive should produce similar swell as conventional petroleum-derived fuels, be effective at low concentration, not introduce significant environmental or toxicity hazards and not alter fuel properties adversely (27). The results in the table were compared to the swelling values obtained for conventional jet fuel (JP-5) and synthetic jet fuel (S-5) which were 16.2 ± 1.0 and

0.7±0.2 respectively (27). These results should be viewed with caution, however, as it is uncertain whether equilibrium had been reached.

Graham *et al.* (2) compared the swelling of "as received" and deplasticised samples exposed to Jet A and SPK. They study also looked at 8% blends of 10 hydrocarbon aromatics with SPK. This study extended beyond NBR to include fluorosilicone and fluorocarbon O-rings and sealant materials such as polythioethers and polysulfides. While fluorosilicone was shown to have some response to aromatic types, NBR was much more sensitive to fuel changes. Fluorocarbon O-rings were effectively inert. Experiments with NBR were performed on new as well as deplasticised O-rings.

The use of deplasticised samples allow for more realistic in service conditions to be simulated as well as reducing time of samples to reach equilibrium. Graham *et al.* extracted the plasticiser from the "as received" O-ring samples by soaking them in acetone for 24 hours, then rinsing them with fresh acetone and repeating this step 3 more times. Following the plasticiser extraction the samples were air dried for 24 hours followed by drying in a convection oven at 60°C for 1 hour (2).

As general rule it was found that the extent of swell increased with decreasing molar volume and increasing δ_p and δ_h. Of these parameters they felt that molar volume had the least influence and δ_h the most. Graham *et al.* (2) made measurements after only 40h. It is clear that in many experiments, equilibrium had not been reached even though they used small O-rings (2mm X 2mm). Nevertheless, these authors felt that this time was still sufficient to allow discrimination between fuels.

Most recently the effect of blends of toluene and naphthalene in GTL kerosene has been assessed by Anderson (3). Anderson investigated the swelling interaction by monitoring stress relaxation of "as received" nitrile O-rings at 30°C for 5 days. He compared swelling data of blends of GTL SPK and aromatics with stress relaxation data with that for samples exposed to Jet A-1. It was shown that as the aromatic content in the fuel is increased the percentage stress relaxation decreases. The study raised questions about the minimum aromatic specification as blends of GTL SPK + 8%

toluene did not appear to have as great an effect on the stress relaxation behaviour as naphthalene (3).

Anderson concluded that care needs to be taken when adding aromatics to the minimum aromatic specification. Further this study showed that the strength of the interaction between the polymer and the solvent plays a significant role and may be more important that molar volume effects (3).

CHAPTER 3

3. EXPERIMENTAL PROCEDURES

3.1. Materials Used

The nitrile rubber (NBR) O-rings, used in this study, were supplied by Bearing Man Ltd (Johannesburg, South Africa). These had an inside diameter of 20mm, a 2.5mm cross-sectional diameter and a Shore-A hardness of approximately 70. Later dilatometric measurements were performed on smaller O-rings of inside diameter 4.2mm and cross-sectional diameter 1.9mm and Shore-A hardness 70. These were also supplied by Bearing Man Ltd. The decision to use NBR O-rings in this study was made because NBR components show the greatest swelling sensitivity to the aromatic content in fuels when compared to other polymers typically found in aviation seals (2) (10). The response, therefore, of NBR components to solvents would thus be the extreme case.

Investigations into the behaviour of polymeric seals were conducted on "as received" O-rings, and conditioned, *i.e.* deplasticised samples. The conditioning process is described in a section that follows.

Commercially available fuels and fuel components used in this investigation included petroleum-derived jet fuel (Jet A-1) from the Natref refinery, and CTL SPK and GTL SPK from Sasol.

Table 3.1 indicates pure solvents used in this study as well as their purity, their solubility parameters and their molar volume. These were supplied by Sigma-Aldrich (St Louis, USA) unless stated otherwise. Other suppliers were Merck (Darmstadt, Germany) and Kimix (Cape Town, South Africa).

Unless specified otherwise, the use of SPK in the rest of the document will refer to CTL SPK.

Table 3.1: Solvents used in study with indication of grade, solubility parameter and molar volume (47)

Chemical class	Solvent	Purity	Solubility parameters ($(MPa)^{1/2}$)				Molar volume at 20°C $ (cm^3mol^{-1})
			δ_d	δ_p	δ_h	δ_{Total}	
Hydrocarbons							
Normal	n-Hexane	(96%)	14.9	0.0	0.0	14.9	131.6
	n-Octane*	(99%)	15.5	0.0	0.0	15.5	162.5
	n-Dodecane*	(99%)	16.0	0.0	0.0	16.0	227.1
	n-Tetradecane*	(99%)	16.2	0.0	0.0	16.3	260.4
Branched	iso-Octane	(98%)	14.1	0.0	0.0	14.1	166.1
	Iso-Dodecane	***	14.7#	0.0#	0.0#	14.7#	228.3
Cyclic	Cyclohexane	(99%)	16.8	0.0	0.2	16.8	108.7
	Methylcyclohexane	(99%)	16.0	0.0	1.0	16.0	128.3
	1,2-Dimethylcyclohexane	(99%)	16.7#	0.0#	0#	16.7#	144.2
	Cyclooctane	(99%)	17.2#	0.0#	0#	17.2#	134.5
Aromatic	Toluene**	(98%)	18.0	1.4	2.0	18.1	106.3
	o-Xylene	(99%)	17.8	1.0	3.1	18.2	120.6
	Ethylbenzene	(99%)	17.8	0.6	1.4	17.9	122.5
	Mesitylene	(99%)	18.0	0.0	0.6	18.0	139.1
	Cumene	(99%)	18.1	1.2	1.2	18.2	139.4
	p-Cymene	(99%)	17.6#	1.2#	1.2#	17.7#	156.6
	n-Butylbenzene	(99%)	17.4	0.1	1.1	17.4	156.1
	sec-Butylbenzene	(99%)	17.9#	1.2#	1.2#	18.0#	155.5
	Tetralin	(99%)	19.6	2.0	2.9	19.9	136.3
Oxygenates							
Linear	Diethylene Glycol Monomethyl Ether (DiGME)	(99%)	16.2	7.8	12.6	22.0	118.1
Aromatic	Anisole	(99%)	17.8	4.1	6.7	19.5	108.7
	Benzyl Alcohol	(99%)	18.4	6.3	13.7	23.8	103.6
	Benzyl Methyl Ether	(99%)	17.9#	4.9#	4.3#	19.1#	128.7
	Dibenzyl Ether	(99%)	19.6	3.4	5.2	20.6	190.1
Other							
	Dichloromethane (CH_2Cl_2)**	(99%)	18.2	6.3	6.1	20.2	63.9
	Jet A-1	-	16.5#	0.1#	0.3#	16.5#	193.7#
	CTL SPK	-	15.4	0.0#	0.0#	15.4#	212.5#
	GTL SPK	-	15.7#	0.0#	0.0#	25.7#	199.0#

* Supplied by Merck ** Supplied by Kimix *** Mixture of highly branched isomers

Estimated value $ Molar volumes calculated from densities (60)

Where solubility parameters in Table 3.1 were estimated, they are estimated using group contributions in Hansen (52) . Solubility parameters of the fuels were estimated from their molecular compositions. The solubility parameters of the component molecules were first estimated using the group contributions in Hansen (52). The overall solubility parameters were found by using the volume weighted average of the individual solubility parameters.

3.2. Equipment Used

In order to determine the effect that different solvents have on NBR O-rings, a variety of exposure experiments were carried out. These allowed the differences in swelling characteristics of chemicals from different structural classes to be studied. These experiments were conducted using static exposure techniques as well as an elastomer compression rig which measures the dilation of an O-ring when exposed to solvent. A description of the experimental equipment is supplied in the following sections.

3.2.1. Mass measurements

During static exposure experiments, mass measurements were made using a Mettler Toledo AT20 analytical balance with an accuracy of ±2μg.

3.2.2. Dilatometric measurements

Volumetric measurements were calculated from the diameter and area data obtained using a Nikon ShuttlePix P-MFSC microscope with an resolution of ±1μm.

3.2.3. SAFL Elastomer Compression Rig

An elastomer compression rig was designed and built at SAFL to provide continuous dilatometric measurements of O-rings undergoing exposure treatment. The rig was specifically designed for the use of O-rings with an internal diameter of 20mm and a cross-sectional diameter of 2.5mm (17). The rig consists of six modules, allowing different solvents to be tested simultaneously. A more detailed description of the rig may be found Appendix B.

3.2.4. Thermogravimetric Analyser

A Q5000IR thermogravimetric analyser (TGA), supplied by TA Instruments (New Castle, USA), was used in this study. The TGA measures changes in weight as a function of temperature. The sample is placed on a high precision balance with an accuracy ±0.5μg in an electrically heated infrared furnace. The instrument was calibrated for mass using reference weights and for temperature using a calibrated thermometer (ambient temperature) and the Curie temperature of Ni (358°C) (61).

3.3. Experimental Methods

The procedures used to investigate swelling were based on the methods in ASTM D1414 (Standard Test Method for Rubber O-rings) (15), ASTM D471 (Standard Test Method for Rubber Property-Effect of Liquids) (16) and the study of Visram (17). Both gravimetric and dilatometric data were collected.

3.3.1. O-ring Conditioning Procedure

The conditioning of O-rings removes plasticisers and extractable curatives present in the nitrile rubber O-rings. Because this process occurs naturally in service, a greater understanding of the degree and rate of extraction was required. Furthermore, because the plasticisers have been removed before seal swell experiments, a simpler swelling process occurs allowing only solvent transport into the seals to be investigated. Using deplasticised O-rings eliminates the contribution of plasticiser extraction to any changes in seal swell.

The conditioning procedure was conducted as follows:

- 20 O-rings were placed in 800mL of CH_2Cl_2 in a 1L sealable Schott bottle.
- The O-rings were left in solution for 3 days at a constant temperature of 23°C.
- The solvent was replaced with fresh supply and samples were left for an additional 3 days.

After the extraction of plasticiser the solvent in the O-ring was removed. The samples were allowed to dry in a fumehood at ambient conditions for 1 day, followed by

vacuum extraction at 50°C for 5 days at -0.80bar. A Scientific Manufacturing CC vacuum oven was used in this study for this purpose.

3.3.2. Static Exposure Treatments

ASTM method D1414 (Standard Test Method for Rubber O-rings) (15) and D471 (Standard Test Method for Rubber Property-Effect of Liquids) (16) contain the base methods for the solution exposure experiments. Variations on these are described in the appropriate sections.

3.3.2.1. Gravimetric Method

The static gravimetric method was conducted as follows:

- The initial masses of the samples were recorded.
- The samples were then placed in the relevant solvent.
- At specified times the samples were removed from the solvent and blotted dry whereafter they were weighed.
- Finally the samples were returned to the solvent.

The containers were placed inside a closed box in order to eliminate any influence of light exposure. Although this is not specified in the ASTM methods it was, however, deemed important for the long exposure experiments conducted in this study.

The procedure was continued until the samples had reached equilibrium, *i.e.* until a change of mass was no longer observed. From the data the mass swelling ratio (Q%) was determined as a function of time.

$$Q\% = 100\frac{m_t - m_o}{m_o} \qquad (3.1)$$

where:

m_0 = mass before swelling

m_t = mass at time, t

For certain experiments the O-rings were removed from solution after equilibrium had been reached and exposed to air in a fumehood for 1 day, allowing the bulk of the remaining fuel in the polymer to evaporate. The sample was then placed in a vacuum oven at 50°C for 5 days. Final mass measurements after solvent extraction where then made to allow the extent of mass loss due to plasticiser extraction to be determined.

3.3.2.2. Optical Dilatometric Method

In ASTM D1414 volume changes may be observed using a hand micrometer of O-ring diameter according in which the cross-sectional diameter is measured at four points equally distributed around the circumference (15). It has been found that this is inaccurate; so optical microscopy was used instead (44).

A similar experimental procedure was used to that of gravimetric method. However, the change in O-ring volume was determined using an optical microscope at 40x (optical) magnification. The average diameter of the O-rings were measured from six points equally distributed around the sample by taking images of the O-rings undergoing solution treatment. Each diameter reading was determined using the circular measurement option of the ShuttlePix software. This allowed for the inside diameter (i.d.) and outside diameter (o.d.) to be measured and thus the thickness of the sample to be determined at one of the six measuring points. The circular measurement selection of the required three points can be seen in Figure 3.1 for both the inner and outer diameters.

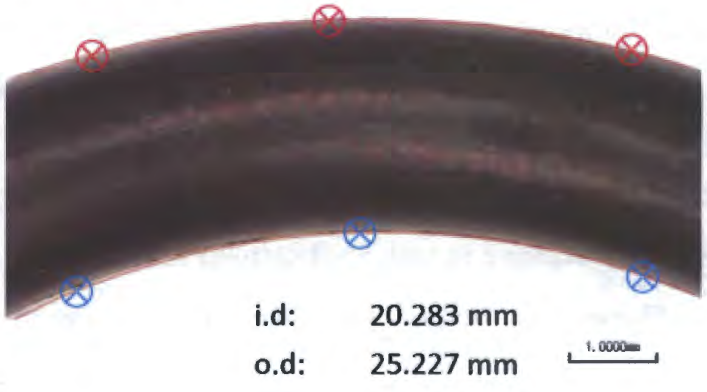

Figure 3.1: Microscope image of a magnified O-ring indicating the selection of the three points required to obtain the inner (i.d.) or outer (o.d.) diameter

Because the O-rings are not under any load, isotropic swelling may be assumed. The change in cross-sectional area can be used to determine the change in the samples volume (49). This allows for the volume swelling ratio (R%) to be calculated.

$$R\% = 100\left(\left(\frac{d_f}{d_o}\right)^3 - 1\right) \tag{3.2}$$

where:

d_o = initial cross-sectional diameter

d_f = cross-sectional diameter at time, t

Because of uncertainties introduced by the fact that volume swell is calculated from the cube of the one-dimensional expansion, a modified method was introduced in which volume swell was determined from increases in the area observed under a microscope. This is an adaptation of the method of Graham *et al* (49).

Again an optical microscope at 40x (optical) magnification was used. The average projected area of the O-rings were measured three times. During each measurement the areas within the outer diameter and the inner diameter were calculated using the ShuttlePix software. The projected area was then calculated by difference. An example of such an area be seen in Figure 3.2 .

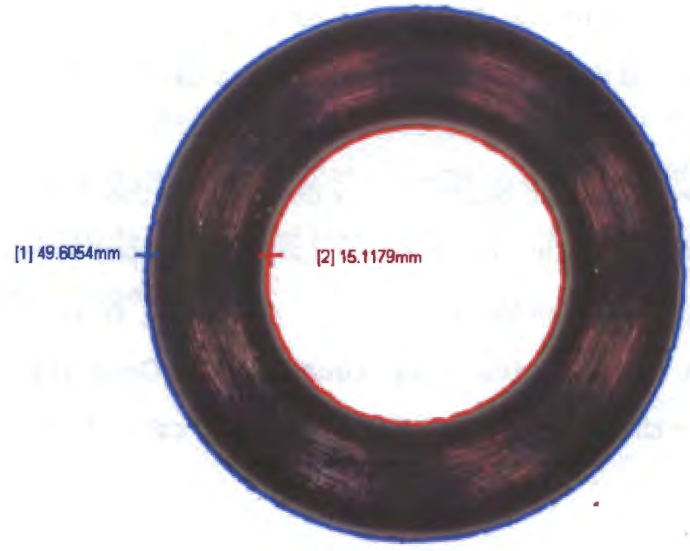

Figure 3.2: Illustration of the determination of projected area of an O-ring

Because this technique requires the entire O-ring to be within the field of view of the microscope, the smaller O-rings supplied by Bearing Man Ltd were used.

This allows for the volume swelling ratio (R%) to be calculated.

$$R\% = 100\left(\left(\frac{A_f}{A_o}\right)^{3/2} - 1\right) \tag{3.3}$$

where:

A_o = initial projected area

A_f = projected area at time, t

3.3.3. Dynamic Experiments Using the Elastomer Compression Rig

The operation of the elastomer compression rig was as follows:

- The displacement transducer and compressed air inlet were disconnected from each cylinder.
- The base on the cylinder was unscrewed and a single O-ring was placed inside the O-ring groove.
- The cylinder was then reconnected and run under compression for 24 hours to allow for the rig to settle.
- 80mL of solvent was introduced to the fuel chamber in the base of each cylinder, and the compression rig started so data could be collected.

Knowing the O-ring groove depth and by determining the difference in position (ΔX) between the position when the O-ring is fully compressed (maximum pressure) and when it was fully expanded (pressure = zero), the cross-sectional diameter of the O-ring can be calculated using Equation 3.4. Once the O-ring diameter is determined, the change in swelling ratio (R%) can be calculated using Equation 3.2.

$$\text{O-ring diameter} = g.d + \Delta X \qquad (3.4)$$

where:

g.d. = groove depth

ΔX = difference in position

3.3.4. Method Refinement

Before the effect of different chemical classes on swell could be assessed, a number of preliminary experiments were conducted in order to investigate certain experimental variables. The effects of solvent to polymer ratio, of cutting samples, of temperature and measurement technique (gravimetric *vs.* dilatometric) were initially investigated in order to minimise experimental uncertainty and to determine repeatability. The preliminary experimental procedures are discussed in the following sections and relied heavily on static gravimetric measurements.

To reduce solvent usage, it was decided to conduct static gravimetric exposure experiments on bisected samples, unless otherwise stated. The use of entire O-rings was used in the volumetric experiments in order to reduce any inaccuracies caused by distortion after bisecting the sample. Entire O-rings were used in the compression rig studies because of the nature of the rig's design.

3.3.4.1. Degree of Repeatability

The degree of repeatability was investigated by treating a number of O-ring samples under the same conditions in solvents that showed significantly different swelling. Table 3.2 shows the solvents used in this investigation along with an indication of the number of experiments undertaken.

Table 3.2: Sample number and solvents used to determine the degree of repeatability for the various experimental methods

Gravimetric measurements	Dilatometric measurements	Compression rig measurements
10 samples in Jet A-1	10 samples in Jet A-1	10 samples in Jet A-1
5 samples in toluene	5 samples in toluene	
5 samples in n-dodecane	5 samples in n-dodecane	

Repeatability of volume swell, determined from projected area measurements on smaller O-rings, was estimated using the average coefficient of variation of the volume swell of 3 samples in 28 different solutions.

3.3.4.2. Solvent to Polymer Ratio Effects

The effect of the solvent to polymer ratio was investigated by using gravimetric measurements for different volumes of Jet A-1 for each swelling experiment. Swelling was undertaken in 15mL, 20mL, 40mL and 80mL of Jet A-1 at 50°C using entire O-rings with mass and volume of approximately 0.42g ± 0.01g and 0.34 cm^3 ± 0.02cm^3 respectively. The ratios used are above and below the required volume ratio described in the ASTM D1414 and D471 methods of approximately 30mL of solvent per O-ring (15) (16). 80mL:O-ring is the ratio at which the compression rig is designed to operate (17)).

3.3.4.3. The Effect of Temperature

In order to investigate the effect of temperature, experiments were conducted at 23°C and 50°C. The experiments conducted at 23°C were done in a thermostatically controlled room, while for experiments at 50°C samples were placed inside an oven.

3.3.4.4. The Effect of Plasticiser Extraction

The effects that the presence/absence of plasticiser have on the mass swelling ratio was investigated by performing experiments on both plasticised and deplasticised O-ring samples in 20mL of solutions at 50°C.

3.3.5. Investigation into the Effect of Chemical Class and Structure

The main focus of this study was to determine the effects that various chemical classes have on the swelling of elastomeric O-rings and to determine the level of blending compounds required to produce a fungible fuel. Previous studies into this effect have been carried out using a number of techniques including gravimetric measurements, optical dilatometry and elastomer stress relaxation (3) (10) (14) (27) (43) (57). In this study, only gravimetric measurements and optical dilatometry were used to investigate changes in swelling.

The effects of various chemical classes on seal swell were studied using bisected O-rings. A delay in obtaining the microscope for optical measurements resulted in gravimetric studies being initially focused on. In these situations the changes in volume are calculated from the mass of fuel/solvent that is absorbed. The methods for calculating this may be found in Appendix D. In later experiments, both optical and gravimetric measurements were made.

Each investigation was carried out on a single section of the O-ring sealed inside Schott bottles with 20mL of solvent at 50°C. Both experiments on "as received" samples and deplasticised samples were performed. The chemical classes specifically focused on in the study were: n-, iso- and cyclic-paraffinic, aromatics compounds and oxygenates such as ethers. The compounds used are listed in Table 3.1.

3.3.5.1. Blends with SPK

Molecules such as aromatics have the effect of increasing the degree of seal swell when added to highly paraffinic fuels. These effects where investigated by making solutions of the respective blending components in SPK. All solution blends used in this study were prepared by volume according to standard laboratory practice. Typically 8% blends (v/v) in SPK were tested.

3.3.5.2. Switch-load Testing

The final experimental procedure undertaken on seal swell was an investigation into switching from petroleum-derived fuel to synthetic fuels, known as switch loading.

These experiments were done in order to represent more realistic conditions that an O-ring may face in service should the fuel chemistry be changed.

Initial switch loading experiments were run on statically treated O-ring samples by switching solvents every 7 days from Jet A-1 to SPK, and recording mass changes. This was followed by experiments on blends of SPK and low level additional components.

3.3.6. Density Determination

Because extractables are removed from new O-rings when exposed to solvent, the density of the O-rings changes, the extent of any density changes were measured. The density measured from the deplasticised samples allowed for a comparison of directly measured and calculated volumetric changes. This allows for preferential absorption in mixed solvents to be studied.

Density investigations were made using a 25 mL Marienfeld density bottle. Each O-ring was cut into four segments and then placed into the density bottle together with distilled water. Care was taken to ensure no air bubbles were present on the samples or in the density bottle.

The density of the samples was calculated as follows:

$$\rho = \frac{\rho_L m_s}{m_L - (m_t - m_b - m_s)} \tag{3.5}$$

where:

m_L = mass of liquid required to fill the bottle on its own

m_t = total mass of density bottle with sample and liquid

m_b = mass of density bottle

m_s = mass of sample

ρ_L = density of liquid used

3.3.7. Thermogravimetric Analysis

TGA experiments were carried out on "as received" and deplasticised O-ring segments of approximately 10μg by placing them in a 50μL platinum pan. The samples were subjected to heating rate of 5°C/min using normal TGA operation mode. The percentage mass change was recorded from 23°C to 650°C. High purity nitrogen gas, supplied by Air Products (Johannesburg, South Africa) was used as purge gas at a flow rate of 25mL/min. The data obtained from the TGA was analysed using TA Instrument Universal Analysis 2000 software.

CHAPTER 4

4. METHOD REFINEMENT

Previous investigations into polymer swell have been carried out using a number of different experimental procedures (2) (14) (27) (43) (57). Some of the effects investigated were the influence of temperature, solvent to polymer ratio, polymer composition, polymer thickness and the sampling method. These variables are expected to alter the observed swell; thus comparing data from the various research groups is made more challenging. In this study it was decided to look into some of these factors in more detail.

4.1. Static Solution Exposure Investigation

Figure 4.1 shows the mass swelling ratio for "as received" O-rings exposed to Jet A-1 and SPK at 50°C. This is illustrative of the effect of varying the nature of the fuel.

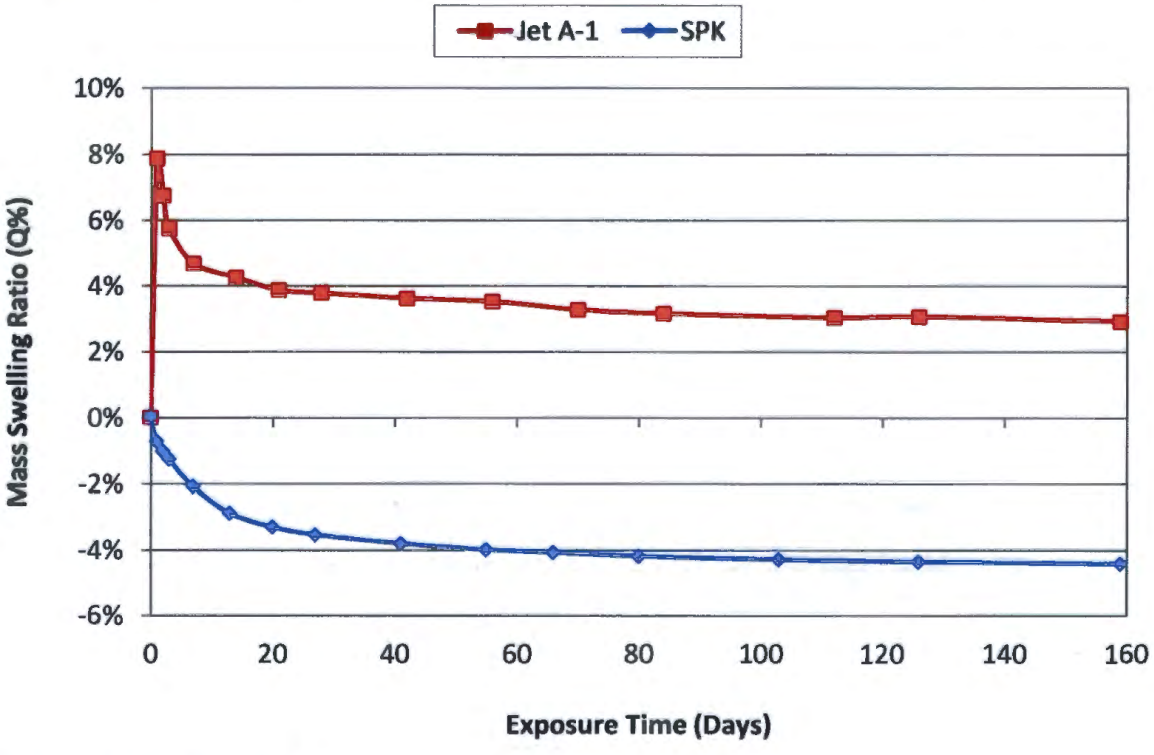

Graphs are plotted as the average of three experiments.

Figure 4.1: Comparison of "as received" O-rings exposed to Jet A-1 and SPK at 50°C

Samples swollen in Jet A-1 approach an equilibrium mass swelling ratio of approximately 3% whereas the samples exposed to SPK approach a negative mass swelling ratio of slightly below -4%.

It can thus be expected that should a petroleum-derived fuel be switched to pure synthetic paraffinic kerosene, a dramatic decrease in seal swell could result which might cause leakage.

In this study, both gravimetric (Q%) and volumetric measurements (R%) were recorded at various time intervals. Mass measurements were deemed adequate to investigate a number of the preliminary studies, such as the effects of temperature, solvent to polymer ratio, conditioning procedure and the effect of plasticiser extraction.

Certain volumetric measurements were also carried out in this section in order to determine the repeatability of such measurements and the relationship between mass and volume measurements.

4.1.1. Static Gravimetric Experiments

The static validation experiments were run as preliminary experiments in order to investigate the effects of solvent to polymer ratio, repeatability of method and the effects of temperature.

4.1.1.1. Solvent to Polymer Ratio

First, an appropriate solvent to polymer ratio had to be chosen. The data obtained from the investigation into the effects of solvent ratio can be seen in Figure 4.2. Samples were exposed to 15mL (± 50:1 by volume), 20mL (± 60:1), 40mL (± 120:1) and 80mL (±240:1) of Jet A-1. The numbers in brackets are the approximate solvent to polymer ratios. This was done in order to see whether the solvent to polymer ratio would affect the extent and rate of plasticiser extraction. Little distinction can be seen between the four graphs plotted where the ratio is greater than or less than the recommended solvent to polymer volume ratio described in the ASTM D471 method

of approximately 30mL per O-ring (16). Thus the effect of plasticiser concentration in the solution seems to have very little effect on seal swell so it was decided to continue with a ratio of 40mL solvent per O-ring.

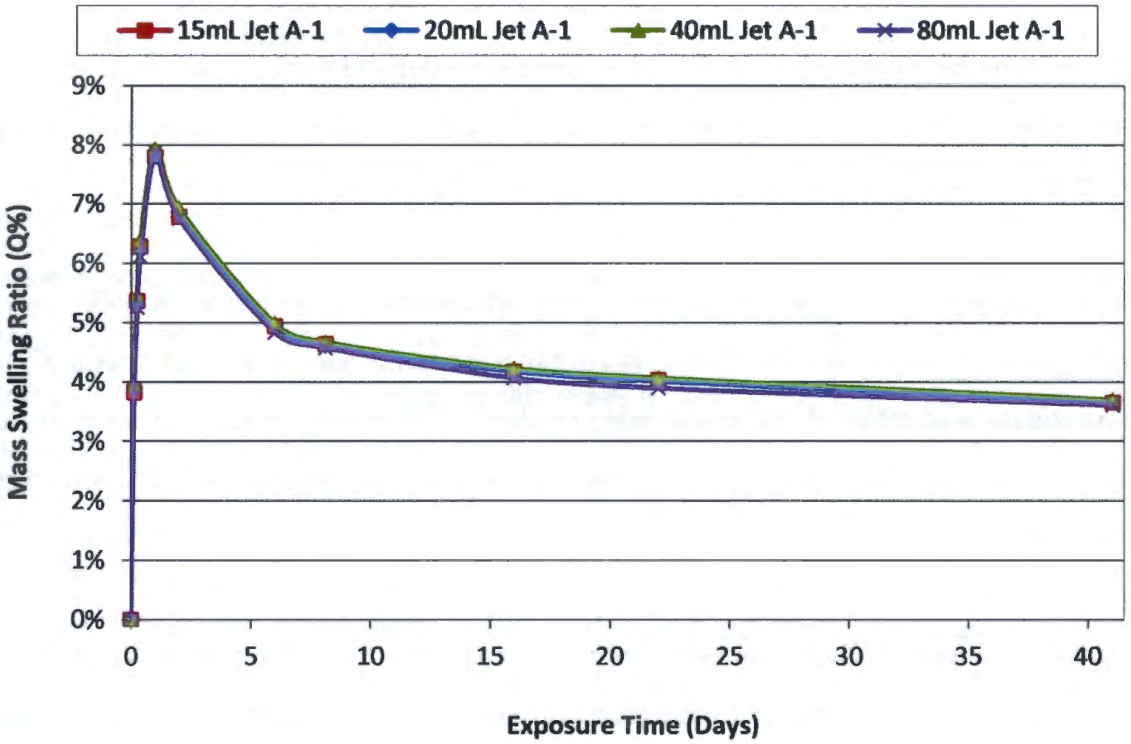

Graphs are plotted as the average of three experiments.

Figure 4.2: Solvent ratio effects on the swelling of "as received" O-rings treated in Jet A-1 at 50°C

4.1.1.2. Repeatability of Gravimetric Measurements

The level of repeatability was then assessed by exposing "as received" samples to toluene, n-dodecane and Jet A-1 at 50°C. Figures 4.3 – 4.5 illustrates the high degree of repeatability obtained.

Toluene is representative of very high swell conditions, while n-dodecane is illustrative of the repeatability of experiments in the negative mass swelling range such as might be expected for an SPK. Additionally samples were exposed to Jet A-1 to show behaviour for intermediate swelling values.

Table 4.1 summarises the data.

Table 4.1: Repeatability of mass measurements of samples exposed to various solvents across a range of solubility parameters (47)

Solvent	δ ((MPa)$^{1/2}$)	Sample size	Average swelling at 7days (%)	Coefficient of variation (%)
Toluene	18.1	5	77.5 ± 2.1	2.0
Jet A-1	16.5	10	4.5 ± 0.1	1.0
n-Dodecane	16.0	5	-2.8 ± 0.1	1.0

The uncertainty values for the average mass swelling ratio reflect the 95% confidence interval

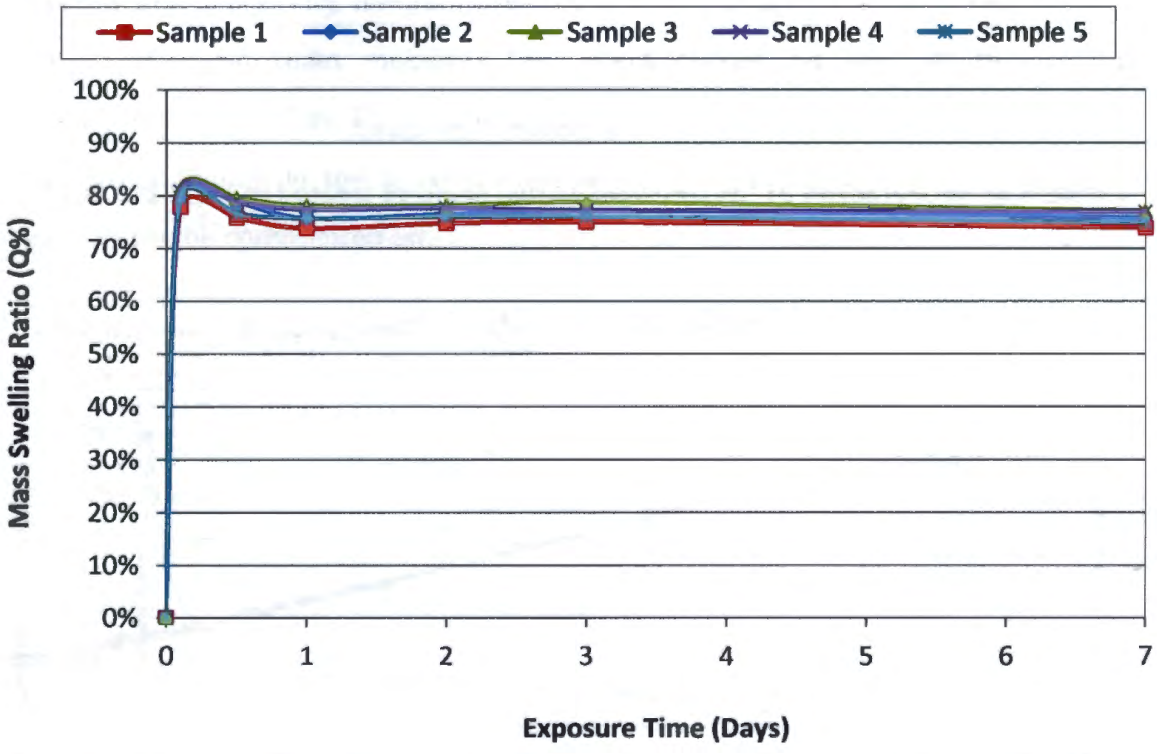

Figure 4.3: Repeatability of "as received" O-ring samples treated in toluene at 50°C

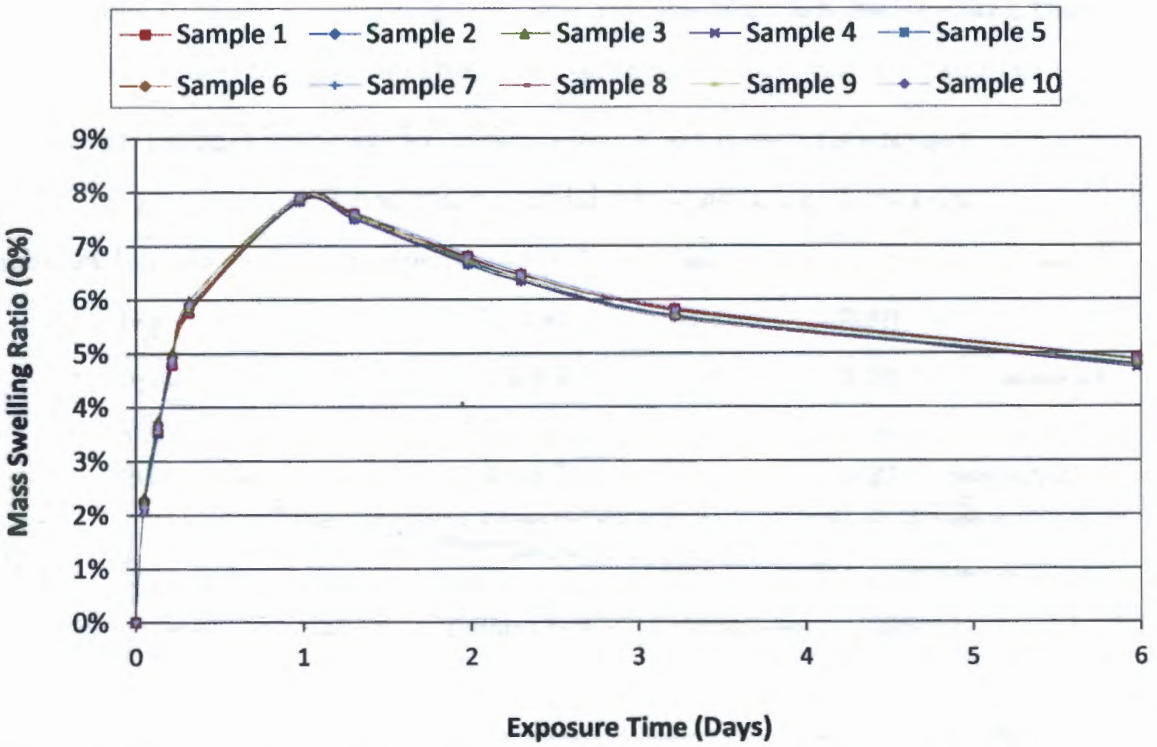

Figure 4.4: Repeatability of "as received" O-ring samples treated in Jet A-1 at 50°C

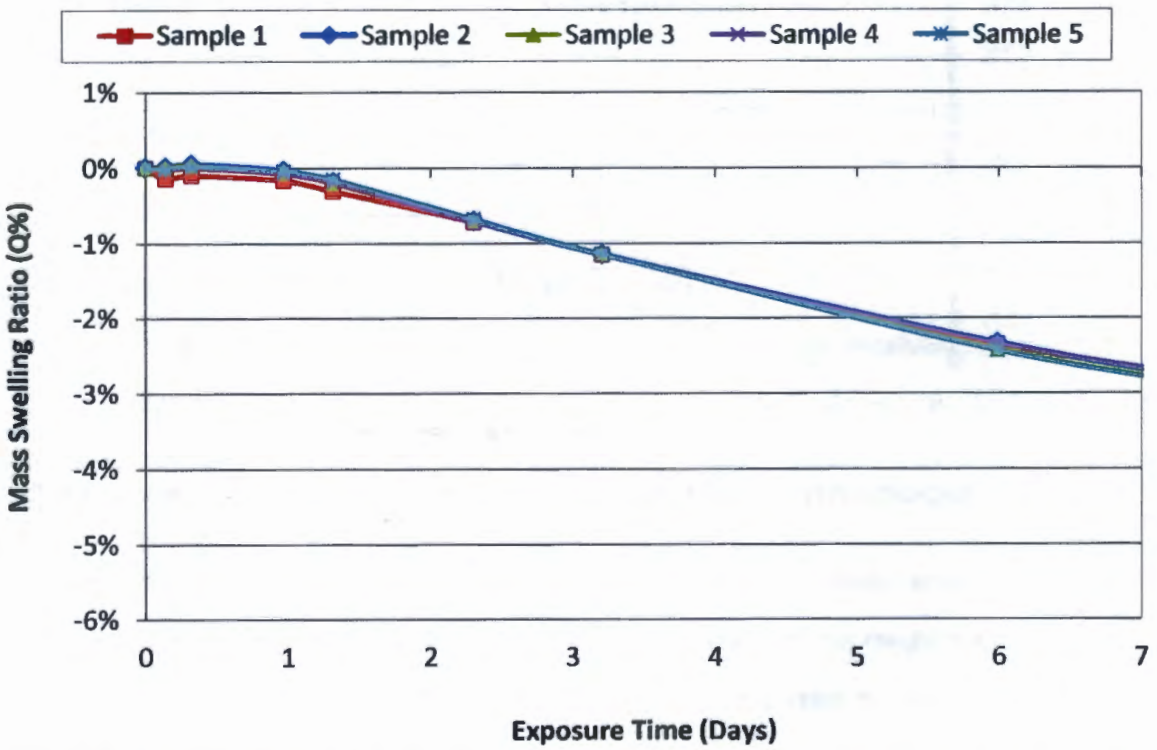

Figure 4.5: Repeatability of "as received" O-ring samples treated in n-dodecane at 50°C

4.1.1.3. The Effect of Temperature on Seal Swell

Figure 4.6 and Figure 4.7 show the effect temperature has on the swelling of "as received" samples exposed to Jet A-1 and o-xylene. o-Xylene was chosen to allow a comparison with Mostafa *et al.* (43). Jet A-1 was chosen to allow temperature effects of commercial fuels to be studied. In both experiments, the maximum and equilibrium mass swelling ratio were reached earlier in samples treated at the higher temperature due to increased molecular transport kinetics.

The effects that temperature has on the rate of molecular transport can be specifically seen when comparing the two curves in Figure 4.6. Based on the literature, (58) it was expected that increasing temperature would result in an increase in swell due to greater polymeric chain mobility. This effect cannot be seen in temperature experiments in this study. The samples exposed to Jet A-1 at 23°C appear not to have reached equilibrium in the allowed time and therefore only the rate of molecular transport can be commented on.

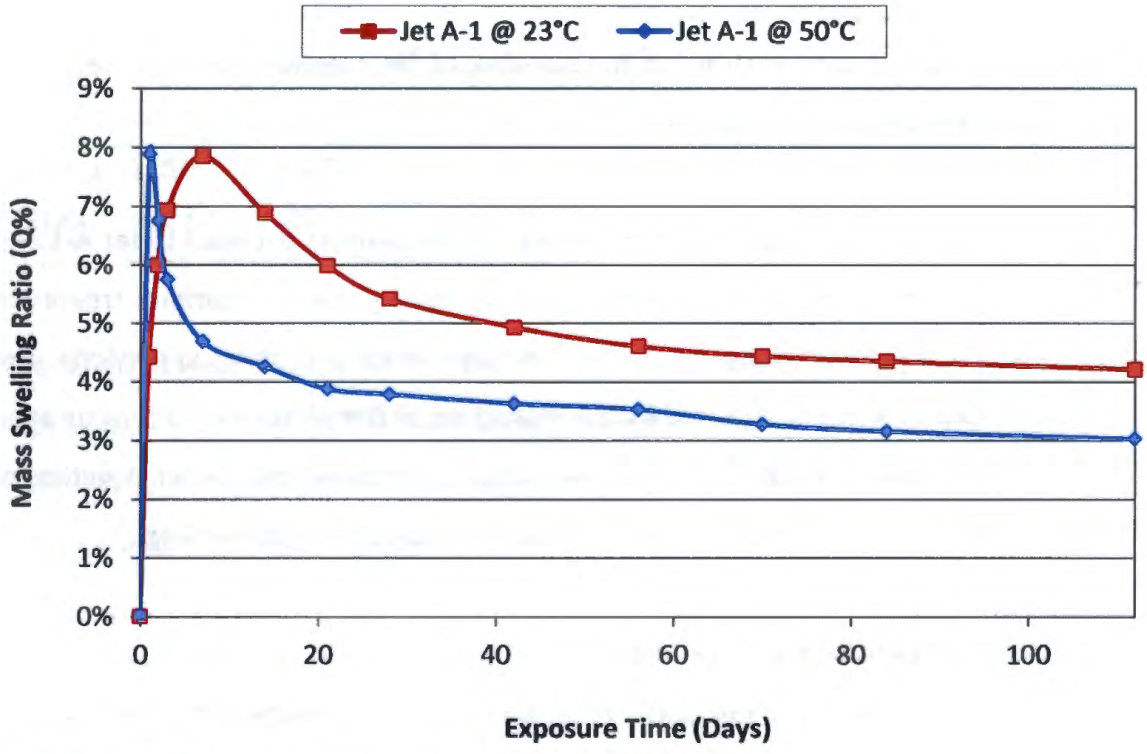

Graphs are plotted as the average of three experiments.

Figure 4.6: Effect of temperature on the swelling of "as received" O-rings treated in Jet A-1 at 23°C and 50°C

Samples exposed to o-xylene appear to have very similar equilibrium mass swelling ratios at the different temperatures.

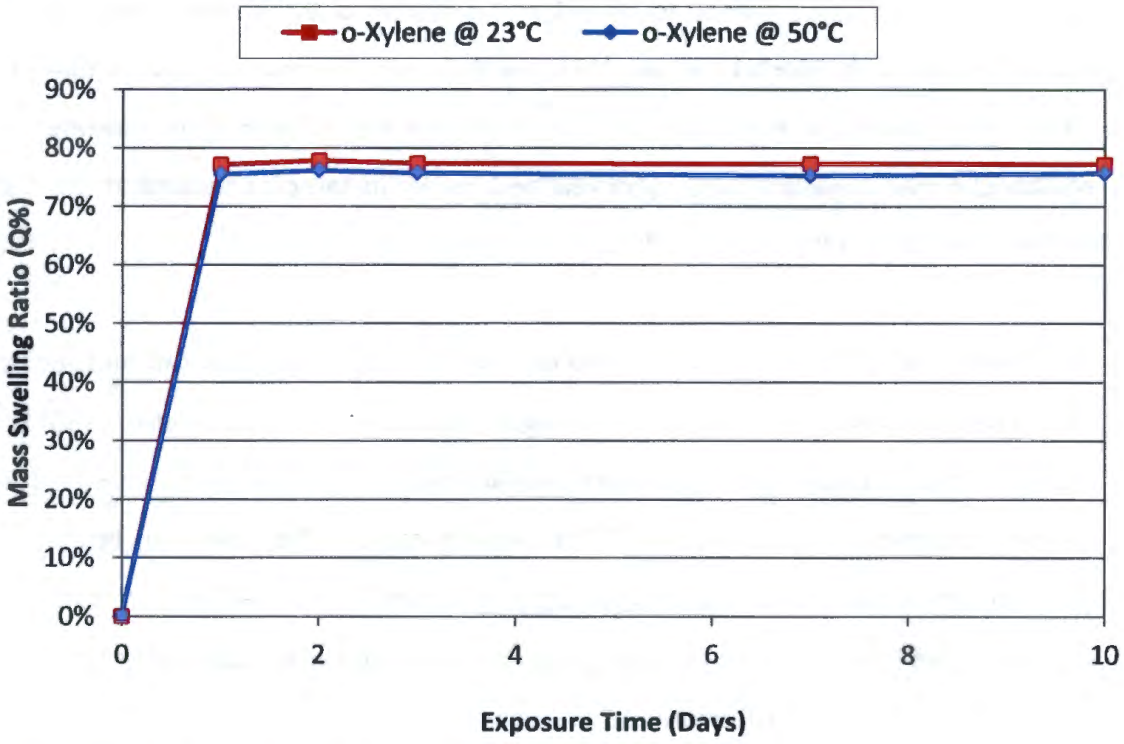

Graphs are plotted as the average of three experiments.

Figure 4.7: Effect of temperature on the swelling of "as received" O-rings treated in o-xylene at 23°C and 50°C

Importantly, the differences in the time scales for the samples exposed to Jet A-1 and o-xylene should be noted. The equilibrium mass swelling ratio for samples treated in Jet A-1 takes considerably longer to be reached compared to samples in o-xylene. The distinctive decrease in mass caused by the extraction of the plasticiser cannot be seen clearly with samples treated in o-xylene. This is because the faster kinetics of plasticizer extraction dominates, as well as the very high degree of swelling.

4.1.2. O-ring Conditioning Procedure

The negative gradient observed in the Jet A-1 exposure treatment (Figure 4.1) can be explained by the extraction of molecules such as plasticiser and extractable curatives from the O-ring. The rate at which this process takes place is related to the diffusion coefficient of these extractables which is affected by temperature, relative solubility parameter of the solvent and the molar volumes of the solvent and plasticiser.

In-service, plasticiser is likely to be rapidly lost and for a large part of an O-ring's service life there will be little plasticiser present in the O-ring. The effects that different chemical classes have on O-rings in-service can thus best be shown on deplasticised samples. The development of a conditioning process to best reproduce samples found in service was thus necessary.

In this investigation, O-rings were exposed to Jet A-1 and dichloromethane (CH_2Cl_2) to investigate plasticiser extraction. The decision to use CH_2Cl_2 was based on the expected acceleration of plasticiser extraction since CH_2Cl_2 has a similar solubility parameter to that of NBR and its extractable additives. It was found that O-rings exposed to CH_2Cl_2 displayed a far greater rate of solvent absorption and extent of swelling ratio than Jet A-1. Table 4.2 summarises the key information obtained from the respective experiments.

Table 4.2: Gravimetric measurements on "as received" O-rings swollen in Jet A-1 and CH_2Cl_2 (17)

Solvent		δ ($(MPa)^{1/2}$)	Percentage mass swell at 6 days (%)	Percentage mass swell at 14 days (%)
Jet A-1	at 50°C	16.5	4.8 (0.1)	3.8 (0.1)
CH_2Cl_2	at 23°C	20.2	232.9 (8.7)	235.5 (11.9)

The values in brackets are the standard deviations of the mean. N = 3.

The larger standard deviation for the CH_2Cl_2 measurements are because of the very high volatility of CH_2Cl_2. The data shows that after 6 days the samples exposed to CH_2Cl_2 at 23°C had reached equilibrium unlike the samples in Jet A-1 at 50°C. After 6 days, the solvent was evaporated (see section 3.3.1).

Figure 4.8 provides an indication of the amount of solvent extracted under extended vacuum. CH_2Cl_2 evaporates considerably faster than Jet A-1 under these conditions. This is because the boiling point of CH_2Cl_2 is 39.6°C while typical jet fuel has a boiling range of 160 - 260°C and thus CH_2Cl_2 is rapidly removed from the O-ring at 50°C (28) (62).

The percentage mass change after the extraction process reached equilibrium in CH_2Cl_2 was -10.0% ± 0.2%.

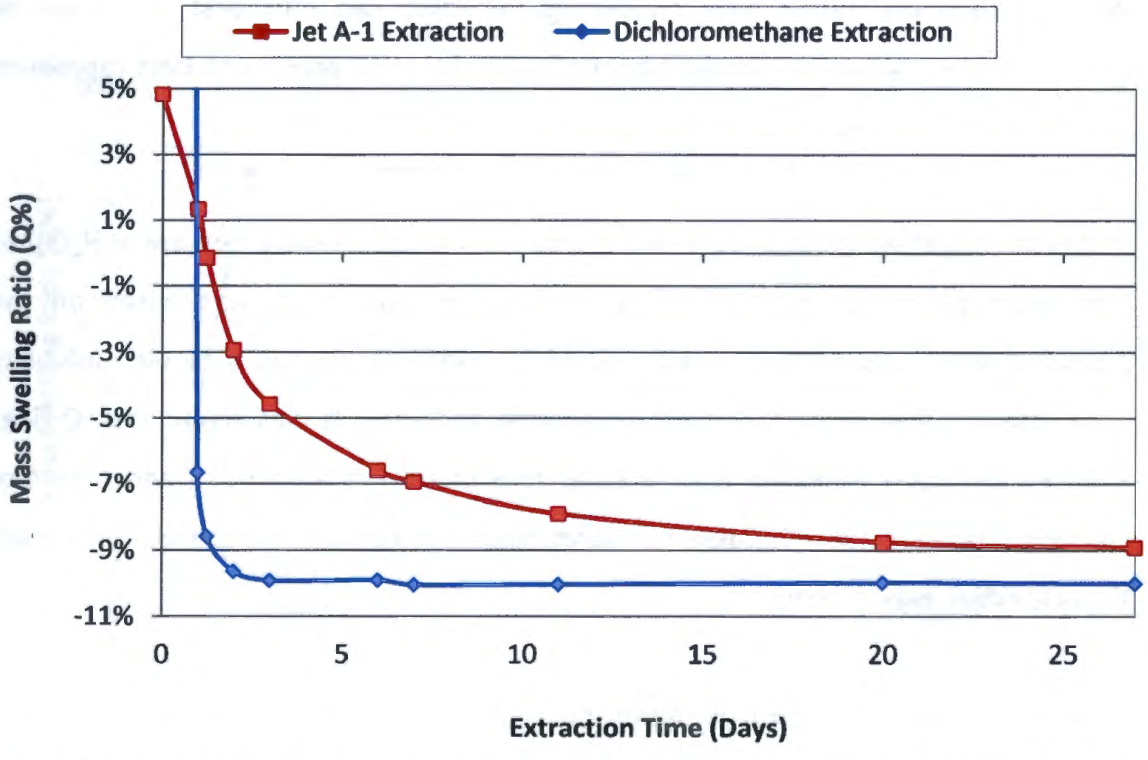

Graphs are plotted as the average of five experiments. Confidence intervals are not provided because they are hidden by the data point due to their small size. The average confidence interval was 0.2%

Figure 4.8: Extraction of Jet A-1 and CH_2Cl_2 from O-rings under vacuum

The level of extractables present in the samples was further investigated using thermal gravimetric analysis (TGA). A sample thermogram can be seen in Figure 4.9 for a 5°C/min heating rate.

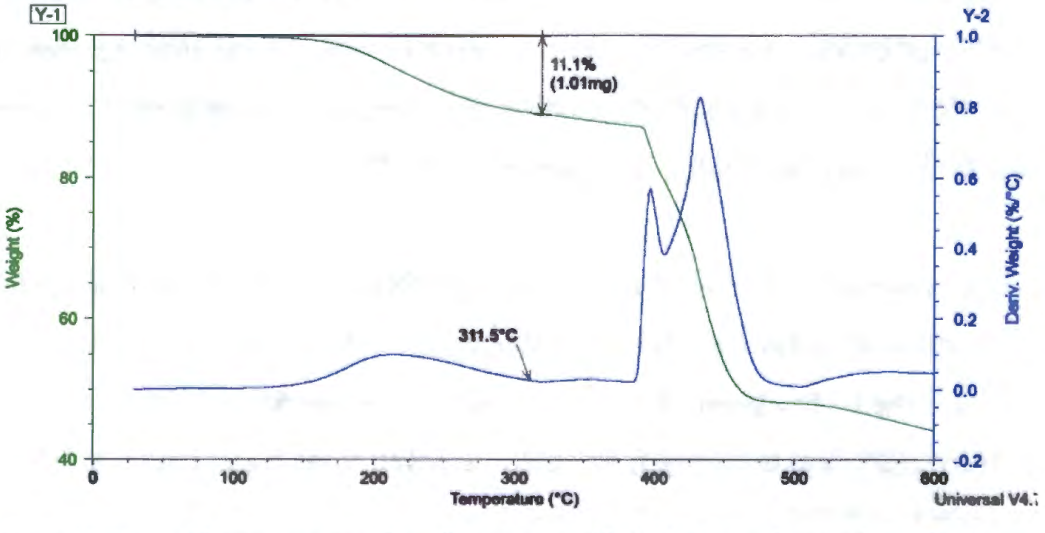

Figure 4.9: Thermogram of an "as received" NBR O-ring heated at 5°C/min.

The TGA data shows that the level of volatile in the O-rings is of the order 10-11%. This value obtained at the minimum of the derivative of 11.1% in Figure 4.9 at 311°C. Figure 4.10 shows the thermogram for a deplasticised sample. It indicates that there is some decomposition of NBR by 311.5°C indicating that TGA experiments would likely overestimate the level of plasticiser.

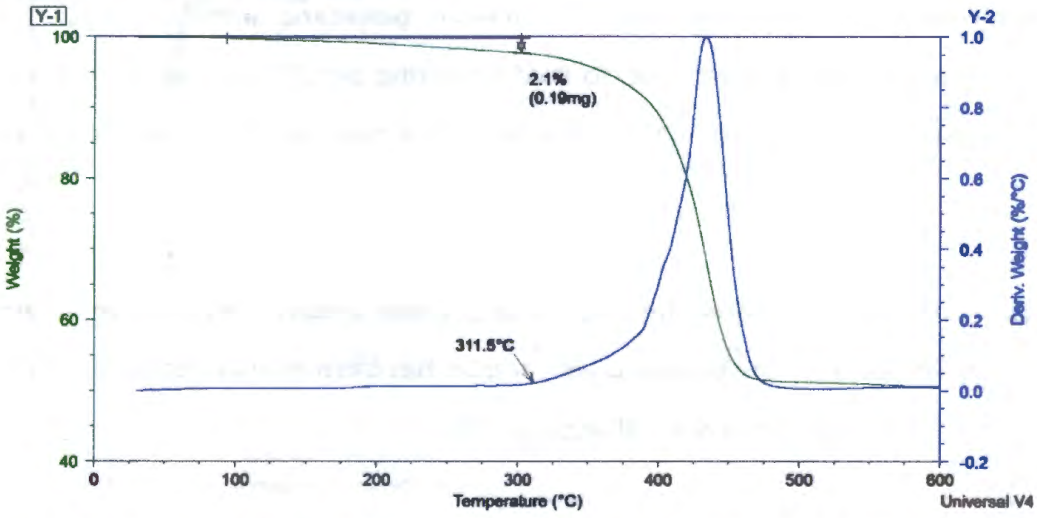

Figure 4.10: Thermogram of a deplasticised NBR O-ring heated at 5°C/min.

Interestingly, multiple thermograms of the "as received" O-rings displayed a sharp change in the rate of mass loss near 400°C (Figure 4.9). This was not observed with deplasticized O-rings (Figure 4.10). Investigations into the reasons for this were, however, beyond the scope of this study.

4.1.3. Determination of the Density of NBR Samples Before and After Plasticiser Extraction

The densities of "as received" and deplasticised samples (see Appendix C) were determined and are tabulated below. These values were subsequently used to convert mass to volumetric measurements in sections 4.2.1 and 5.2.2.

Table 4.3: Density of "as received" and deplasticised O-rings

Sample	Density (g/cm^3)
"As received"	1.238 ± 0.008
Deplasticised	1.274 ± 0.008

The confidence interval is at the 95% level. N = 5.

The increase in density is because the density of typical plasticisers is less than 1g/cm^3 (60). The data in Table 4.3 implies a 12.5% decrease in volume after the removal of extractables.

4.1.4. Effect of Plasticiser Extraction on Seal Swell

An investigation into the effect that extractable polymeric additives, such as plasticisers have on seal swell were performed on O-ring samples exposed to Jet A-1 and n-dodecane. n-Dodecane was chosen because it is a main paraffinic component of jet fuel.

Figure 4.11 and Figure 4.12 show the effect that polymer additives have on the mass swelling ratio. The data for the deplasticised samples has been adjusted to account for plasticiser loss. Hence the initial mass change is -10%.

The dotted line is an indication of the expected swell should equilibrium be maintained. The dotted line, however, does not take into account any possible ageing of the polymeric material due to thermal effects *e.g.* hardening.

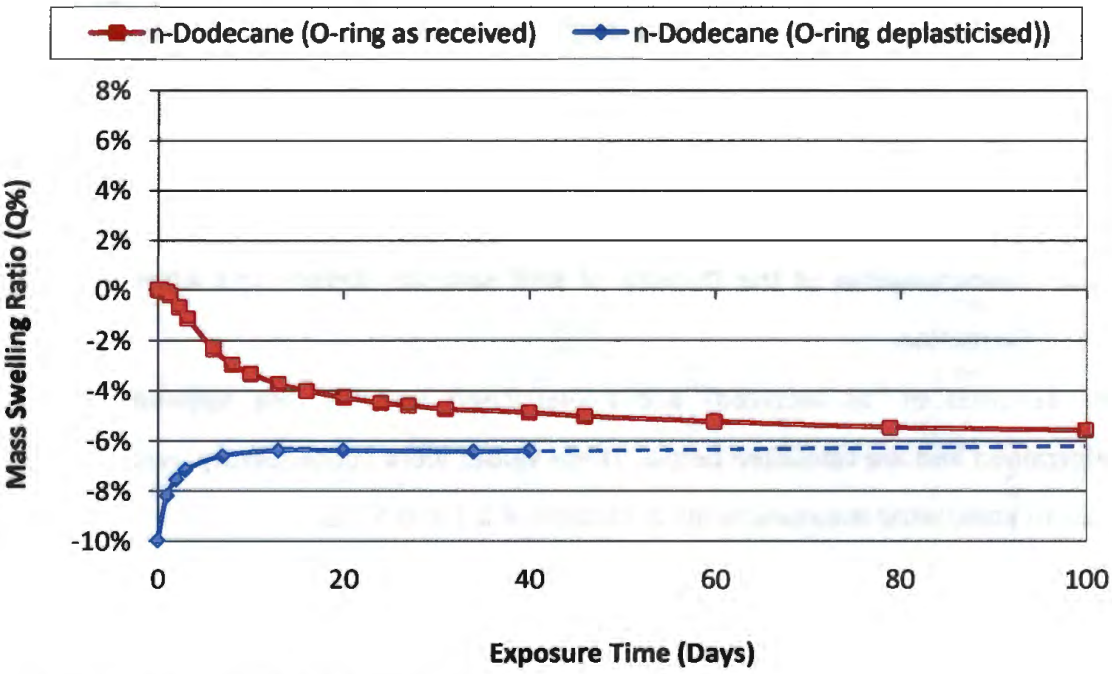

Graphs are plotted as the average of three experiments.

Figure 4.11: Comparison between the average of three "as received" and deplasticised O-rings exposed to n-dodecane at 50°C

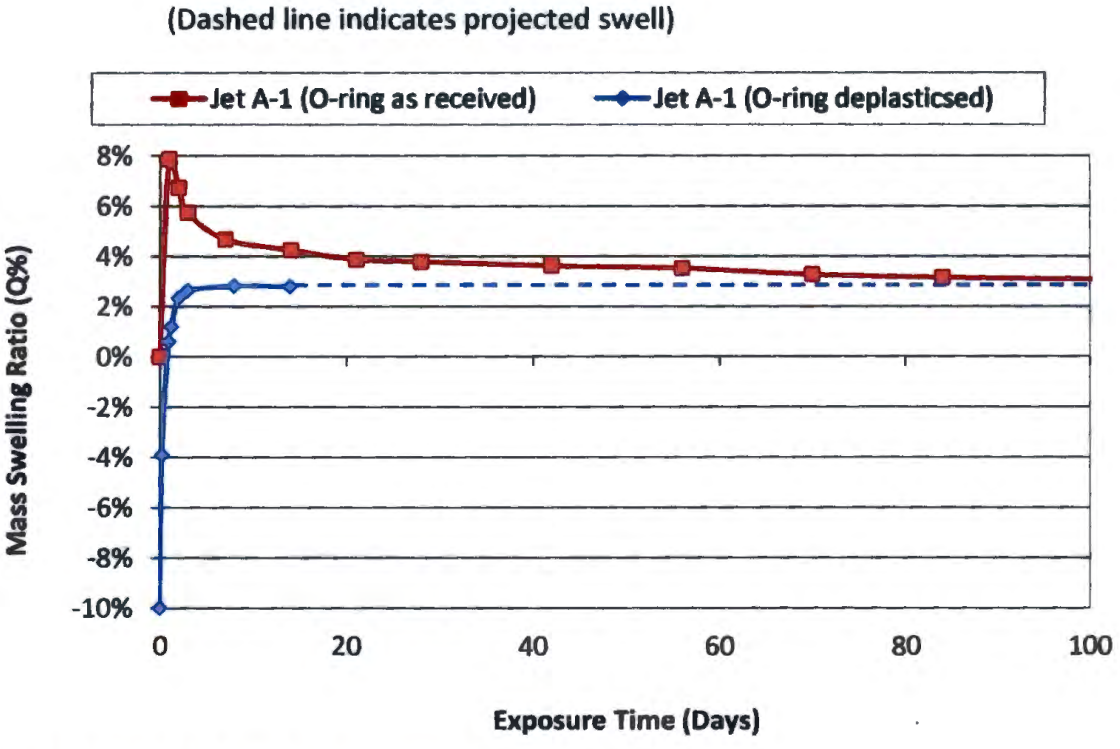

Graphs are plotted as the average of three experiments.

Figure 4.12: Comparison between the average of three "as received" and deplasticised O-rings exposed to Jet A-1 at 50°C
(Dashed line indicates projected swell)

The graphs illustrate that if only "as received" samples were investigated, it would be difficult to separate the plasticiser extraction and solvent absorption from the overall seal swell. Figure 4.12 indicates that similar equilibrium swell is observed for "as received" and deplasticised samples. The ageing of the polymeric materials does not appear to affect the final swell obtained.

The dodecane results in Figure 4.11 do not reach the same final swell. This is because in this case the "as received" O-rings are not at equilibrium. This is not surprising given dodecane's low solubility parameter which is quite different to typical plasticisers thereby lowering the driving force for plasticiser extraction.

4.1.5. Volumetric Measurements

Failure of O-rings in service due to switching fuel classes will most likely be caused by a change in O-ring volume. Consequently volume changes cannot be ignored.

4.1.5.1. Optical Dilatometry

Optical measurements were made by placing the samples under an optical microscope. Initial experiments were conducted on "as received" samples exposed to Jet A-1, n-dodecane and toluene to determine the repeatability of these experiments. Table 4.4 summarises the results.

Table 4.4: Volumes changes of "as received" O-rings exposed to varying solvents at 50°C

Solvent	δ $((MPa)^{1/2})$	Sample size	Average swelling at 7days (%)	Coefficient of variation (%)
Toluene	18.1	5	113.3 ± 6.2	3.7
Jet A-1	16.5	10	7.0 ± 0.5	3.5
n-Dodecane	16.0	5	1.6 ± 0.4	3.9

The uncertainty values for the average mass swelling ratio reflect the 95% confidence interval

When comparing the results with the gravimetric measurements in Table 4.1, the average volume changes at 7 days can be seen to be larger than the gravimetric measurements. This is expected since the densities of the solvents/fuel are lower than that of the rubber and filler.

When comparing the coefficient of variation (CV) of the optical measurements with the values obtained in mass experiments, it can be seen that that the CV values for the optical method is slightly higher. This is a result of one cubing the cross-sectional diameter (Equation 3.2 in section 3.3.2.2). The coefficient of variation of the one-dimensional dilation is 0.6-0.7%.

The average coefficient of variation for the equilibrium volume swell calculated from projected areas of small O-rings exposed to 28 solutions at 50°C was calculated. Each of these exposure experiments involved three O-rings. The average was 2.6%. The average coefficient of variation of the mass swell was 3.8%. The reason for the larger coefficient of variation for the mass measurements is that smaller O-rings have larger surface area to volume ratios which means that any variation in the amount of solvent

on the outer surface is more significant than for larger O-rings. Note also that these estimates are for 3 O-rings in each test, not 5 as before. What is important is that the uncertainty in volume changes is much closer to that of mass changes for smaller O-rings.

Data obtained from optical measurements of deplasticised samples exposed to Jet A-1 and SPK is presented in Figure 4.13.

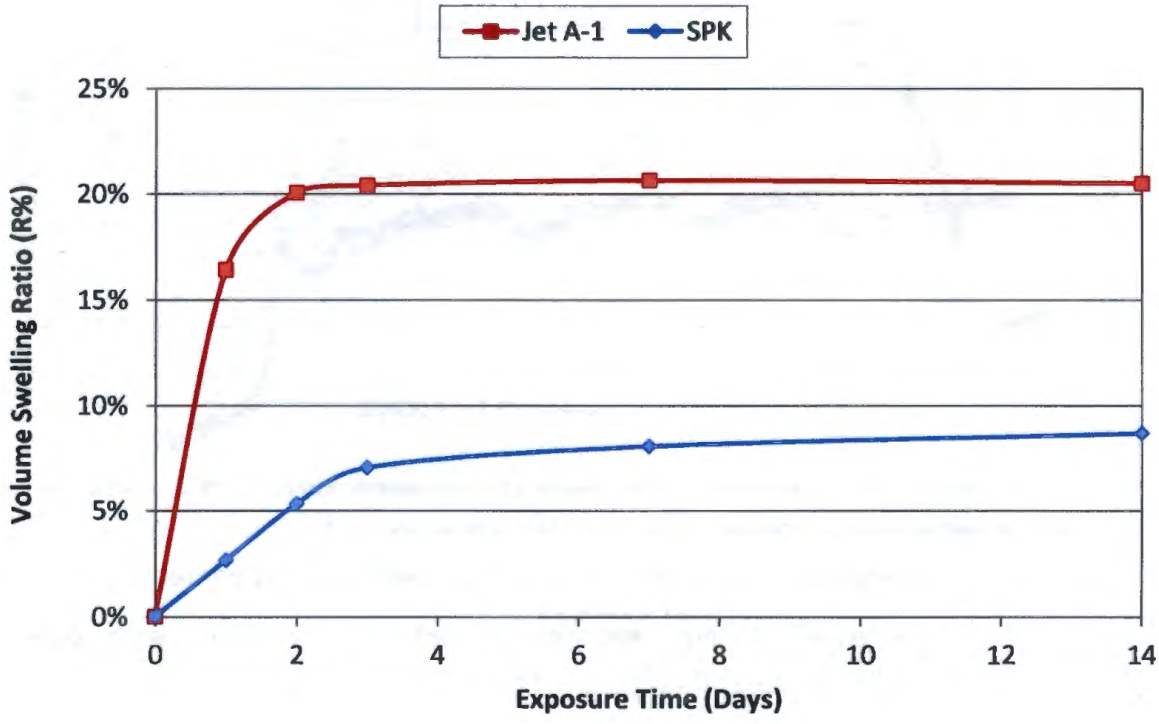

Graphs are plotted as the average of three experiments.

Figure 4.14.: Volume swelling ratio versus exposure time for deplasticised O-rings exposed to Jet A-1 and SPK at 50°C

4.1.5.2. Elastomer Compression Rig

Because the previous study at SAFL had been conducted using the elastomer compression rig, it was deemed important to further investigate this method (17).

Prior to collecting data, the rig was previously run without fuel for 24 hours with an O-ring placed inside each groove. This allowed for any settling in of the rig to be eliminated from the main data as well as to observe any changes in O-ring shape.

Figure 4. shows the repeatability of volume swelling of O-rings exposed to Jet A-1 at 50°C. Data from static and compression rig experiments are compared.

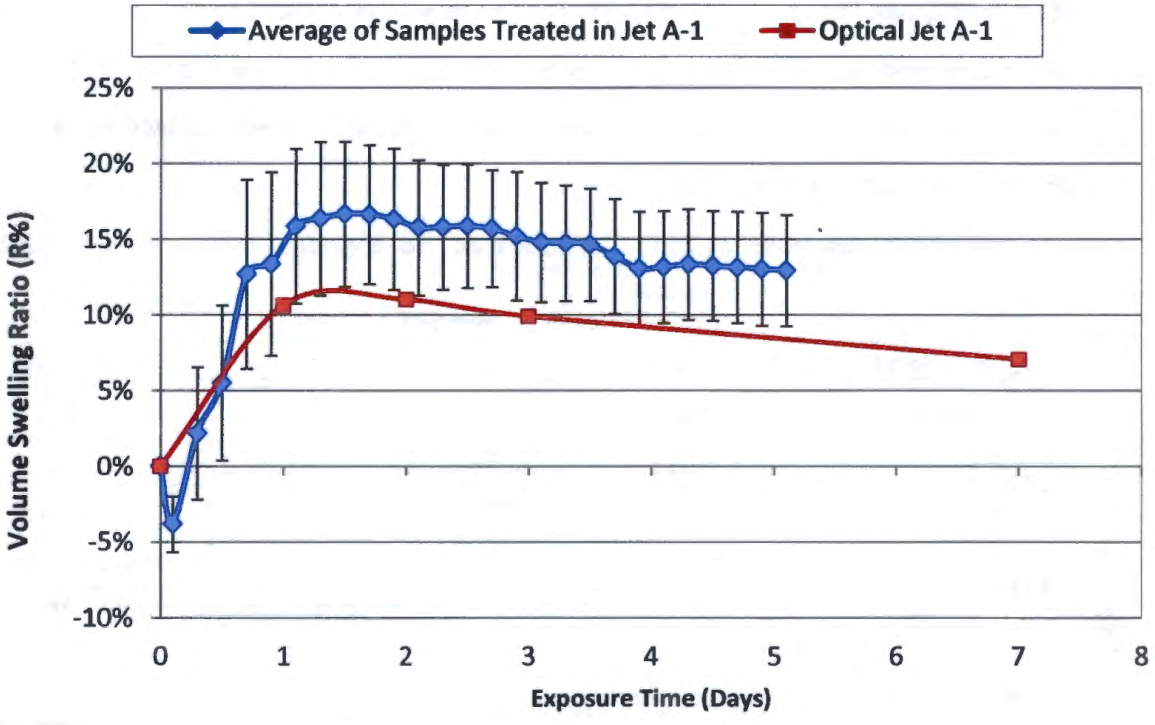

The compression rig data is the average of ten experiments. The error bars represent the 95% confidence interval. No error bars are shown on the optical volume curve because they are smaller than the value marker.

Figure 4.14: Repeatability of compression rig swelling experiments for 10 "as received" O-rings exposed to Jet A-1 at 50°C, with optical measurements for reference

The average coefficient of variation values obtained for the samples swollen in Jet A-1 at 50°C were calculated to be 38.8%. The one-dimensional (cross-sectional diameter) coefficient of variation is between 5 and 6% illustrating the propagation of error when the one-dimensional dilation is cubed. It can be seen that the rig has a considerably higher uncertainty than static volumetric measurements.

As the O-ring is subjected to compression forces at elevated temperatures, the deformation of the sample may occur fairly rapidly. The recovery of this deformation may be taking considerably longer than allowed for in the experimental cycle because NBR is a viscoelastic material. This is apparent in the initial decrease in volume in seal

swell rig data. It is also thus likely that dilation is not isotropic which would make Equation 3.2 an approximation. No further investigation, however, was carried out to determine the extent of this effect.

Curve 2 in Figure 4.15 illustrates this initial set where an initial decrease in measured diameter occurs. Here O-rings without fuel were placed in the compression rig.

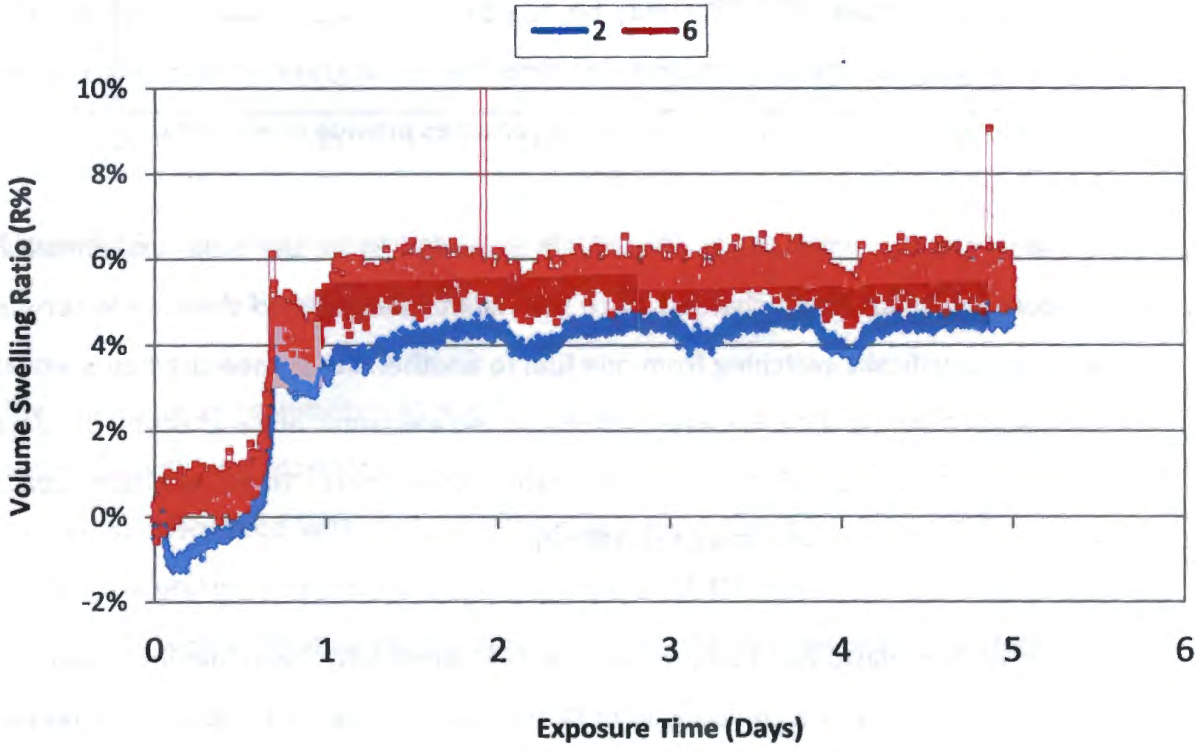

Figure 4.15: Compression rig swelling experiments with no fuel at room temperature for two cylinders

It was found in other experiments run under similar conditions, that jumps in the data (around 0.7 days in Figure 4.15) also occurred. Visram did not observe such anomalies (17). It was decided that no further investigation using the rig would be performed. These unexpected jumps were likely the result of ageing of the rig, *e.g.* corrosion causing the rig to stick and then spring loose. Rig modification would be required. This, however, was outside the scope of this study.

4.2. Discussion

The development of the conditioning procedure, the effects of temperature on seal swell and experimental duration were essential for further experiments, designed to look into the effects of various chemical classes on seal swell.

4.2.1. Measurement Approach

Since in service failure of O-rings may be due to a decrease in sample volume, the benefits of using volumetric measurements over the use of gravimetric measurements are therefore apparent. Nonetheless both approaches provide useful data.

The use of the compression rig was initially intended to be the main experimental procedure for dilatometric changes since the rig was designed to simulate in-service operation, specifically switching from one fuel to another. Static measurements would have validated the rig data. Because of unexplained electronic noise affecting the data collected, it was decided to focus on static experiments. These are the typical measurements found in literature (2) (10) (49).

The use of the elastomer compression rig had previously been demonstrated by Visram (17). Figure 4. is a comparison of O-rings tested in Jet A-1 and CTL SPK (Ker0A in the figure) at 50°C. λ is the one-dimensional dilation in cross-sectional diameter in the direction of original compression. Note the similarity in shape with Figure 4.4.

Although the rig could in principle provide volumetric changes due to swell and allow easy study of fuel switches, increased electronic noise meant that it was not reliable enough to be used further.

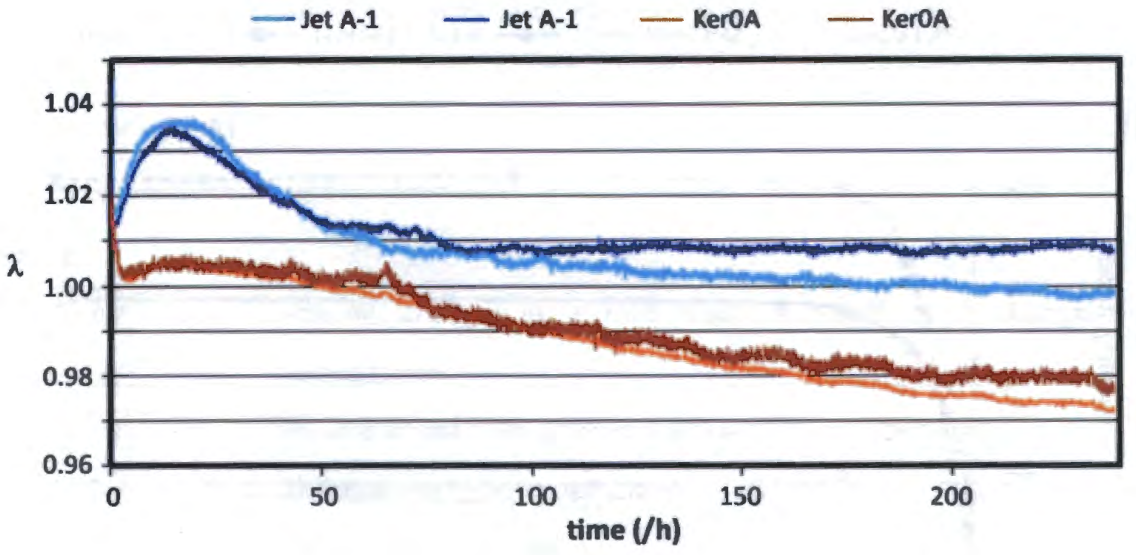

Figure 4.16: Elastomer compression rig dilation of "as received" O-rings exposed to Jet A-1 and SPK at 50°C (17)

The degree of repeatability obtained using optical dilatometry was better than that observed with the elastomer compression rig. Some uncertainty arises because of difficulties associated with making microscopy measurements. These difficulties are due to the presence of flash lines and distortion of the samples. There is also some uncertainty with estimating the diameters because the samples are not perfect tori.

The high repeatability of both optical and gravimetric measurements led to the decision that in later experiments only three measurements at each time stage were made. It should be noted that in other studies, *e.g.* Graham *et al.* (2) as few as two measurements were made.

Comparing the optical measurements in this study with gravimetric measurements, it can be seen that both experimental methods show similar seal swell trends. Because of density differences between the rubber and the solvent, volume changes are larger. Figure 4.16 below illustrates this clearly. An approximate shrinkage of 13% by volume would occur when fuel is switched from Jet A-1 to SPK. Because of plasticiser removal under in-service conditions, O-rings would be expected to shrink 4 to 5 % from their original size when exposed to SPK.

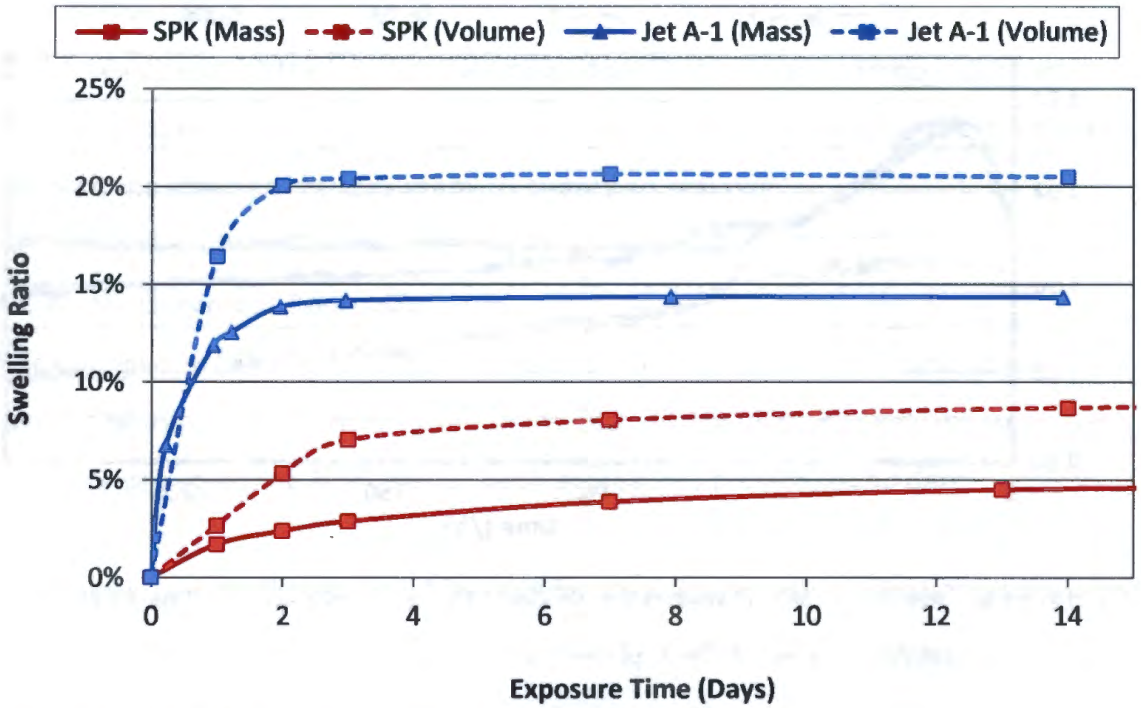

Graphs are plotted as the average of three experiments.

Figure 4.16: Comparisons of optical versus gravimetric measurements for deplasticised O-rings in Jet A-1 and SPK at 50°C

Percentage volume changes can also be estimated from the mass changes. The calculations may be found in Appendix C. It is assumed that the density of fuel in the O-ring is the same as that in the bulk and no preferential uptake of higher or lower density components occurs. This approach is traditionally used to determine the volume fraction of rubber and the volume fraction of solvent during experiments to determine crosslink density.

The densities at 50°C used for Jet A-1 and SPK were calculated using the respective densities at 15°C (4) and the thermal expansion coefficients (63) in Table 4.5.

Table 4.5: Thermal expansion coefficient an densities of Jet A-1 and SPK (4) (63)

Fuels	Thermal expansion coefficient (K^{-1})	Density at 15°C (g/cm^3)	Calculated density at 50°C (g/cm^3)
Jet A-1	9.9×10^{-4}	0.801	0.773
SPK	7.6×10^{-4}	0.765	0.745

The densities at 50°C were calculated using equation 4.1.

$$\Delta V = \beta V_0 \Delta T \qquad (4.1)$$

where:

ΔV = volume change in a unit mass a result of a change in temperature

V_0 = volume of the unit mass at the reference temperature

β = thermal expansion coefficient

ΔT = temperature change

A comparison of the measured and calculated volume swelling ratios is presented in Figure 4.17 and Figure 4.18.

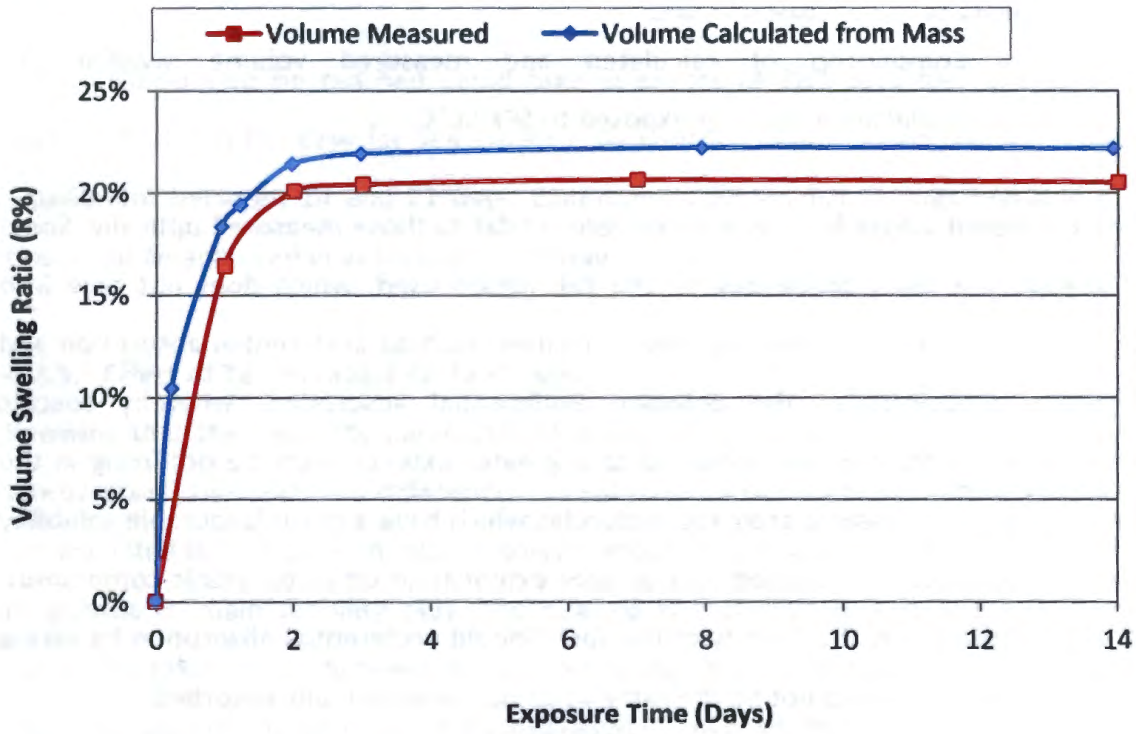

Graphs are plotted as the average of three experiments.

Figure 4.17: Comparison of calculated and measured volume swelling for deplasticised O-rings exposed to Jet A-1 at 50°C

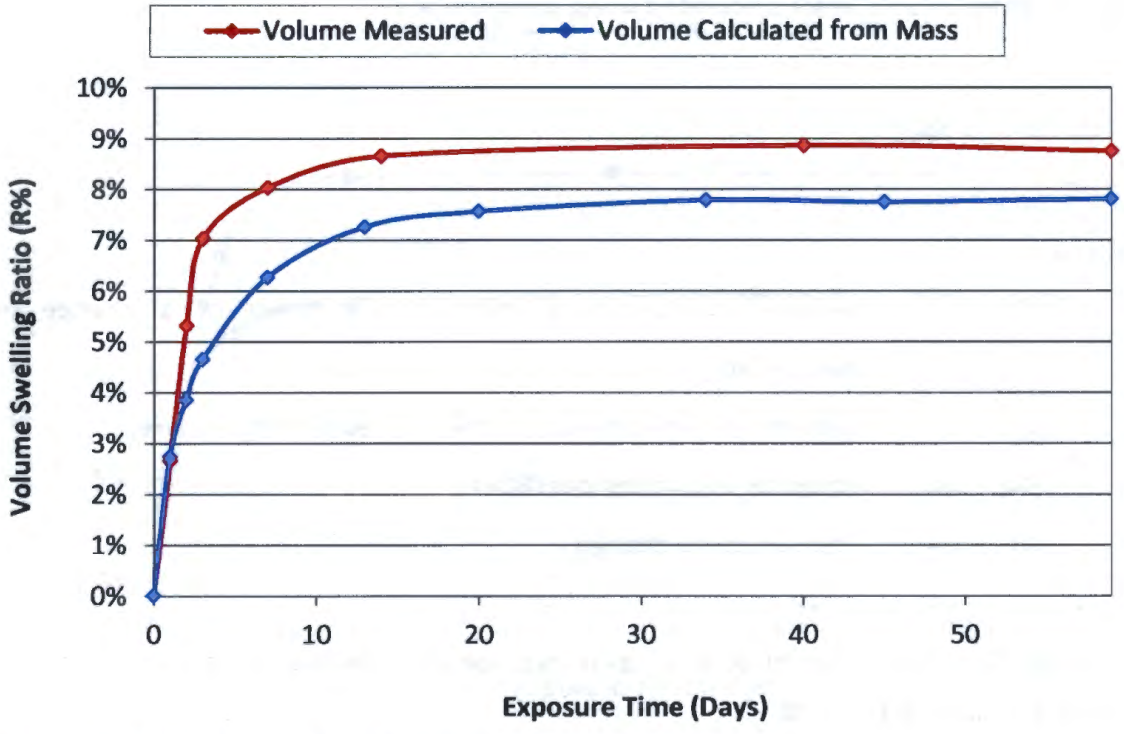

Graphs are plotted as the average of three experiments.

Figure 4.18: Comparison of calculated and measured volume swelling for deplasticised O-rings exposed to SPK 50°C

The calculated values for volume swell are similar to those measured optically. Some discrepancy is likely to be due to the calculation used, which does not take into account all the factors affecting volume change, such as preferential absorption and changes in density of the polymer. Preferential absorption, whereby specific compounds in the fuel are absorbed to a greater extent, might be occurring in the Jet A-1 case. For example aromatic molecules which have a more favourable solubility parameter might be absorbed to a greater extent than other paraffinic compounds. The calculation uses the density of the fuel. Should preferential absorption be taking place this density would not be the same as components actually absorbed.

There is some evidence for this in the literature Graham *et al.* (2). In the case of Jet A-1, this means that the density of the jet fuel in the O-ring is higher than that in the bulk which would mean the calculation overestimates the volume change slightly. Graham *et al.* (2) also reported that in SPK the lower density, lighter (smaller carbon number) alkanes are slightly concentrated in the O-ring. This would lead to the

calculated volume change being a slight underestimate. A look at Figure 4.17 and Figure 4.18 reveals that is the case here.

4.2.2. Duration of Solvent Exposure

Seal swell experiments were continued until equilibrium to eliminate misleading conclusions that could have been drawn from samples still undergoing changes. Allowing samples to reach equilibrium allows the effects of diffusion to be removed (32). Hansen supports this by stating that "using the solubility parameters to determine swell is only suitable at equilibrium, which is not usually reached in previous studies" (64). It was, therefore, decided that subsequent experiments in this study should be run to equilibrium conditions. Equilibrium conditions are likely not achieved in some of the literature. This is surmised because exposure times are often of the order of 2-3 days.

For equilibrium to be reached could take in excess of 180 days for "as received" O-rings. This was the case for SPK swelling. By contrast deplasticised O-rings reached equilibrium between 14 and 21 days. Experiments on smaller O-rings revealed that this could be achieved in as little as 3 to 6 days.

4.2.3. Effect of Temperature on Seal Swell

Knowing that the solubility parameter of a solvent and polymer are independent of temperature, the observed differences in seal swell caused by temperature variations are expected to be due to changes in solvent mobility, molar volume and the increases in polymeric chain mobility (43). The change in molar volume is due to thermal expansion taking place between solvent molecules, thus as temperature is increased the molar volume increases which should result in lower swell (65).

Mostafa *et al.* investigated the effect of temperature on swell (43). Although they exposed 30 X 5 X 2cm NBR moulded disks to motor oil, their results provide insights into the observations made here. The results are presented in Table 4.6.

Table 4.6: Mass swelling ratio at 48 h for varying concentration of carbon black filled NBR moulded disks exposed to motor oil (43)

Temperature (°C)	Mass swelling ratio at 48 h (Q%)	
	NBR sample 1 (0*)	NBR sample 2 (30*)
25	1.82	1.18
70	2.37	1.50
100	4.65	2.35
125	4.80	2.42

* Parts carbon black per hundred of rubber by weight

Mostafa *et al.* established that samples treated at elevated temperatures showed an increase in swell. This effect was explained by postulating that at elevated temperatures chain mobility would increase, resulting in the softening of the rubber leading to greater swell (43).

Mostafa *et al.* however, only recorded data for the first 48 hours. It is highly likely that the samples at lower temperatures had not yet reached equilibrium conditions. Consequently the results should be treated with caution. This highlights the need to ensure that equilibrium has been reached when comparing data.

The effect of temperature was also investigated by Joseph *et al.* using NBR/EVA polymer blends treated in p-xylene (58). NBR/EVA exposed to p-xylene at various temperatures appear to have reached equilibrium and show that samples treated at elevated temperatures show a greater swell. Joseph *et al.* explained the greater swell seen for samples treated at elevated temperatures as being due to the greater polymeric chain mobility at higher temperatures. This temperature relationship, however, was not seen in this study when NBR O-rings were exposed to o-xylene or Jet A-1 (Figure 4.6 and Figure 4.7). The extent of swell actually decreased as temperature rose. This is discussed in more detail in section 5.5.5.

The findings in this study and of Mostafa *et al.* showed that at higher temperatures a faster rate of solvent absorption is seen (43). This is expected since the diffusion coefficient for solvent entering the polymer, and for the plasticiser leaving the

polymer, is larger at elevated temperatures. To save time, later experiments were performed at 50°C. Equilibrium conditions could be achieved far sooner allowing more experiments to be performed.

4.2.4. Plasticiser Effects

Extractable polymeric additives such as plasticisers and curatives complicate the interpretation of swelling data obtained from "as received" samples undergoing solvent exposure. Any mass or volume changes observed during the exposure of plasticised O-rings are the result of a combination of solvent entering the polymer and the extraction of additives. The amount of extractable additives is important as different polymer compounds will contain varying amounts of additives, which will affect the overall change in swell. Caution must thus be exercised when comparing two different data sets as the percentage plasticiser may vary significantly despite the samples having a similar hardness. Hardness is a function of both plasticiser/extender oil, filler level, cross-link density and temperature (42) (43).

In order to investigate the effects that these extractable additives have on seal swell, it was important to determine the amount of additives that could be extracted and the rate at which this process occurs. This was achieved by comparing the mass of deplasticised and "as received" O-rings exposed to the same solvent and under similar experimental conditions. The O-rings used here contained about 10% plasticiser. Density measurements indicated this was equivalent to a 12.5% change in volume.

Plasticised samples initially passed through an absorption peak before losing mass. Such behaviour is typical of plasticised samples (57). Experiments on deplasticised samples displayed a classic monotonic uptake curve to an equilibrium plateau.

The swelling data from "as received" O-rings exposed to n-dodecane showed only a decrease in mass. This is most likely to be due to the mass of plasticiser extraction being greater than the solvent being absorbed.

4.2.5. O-ring Conditioning

Corporan *et al.* conducted experiments on deplasticised samples. The method of plasticiser extraction process was, however, omitted by Corporan *et al.* (10). It was found in this study that solvents that show high seal swell potential will remove plasticisers rapidly from the O-rings. CH_2Cl_2 was chosen because it is highly volatile and can be extracted rapidly from the sample following plasticiser extraction.

Additional extraction experiments conducted on prior conditioned samples showed no further mass loss. This is supported by TGA thermograms in which plasticiser appears to be absent. By contrast it was difficult to remove all the Jet A-1 from the deswollen samples in a reasonable time.

Deplasticised O-rings are likely to be more representative of O-rings after a few months of service. Running the plasticised and deplasticised experiments separately allows the effect of plasticiser extraction to be distilled. This is illustrated in Figure 4.19.

These curves allow the rate of solvent absorption and plasticiser extraction to be seen separately. The deplasticised O-ring curve shows the rate of solvent absorption. By subtracting the absorption curve for the deplasticised O-ring from the absorption curve for an "as received" O-ring the plasticiser extraction curve can be obtained. When one compares the deplasticised case with the calculated plasticiser extraction curve, it can be seen that the rate of solvent absorption (initial slope) is greater than the rate of plasticiser extraction. This can is most likely due to the greater molecular volume of the plasticiser giving rise to a smaller diffusion coefficient. For instance dibutyl phthalate has a molar volume of 266cm^3 compared to a molar volume of two common components of jet fuel, n-butylbenzene (156cm^3) and n-dodecane (227cm^3).

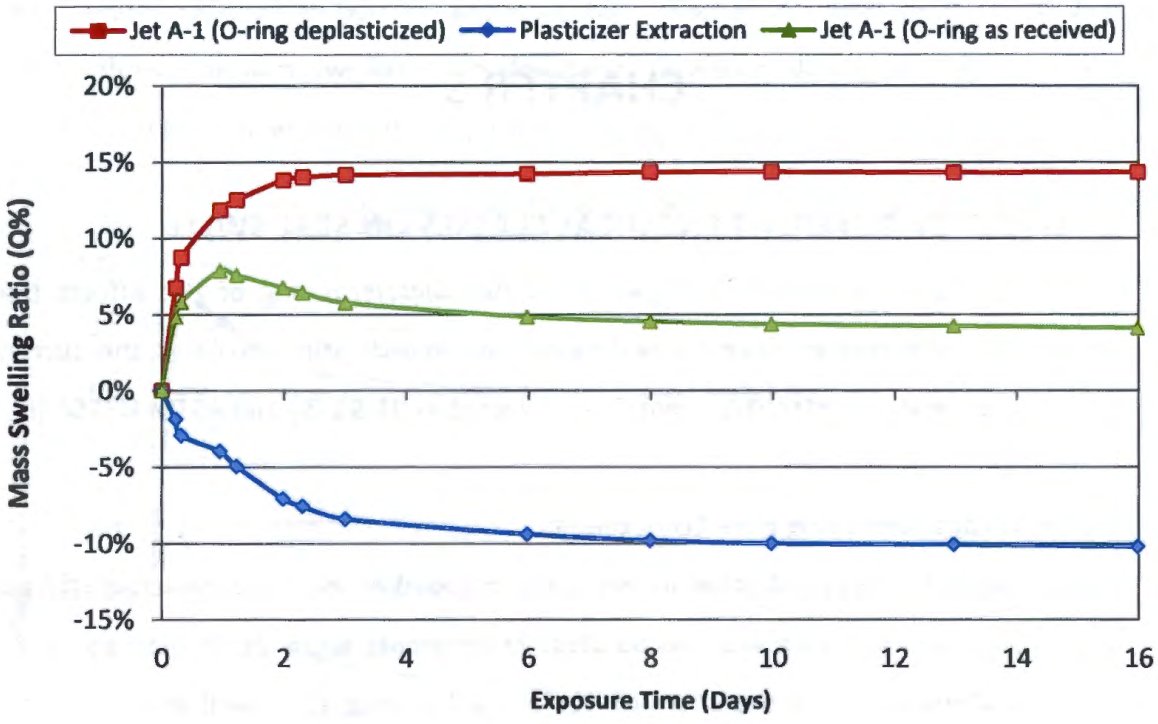

Graphs are plotted as the average of three experiments.

Figure 4.19: Plasticiser extraction from "as received" O-rings exposed to Jet A-1.

CHAPTER 5

5. EFFECT OF DIFFERENT CHEMICAL CLASSES ON SEAL SWELL

This study was commissioned to gain a greater understanding of the effects that various chemical classes have on seal swell. The investigation explores the current minimum aromatic specification contained in Def Stan 91-91 (5) and ASTM D7566 (6).

5.1. Investigations using Pure Components

The chemical classes investigated in this study included n-, iso-, and cyclic-paraffins as well as various aromatics and oxygenates. Experiments were performed to gain a greater understanding of the chemical factors influencing seal swell and to provide insight for the investigation into later blending studies.

5.1.1. Paraffinic Isomers

An iso-paraffinic synthetic kerosene, produced via CTL FT processes, is currently approved for use as a jet fuel blending component (4). Future production of synthetic jet fuel may use alternative feedstocks and production processes which may alter the fuel chemistry. Thus, the effects that changing the paraffinic isomers have on seal swell were investigated. In this study, isomers of octane and dodecane were used to better illustrate the effect of various paraffins and their isomers. The swelling of samples exposed to CTL and GTL SPK were also compared.

5.1.1.1. Pure Paraffin Isomers (Octane and Dodecane)

The effect that different isomers of octane have on seal swell can be seen in Figure 5.1. Although octane is lighter than the components found in jet fuel, it was used in addition to dodecane because of the ready availability of two cyclic isomers. It was found that when "as received" O-rings were exposed to n-octane, the mass uptake increased and then rapidly decreased. Iso-Octane, by contrast, displayed a gradual decrease in mass from the onset of the experiment.

The samples exposed to both n- and iso-octane reached equilibrium at similar mass swell values. Samples swollen in cyclooctane, however, displayed a greater mass uptake than was observed in the experiments using the other octane isomers.

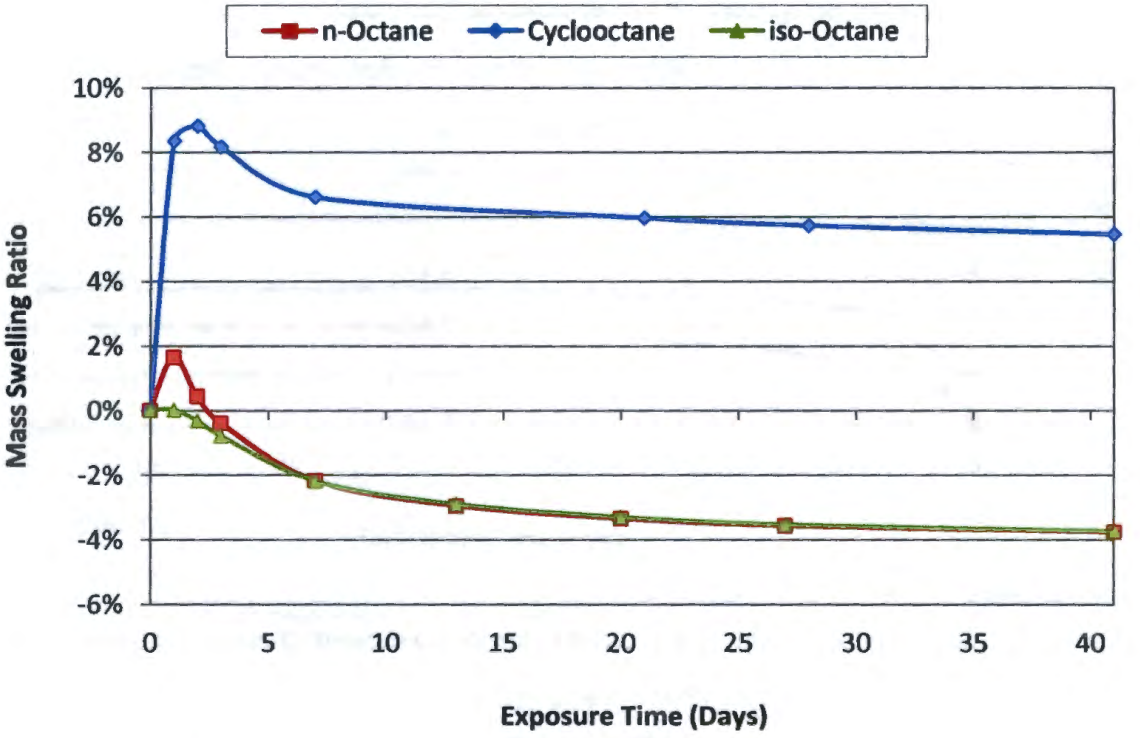

Graphs are plotted as the average of three experiments.

Figure 5.1: Comparison of the mass uptake for "as received" O-rings exposed to various octane isomers at 50°C

To explore this difference in initial uptake further, additional experiments were run on deplasticised O-rings exposed to the isomers of octane and dodecane.

Dodecane was chosen because it lies in the jet fuel boiling range. These results, which can be seen in Figure 5.2 and Figure 5.3, show that the initial absorption rate of the n-isomers is greater than the absorption of their respective iso-isomers. Consequently, samples exposed to n-isomers reached equilibrium sooner than samples exposed to the iso-isomers.

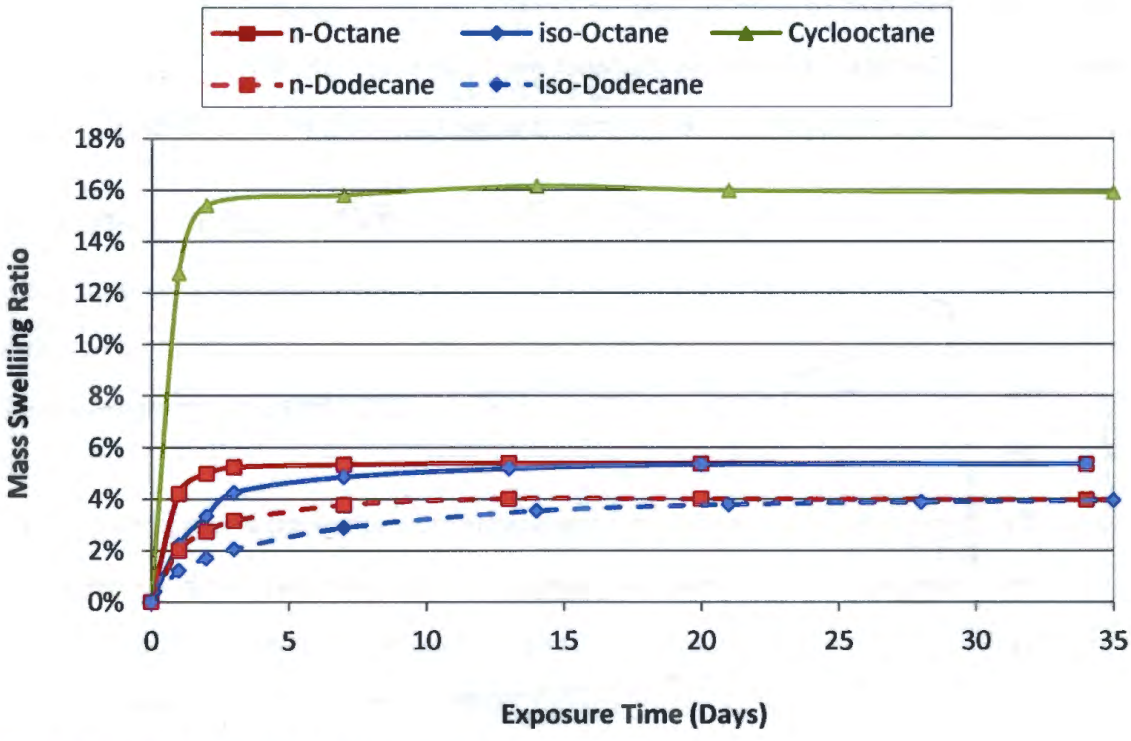

Graphs are plotted as the average of three experiments.

Figure 5.2: Comparison of the mass uptake for deplasticised O-rings exposed to the isomers of octane and dodecane at 50°C

More solvent was absorbed by O-rings when the rings were exposed to the octane isomers than when they were exposed to the isomers of dodecane. This indicates that for iso- and n-paraffins molar volume outweighs solubility parameters. The decrease in volume swell is approximately 30% (in relative terms) from n-octane to n-dodecane while the molar volume increases by almost the same (28%). The solubility parameter and molar volume data are compared in Table 5.1.

The volume data presented in Figure 5.3 and Table 5.1 shows that n-octane swells the O-ring more than iso-octane but the effect is not statistically significant. In the case of the dodecanes, it is significant, but that is likely the result of iso-dodecane not having reached equilibrium at 14 days. The volume measurements show that samples exposed to both cyclic isomers, cyclooctane and 1,2-dimethylcyclohexane, swell more than samples exposed to the n and iso-paraffinic octane isomers. In this case the increase in swell is near double which is much larger than the decrease in molar

volume. This suggests that the solubility parameter also play a role in causing the higher swell of cyclic paraffins, unlike non-cyclic paraffins.

Table 5.1: Solvent properties and volumetric swell changes for isomers of octane and dodecane on deplasticised O-rings at 50°C

Solvent	Molar volume at 20°C (cm^3mol^{-1})	Solubility parameter $(MPa)^{1/2}$	Average volume swelling ratio at 14 days (%)
n-Octane	163.5	15.5	12.6 (0.3)
iso-Octane	166.1	14.1	12.5 (0.3)
1,2-dimethylcyclohexane	144.2	16.7	23.5 (0.4)
Cyclooctane	134.5	17.2	26.9 (0.4)
n-Dodecane	227.1	16.0	8.83 (0.1)
iso-Dodecane	228.0	14.7	7.49 (0.2)

The values in brackets are the standard deviations of the mean.

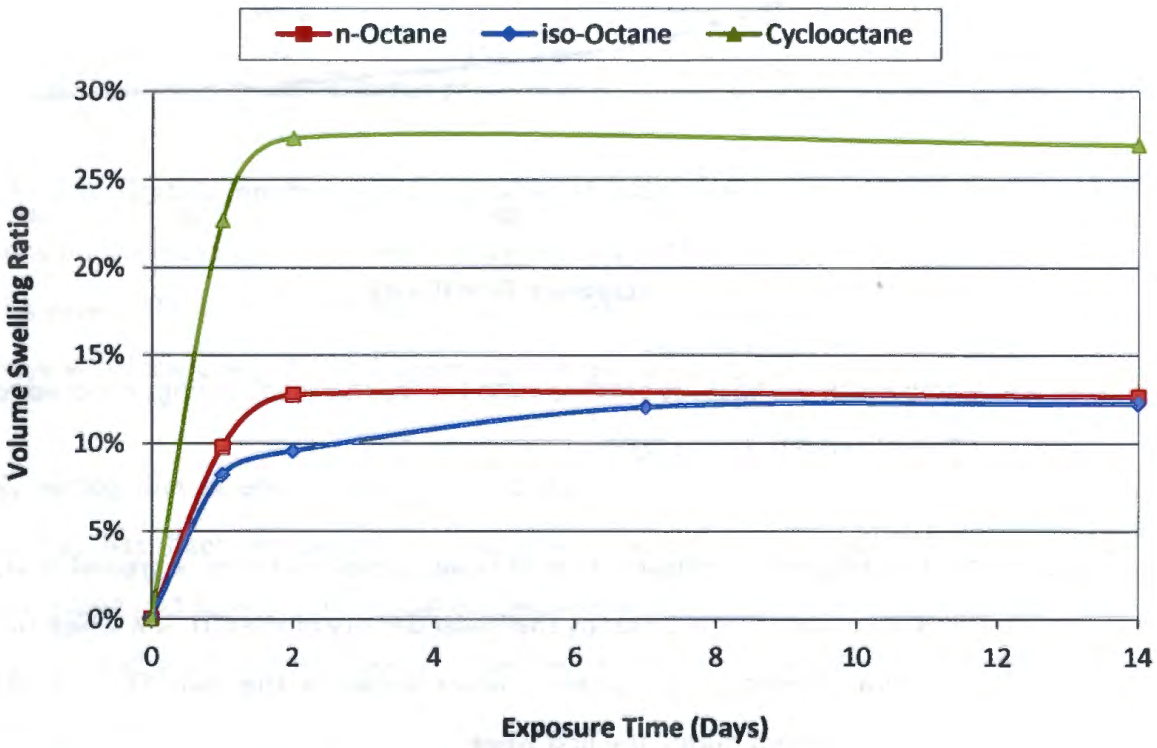

Graphs are plotted as the average of three experiments.

Figure 5.3: Comparison of the volume increase for deplasticised O-rings exposed to isomers of octane at 50°C

5.1.1.2. CTL and GTL SPK

Samples exposed to CTL and GTL SPK display similar seal swell behaviour to that observed with samples swollen in n- and iso-octane, and n- and iso-dodecane. The results can be seen in Figure 5.4. An initial increase in mass is only observed in the GTL SPK case. This GTL SPK contains more n-paraffin than the CTL SPK (4).

Because these experiments were conducted on "as received" O-rings, the samples for which data are presented in Figure 5.4 have not reached final equilibrium.

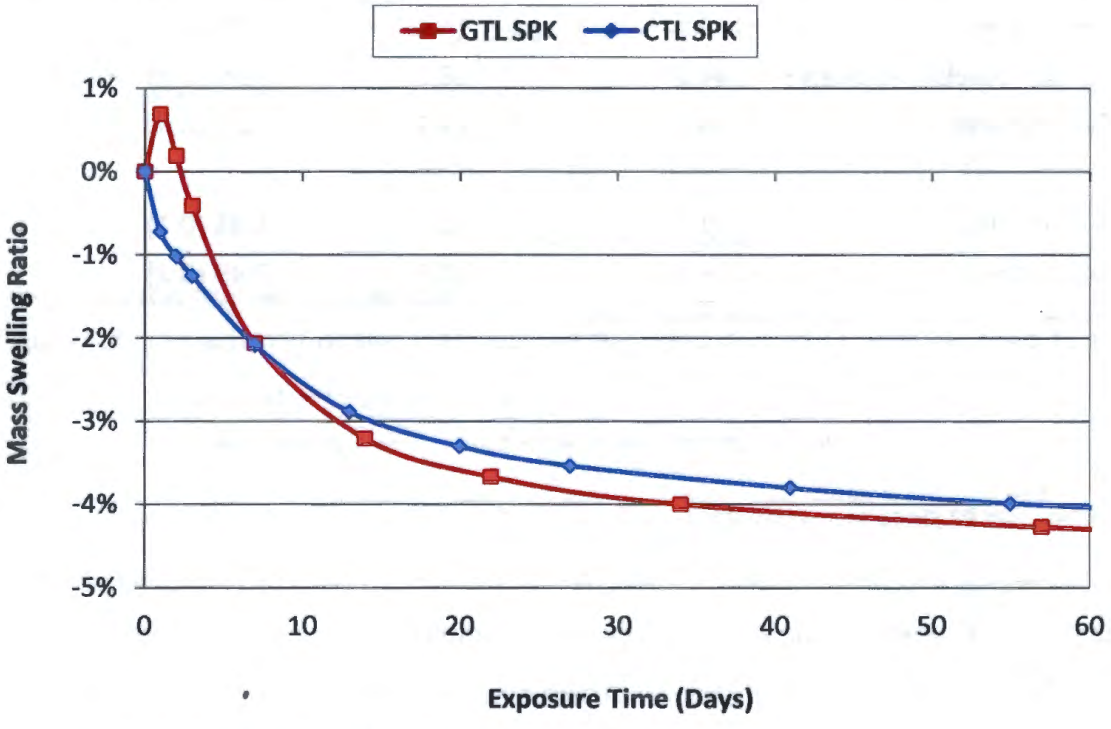

Graphs are plotted as the average of three experiments.

Figure 5.4: Comparison of the mass swelling ratio for "as received" O-rings exposed to CTL SPK and GTL SPK at 50°C

Note that the data presented indicates that at larger exposure times, a greater mass of the CTL SPK is absorbed. This is offset by the lower density of the GTL SPK which has the result that the difference in volume change between the two SPKs is not statistically significant except during the first week.

5.1.2. Effects of Carbon Chain Length on Seal Swell

The data in Section 5.1.1.1 shows that greater swell was observed for samples swollen in octane than those exposed to dodecane. The solubility parameter of n-dodecane is, however, greater than n-octane. The behaviour observed is thus likely driven by the smaller molar volumes of the n- and iso-octanes.

To elucidate this further, an investigation into the effect that molar volume has on seal swell was undertaken. This was carried out on "as received" samples at 50°C exposed to a range of n-paraffins *i.e.* n-hexane, n-octane, n-dodecane and n-tetradecane.

Table 5.2: Solvent properties and experimental summary for "as received" O-rings exposed to different n-paraffins on at 50°C

Solvent	Molar volume at 20°C ($cm^3 mol^{-1}$)	Solubility parameter ($(MPa)^{1/2}$)	Average mass swelling ratio at equilibrium (%)	Calculated volume change at equilibrium (%)
n-Hexane	130.6	14.9	-2.4 (0.1) at 40 d	+1.8
n-Octane	162.5	15.5	-3.9 (0.1) at 80 d	-1.8
n-Dodecane	227.1	16.0	-6.1 (0.0) at 300 d	-6.1
n-Tetradecane	260.4	16.2	-6.3 (0.1) at 300 d	-6.5

The values in brackets are the standard deviations of the mean. N = 3.

The investigation into this set of n-paraffins showed that samples exposed to n-hexane took up the most solvent by mass. It was observed that as molecular volume increased the extent of swelling decreased for the n-paraffins. The solubility parameter seems to have very little effect. Table 5.2 summarises the results obtained.

By noting that at equilibrium the plasticiser, which comprised 10% of the mass the O-ring, has been extracted, the change in volume that results from plasticiser extraction and solvent uptake can be calculated. This is also reported in Table 5.2. The same trend as the mass uptake is observed. These results are discussed more fully in section 5.5.1.2.

5.1.3. Pure Aromatic Hydrocarbon Solvents

The current specification for synthetic jet fuels requires a minimum of 8% by volume aromatic compounds (5). This specification is intended to minimise changes in seal swell when switching fuel types and raise the density of the fuel. The specification does not specify the type of aromatic species. Therefore, the degree of swell caused by different aromatics was investigated to see what effect structural differences within the aromatic class have on seal swell. This was performed with both pure solvents and 8% (v/v) blends with SPK. The blend data may be found in section 5.2. The chemical structures of the aromatic compounds investigated may be found in in Figure 5.5.

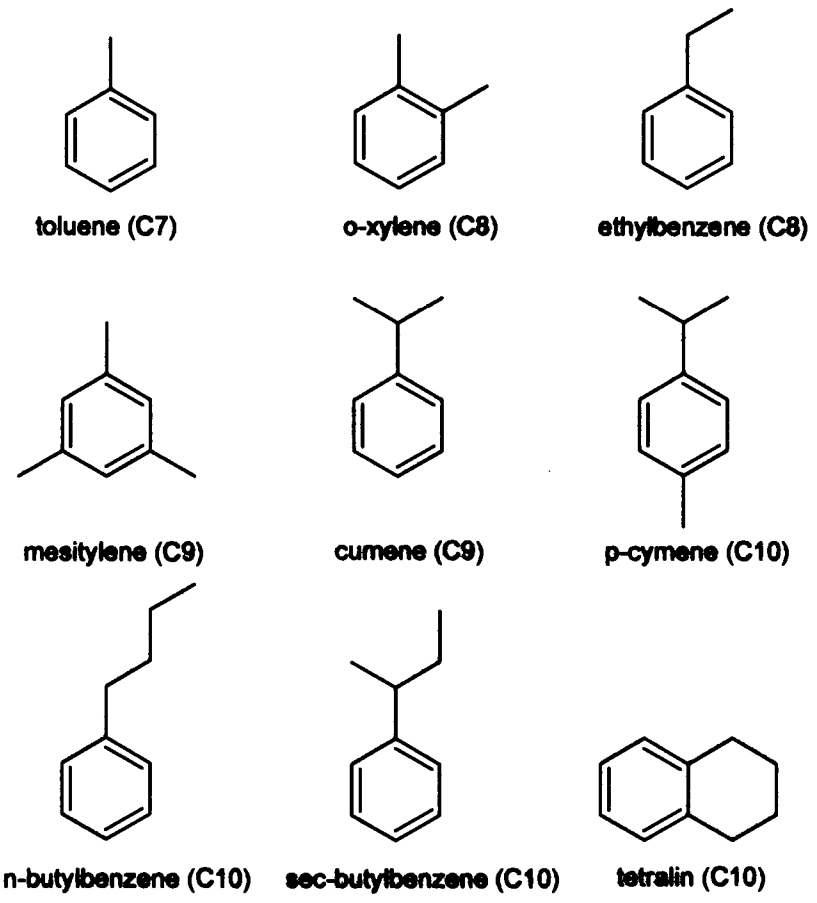

Figure 5.5: Chemical structure of aromatic compounds investigated

These compounds were chosen to span a range of carbon numbers, molecular size and aliphatic chain structure. Of these, toluene, o-xylene, cumene and mesitylene were selected for study as pure compounds.

Exposure to pure hydrocarbon aromatic compounds resulted in rapid swelling of NBR O-rings. The extent of swelling at equilibrium was significantly higher than that of the paraffins tested previously. It was found that there is a wide variation in the extent of seal swell across the aromatic compounds investigated. Table 5.3 summarises the key information from these experiments as well as showing the mass swell ratio after solvent extraction. The volume change at equilibrium is calculated in a similar fashion to that used in section 4.2.1.

Table 5.3: Solvent properties and experimental summary for the exposure of "as received" O-rings to pure aromatic compounds at 50°C

Solvent	Molar volume at 20°C (cm^3mol^{-1})	Solubility parameter ($(MPa)^{1/2}$)				Mass uptake at equilibrium (%)	Calculated volume change at equilibrium (%)	Mass swell after solvent extraction (%)
		δ_d	δ_p	δ_h	δ_{Total}			
Toluene	106.3	18.0	1.4	2.0	18.1	75.3 (2.1)	109.3	-9.9 (0.2)
o-Xylene	120.6	17.8	1.0	3.1	18.2	75.1 (2.0)	107.2	-10.0 (0.2)
Cumene	139.4	18.1	1.2	1.2	18.2	47.4 (1.1)	69.9	-10.2 (0.2)
Mesitylene	139.1	18.0	0	0.6	18.0	46.0 (1.2)	67.7	-10.1 (0.2)

The values in brackets are the standard deviations of the mean. N = 3.

The data shows that the extent of swell is dependent on the aromatic solvent in which swelling occurs. The data suggests that as molecular volume increases swell decreases. However, it can be seen that the swell of o-xylene is very similar to toluene. This suggests that the hydrogen-bonding solubility parameter, δ_h, might be a key determinant of the degree of seal swell. The mass after deswelling with these solvents is consistent with the 10% plasticiser content obtained using dichloromethane. This is further evidence that relatively volatile solvents that swell NBR well are most suitable for O-ring conditioning.

5.1.4. Pure Oxygenated Aromatic Solvents

It has been previously reported that the aromatic alcohol, benzyl alcohol (BzOH), in concentrations as low as 0.5% in SPK can produce significant seal swell (17) (27). The effect that other oxygenated aromatic compounds have on seal swell was, therefore, investigated.

The oxygenated species which were studied are illustrated in Figure 5.6.

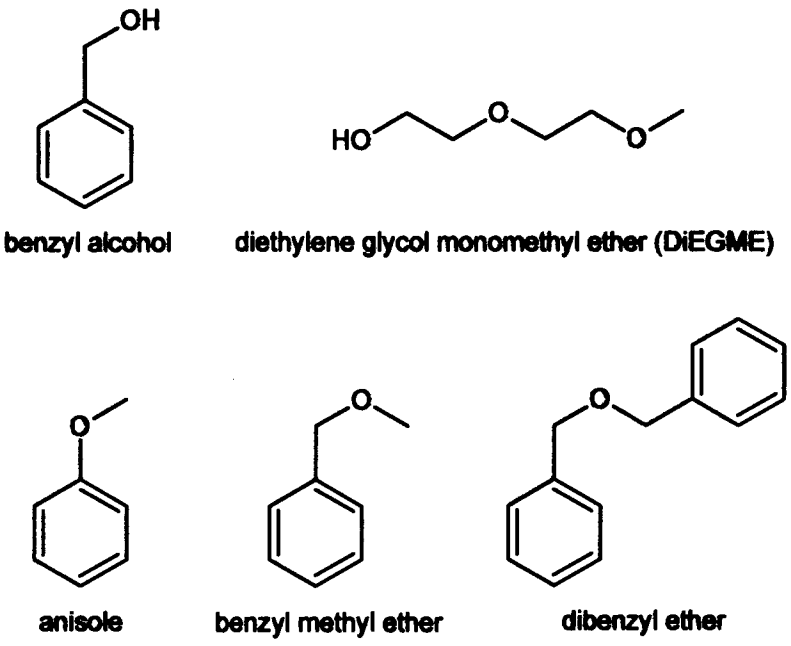

Figure 5.6: Chemical structure of oxygenates investigated

DiEGME was included with the aromatic ethers because it is a non-aromatic polar compound which has similar solubility parameters to benzyl alcohol (see Table 3.1). It is used as an anti-icing agent by the US Air Force (28).

The degree of swell for samples exposed to the pure oxygenates: benzyl alcohol (BzOH), dibenzyl ether and anisole was initially investigated. The increase in mass for these samples may be seen in Figure 5.7. Anisole was selected in order to investigate the effects of the hydrogen bonding since it is similar in structure and size to benzyl alcohol but does not form conventional hydrogen bonds (H- bonds to N or O). Dibenzyl ether was selected to probe the effect of the presence of more than one aromatic ring. Table 5.4 summarises experimental results as well as the solubility parameters and molar volume for the selected solvents. The data for toluene, the monaromatic solvent with the highest extent of swelling, is provided for comparison. Investigations with the other oxygenated species were carried out in 8% blends in SPK. This is discussed in more detail in section 5.2.

Table 5.4: Solvent properties and experimental summary for the exposure of "as received" O-rings to selected oxygenated aromatic solvents at 50°C

Solvent	Molar volume at 20°C (cm^3mol^{-1})	Solubility parameter ($(MPa)^{1/2}$)				Mass uptake at equilibrium (%)	Calculated volume swelling ratio (%)
		δ_d	δ_p	δ_h	δ_{Total}		
Anisole	108.7	17.8	4.1	6.7	19.5	127.4 (4.4)	158.4
Dibenzyl Ether	190.1	19.6	3.4	5.2	20.6	>200*	>230*
Benzyl Alcohol	103.6	18.4	6.3	13.7	23.8	>155*	>190*
Toluene	106.3	18.0	1.4	2.0	18.1	75.3 ± 2.1	109.3

The values in brackets are the standard deviations of the mean. N = 3.

* Samples exposed to dibenzyl ether and benzyl alcohol did not reach equilibrium in the time allowed

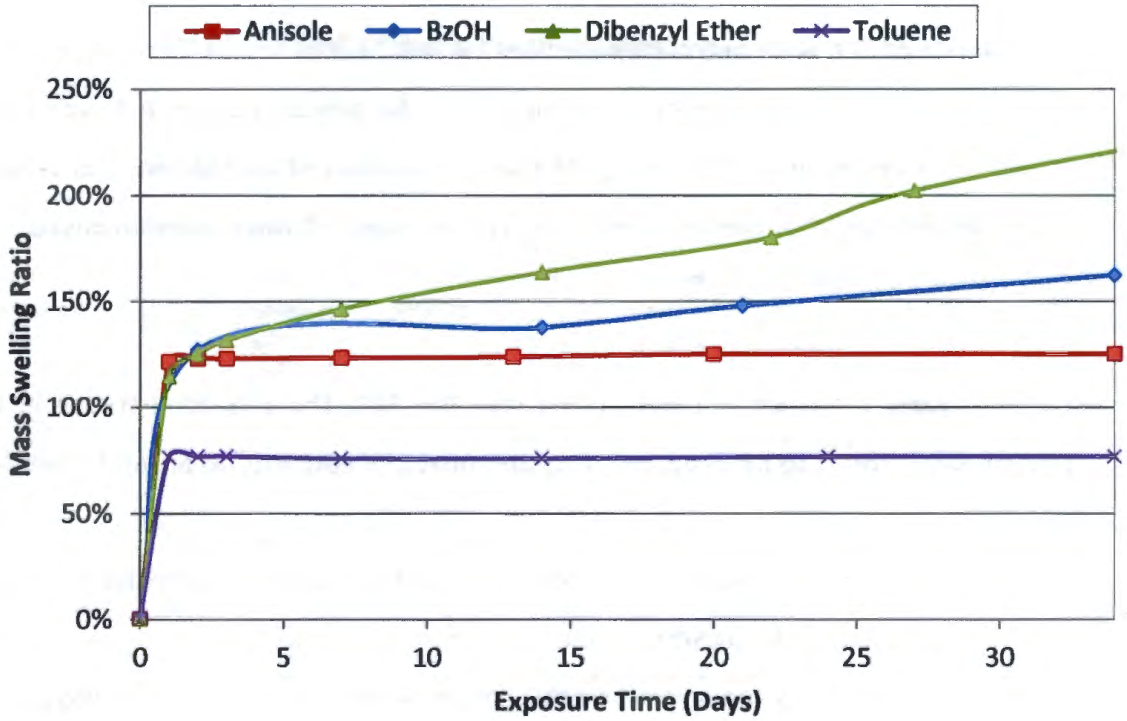

Graphs are plotted as the average of three experiments.

Figure 5.7: Comparison of swelling (measured by mass) ratio for "as received" O-rings exposed to pure anisole, BzOH, dibenzyl ether and toluene at 50°C

Unexpectedly, the extent of mass uptake did not level off when the O-ring was exposed to dibenzyl ether or benzyl alcohol. In the study, it was found that the O-rings exposed to dibenzyl ether could be broken with a minimal effort when pulled apart by hand. Because this effect was not noted when the O-rings were exposed to an 8% (v/v) blend of dibenzyl ether and SPK, it was not explored further.

It is apparent that greater swell occurs when NBR is exposed to aromatic oxygenates than to aromatic hydrocarbons. This is likely the result of increased hydrogen bonding and polar interactions between the nitrile groups of the NBR and the oxygenated solvents. This is reflected in the higher δ_p and δ_h for these solvents than for toluene.

5.2. Blends of SPK with low level components

In a real fuel any such components would be blended at much lower concentrations. The blending of these compounds with SPKs such as those studied here is crucial to determine the effects of their potential use in future applications.

5.2.1. Blends of SPK with petroleum-derived Jet A-1

The specifications for semi-synthetic jet fuel allow the blending of Jet A-1 with up to 50% SPK. In order to assess the effect of the composition of an SSJF on seal swell, a number of SPK : Jet A-1 blends were prepared to which O-rings were exposed. The data is summarised in Table 5.5.

As progressively more Jet A-1 is blended into the SPK, there is an increase in the extent of swell. This is to be expected since the neat SPK contains no aromatic species.

Table 5.5: Swelling of deplasticised O-rings exposed to blends of petroleum-derived Jet A-1 and SPK at 50°C

% Jet A-1	Mass change at equilibrium (%)	Volume change at equilibrium (%) – large O-rings	Volume change at equilibrium (%) – small O-rings
0 (neat SPK)	4.8 (0.1)	8.8 (0.3)	7.7 (0.9)
25	7.0 (0.1)	11.9 (0.3)	11.0 (0.6)
50	9.0 (0.0)	13.9 (0.3)	13.1 (0.4)
75	10.8 (0.1)	17.1 (0.1)	16.1 (0.5)
100 (neat Jet A-1)	14.4 (0.1)	20.7 (0.2)	20.1 (0.6)

The values in brackets are the standard deviations of the mean. The standard deviations for volume changes of small O-rings are larger because the contribution of flash to projected area is larger.

As the Jet A-1 content increases the amount of aromatic species increase and so does swell. The increase in mass uptake and volume change is near linear with % Jet A-1. Note that although deplasticised O-rings swell by 8.9% by volume in SPK, the O-ring has shrunk from its original dimension which it had when it was received because of

the 12.5% volume contraction as a result of plasticiser removal. The trends observed for the small and large O-rings are the same.

5.2.2. Blends of SPK and Aromatic Hydrocarbons

In order to investigate the effect that aromatic blending has on the swelling of O-rings, a number of different blend solutions were prepared. The decision to use predominately 8% volume blends was made so that the stipulated minimum aromatic content required by synthetic jet fuels could be probed (5).

Table 5.6 is a summary of the changes in mass and volume when O-rings are allowed to swell in blends of SPK and aromatic hydrocarbons.

Table 5.6: Solvent properties and experimental summary for the exposure of deplasticised O-rings to blends of aromatic hydrocarbons and SPK at 50°C

Blend component	C No	Molar volume at 20°C (cm^3mol^{-1})	Solubility parameter ($(MPa)^{1/2}$)				Equilibrium mass swelling ratio (%) – large O rings	Calculated volume change due to aromatic (%) – large O-rings	Equilibrium mass swelling ratio (%) – small O rings	Calculated volume change due to aromatic (%) – small O-rings
			δ_d	δ_p	δ_h	δ_{Total}				
Toluene	7	106.3	18.0	1.4	2.0	18.1	9.0 (0.1)	6.2	15.1 (0.5)	7.4
o-Xylene	8	120.6	17.8	1.0	3.1	18.2	8.8 (0.1)	5.8	13.3 (0.4)	5.6
Ethylbenzene	8	122.5	17.8	0.6	1.4	17.9	8.3 (0.1)	5.1	12.8 (0.8)	5.1
Mesitylene	9	139.1	18.0	0.0	0.6	18.0	7.7 (0.1))	4.3	11.8 (0.8)	4.1
Cumene	9	139.4	18.1	1.2	1.2	18.2	7.6 (0.1)	4.1	12.0 (0.5)	4.3
p-Cymene	9	156.6	17.6	1.2	1.2	17.7	6.9 (0.1)	3.8	11.5 (0.2)	3.8
n-Butylbenzene	10	156.1	17.4	0.1	1.1	17.4	7.3 (0.1)	3.7	11.2 (0.5)	3.5
s-Butylbenzene	10	155.5	17.9	1.2	1.2	18.0	7.1 (0.1)	3.4	11.6 (0.5)	3.8
Tetralin	10	136.3	19.6	2.0	2.9	19.9	9.3 (0.1)	5.9	13.7 (0.5)	6.0

The values in brackets are the standard deviations of the mean. Solubility parameters are for the pure blend component (not the weighted average of the blend).

Distortion of the O-rings affected the volume changes measured by observed changes in cross-sectional diameter. This distortion was the consequence of the large O-rings not being perfectly circular. Such deviations from circularity are not an issue when making projected area measurements. The uncertainty in the volume changes determined from the swelling of large O-rings and the closeness of the measured values meant that trends were difficult to discern. Hence volume changes were

measured on small O-rings. Volume changes due to the presence of the aromatic component in the blend were also calculated from mass measurements on large O-rings. The smaller uncertainty in mass measurements allows trends to be discerned for large O-rings. These calculated volume changes may also be found in Table 5.6. The method for this calculation which is based on an accepted method used for calculating volume fractions of rubber in swollen gels may be found in Appendix D. Note that the contribution due to the aromatic is calculated by subtracting the contribution due to SPK. Similar trends were observed for 4% blends of these aromatic compounds in SPK. See Appendix E.

The volume changes calculated from the mass increases indicate that as the carbon number increases (down the table) the extent of swell due to the aromatics decreases. The one exception is tetralin which swell more than expected for reasons discussed above.

5.2.3. Blends of SPK and Aromatic Oxygenates

Measurements were also made on 8% blends of aromatic oxygenates and SPK. Table 5.7 is a summary of the changes in mass and volume when O-rings are allowed to swell in blends of SPK and aromatic oxygenates. Data for toluene and tetralin are included for comparison.

It can be seen from the calculated volume increases, that the calculated volume increase due to these aromatic hydrocarbons exceeds the volume increase of toluene (the aromatic hydrocarbon with the greatest swell) by at least 5.1% (7.4% for small O-rings) and in the case of dibenzyl ether by 11.3% (13.3% for small O-rings) in absolute terms. In relative terms, *i.e.* the increase as a percentage of the volume change caused by toluene is at least 80% (benzyl methyl ether) and 180% for dibenzyl ether. The large increase in swell caused by these aromatic hydrocarbons is driven by the significant increase over aromatic hydrocarbons in the hydrogen bonding parameter, δ_h, and to a lesser extent the polar solubility parameter, δ_p. Interestingly the large molecule, dibenzyl ether, swells the most of the oxygenates which do not possess hydroxyl groups to form conventional hydrogen bonds with NBR.

Table 5.7: Solvent properties and experimental summary for the exposure of deplasticised O-rings to blends of aromatic oxygenates and SPK at 50°C

Blend component	Molar volume at 20°C ($cm^3 mol^{-1}$)	Solubility parameter ($(MPa)^{1/2}$)				Equilibrium mass swelling ratio (%) – large O rings	Calculated volume change due to aromatic (%) – large O-rings	Equilibrium mass swelling ratio (%) – small O rings	Calculated volume change due to aromatic (%) – small O-rings
		δ_d	δ_p	δ_h	δ_{Total}				
Anisole	108.7	17.8	4.1	6.7	19.5	14.6 (0.0)	12.5	21.4 (0.3)	13.7
Benzyl methyl ether	128.7	17.9	4.9	4.3	19.1	13.2 (0.1)	11.3		
Dibenzyl ether	190.1	19.6	3.4	5.2	20.6	19.1 (0.1)	17.5	28.7 (0.5)	21.0
Benzyl alcohol*	103.6	18.4	6.3	13.7	23.8	10.1 (0.0)	6.5	12.4 (0.6)	4.8
DiEGME	118.1	16.2	7.8	12.6	22.0	19.4 (0.3)	18.3		
Toluene	106.3	18.0	1.4	2.0	18.1	9.0 (0.1)	7.3	15.1 (0.5)	7.4
Tetralin	136.3	19.6	2.0	2.9	19.9	9.3 (0.1)	7.0	13.7 (0.5)	5.0

The values in brackets are the standard deviations of the mean. Solubility parameters are for the pure blend component (not the weighted average of the blend). DiEGME and benzyl methyl ether were not tested on small O-rings because of a shortage of solvent.
* 0.5% blend

DiEGME was investigated as it is currently being used in US Air Force jet fuel, JP-8 as an icing inhibitor. The DiEGME level in JP-8 is, however, restricted to only 0.15% by volume in order to reduce foaming (5). It was included at 8% for comparative purposes.

The data shows that the samples exposed to the oxygenated blends at 8% (v/v) show greater mass uptake and volume changes than Jet A-1.

Investigations using lower concentrations of dibenzyl ether were consequently performed.

Figure 5.8 shows the swelling of deplasticised samples in SPK + 2%, 4% and 8% dibenzyl ether to investigate the level of blending components required to produce similar swell as seen in samples exposed to Jet A-1. Table 5.8 summarises the key information.

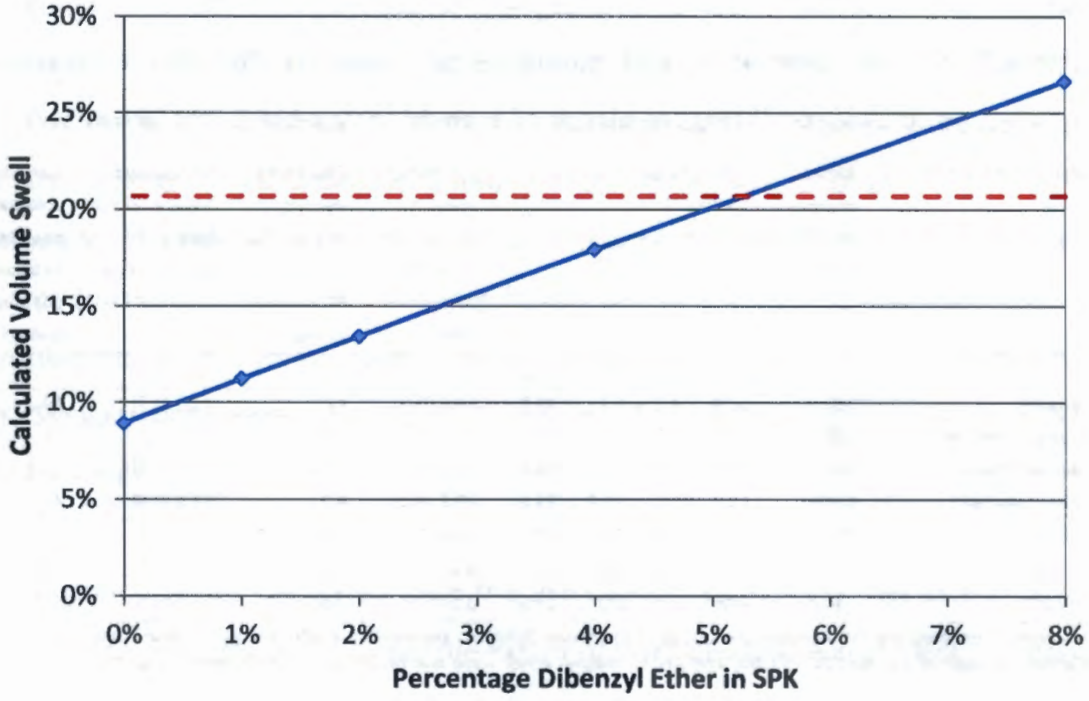

Figure 5.8: Calculated volume swell for deplasticised samples in various concentration of dibenzyl ether in SPK. The red line indicates the swell induced by Jet A-1

Table 5.8: Mass uptake and calculated volume change for deplasticised O-rings in blends of dibenzyl ether with SPK at 50°C

Solution	Average mass uptake at equilibrium (%)	Calculated average volume change at equilibrium (%)*
Jet A-1	14.4 (0.1)	20.7
SPK	4.8 (0.1)	8.9
SPK + 1% Dibenzyl ether	6.7 (0.1)	11.2
SPK + 2% Dibenzyl ether	8.5 (0.1)	13.4
SPK + 4% Dibenzyl ether	12.2 (0.1)	17.9
SPK + 8% Dibenzyl ether	19.3 (0.1)	26.6**

The values in brackets are the standard deviations of the mean. N=3

* includes the volume increase due to SPK component

** Measured change was 26.4

The data suggest that swell similar to Jet A-1 can be achieved with just 5.3% dibenzyl ether and swell, equivalent to that which would be observed for a CTL SPK : JetA-1 blend with 8% aromatics, would lie near 2.2%. The Jet A-1 used in this study contained approximately 18% aromatics by volume (66).

5.2.4. Effect of Temperature on the Swelling of SPK Blends

The effect of temperature on the seal swell ability of SPK additised with benzyl alcohol (BzOH) was investigated because contradictory results were seen in previous research conducted by Visram (17). Visram observed that at ambient temperature the seal swell of samples exposed to Jet A-1 and SPK + 0.5% BzOH had similar seal swell at 48 hours of approximately 8% mass swell. However, in switch loading experiments (where switching occurred every 2 days and that were conducted using the elastomer compression rig at 50°C) a noticeable decrease in swell was observed once the fuel was switch from Jet A-1 to SPK + 0.5% BzOH. This would not be expected if the extent of swell was the same.

The temperature differed between two experiments performed by Visram (17), was the temperature. Bench experiments were performed at ambient temperatures while the rig operated at 50°C.

Figure 5.9 shows the effect of temperature on the swelling of O-rings exposed to SPK + 0.5% BzOH. The graph indicates that O-rings treated at a lower temperature actually reach a greater equilibrium mass swelling ratio which is in excess of the samples exposed to Jet A-1. This is in line with what was observed in Visram's work where it was shown that at 23°C greater swell occurred than Jet A-1. However, at 50°C the behaviour is reversed and the BzOH blend displayed less swell than Jet A-1.

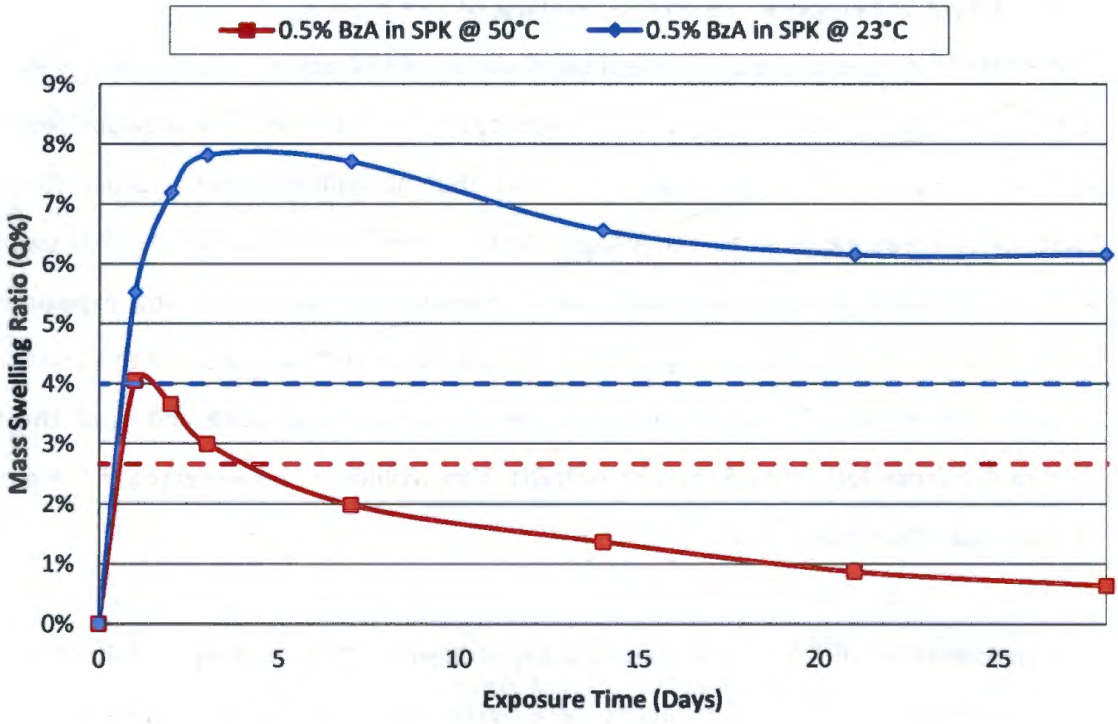

Graphs are plotted as the average of three experiments.

Figure 5.9: The effect of temperature on the swelling of "as received" O-rings in SPK + 0.5% BzOH at 23°C and 50°C. The dashed red and blue lines indicate the extent of swell of samples treated in Jet A-1 at 50°C and 23°C respectively for 300 days.

Further temperature studies were conducted on 8% dibenzyl ether blends. The results obtained for the deplasticised O-rings in SPK + 8% dibenzyl ether for temperatures of 23°C and 50°C can be seen in Figure 5.10. Some of the decrease in swell seen in Figure 5.10 is due to a slight decrease in the swell of SPK (like Jet A-1) as the temperature is increased.

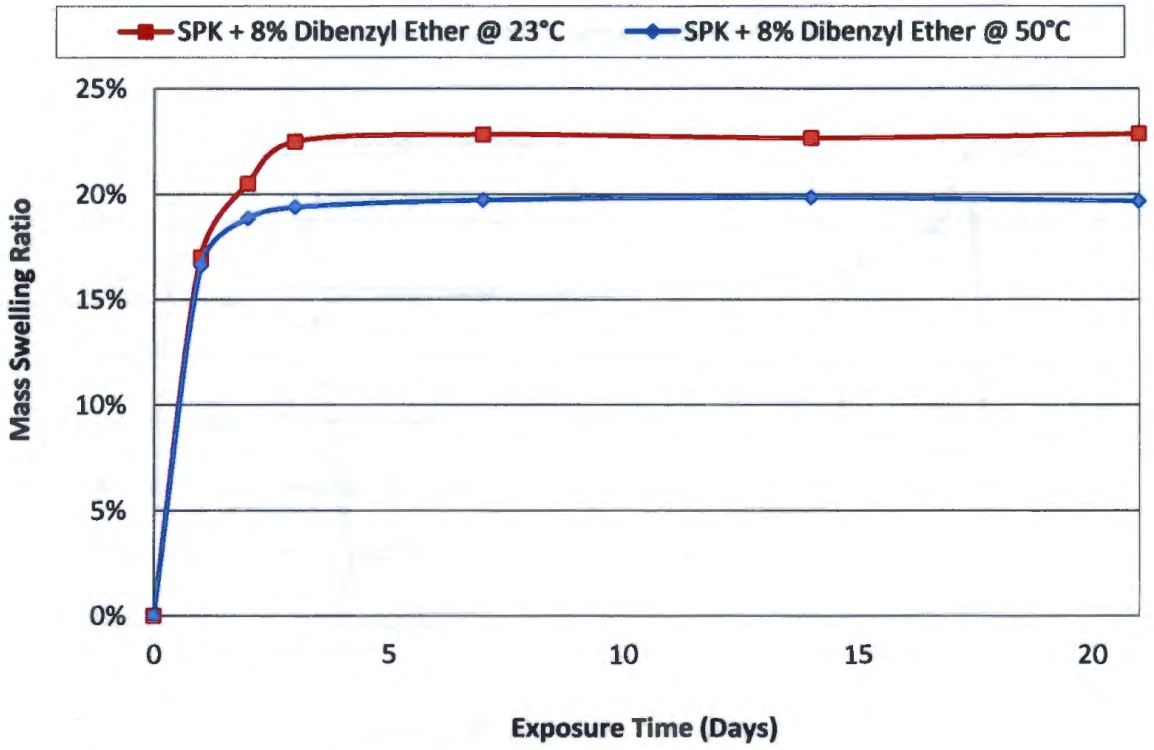

Graphs are plotted as the average of three experiments.

Figure 5.10: Effect of temperature effects on the swelling of deplasticised O-rings in SPK + 8% dibenzyl ether

5.3. Switch Loading

The effect of switching fuel types was investigated by monitoring changes in swell. Figure 5.11 illustrates the potential swelling problem that could arise when switching from Jet A-1 to a purely synthetic paraffinic kerosene without blending components. It can be observed that once the fuel is switched a rapid change in the extent of swelling occurs.

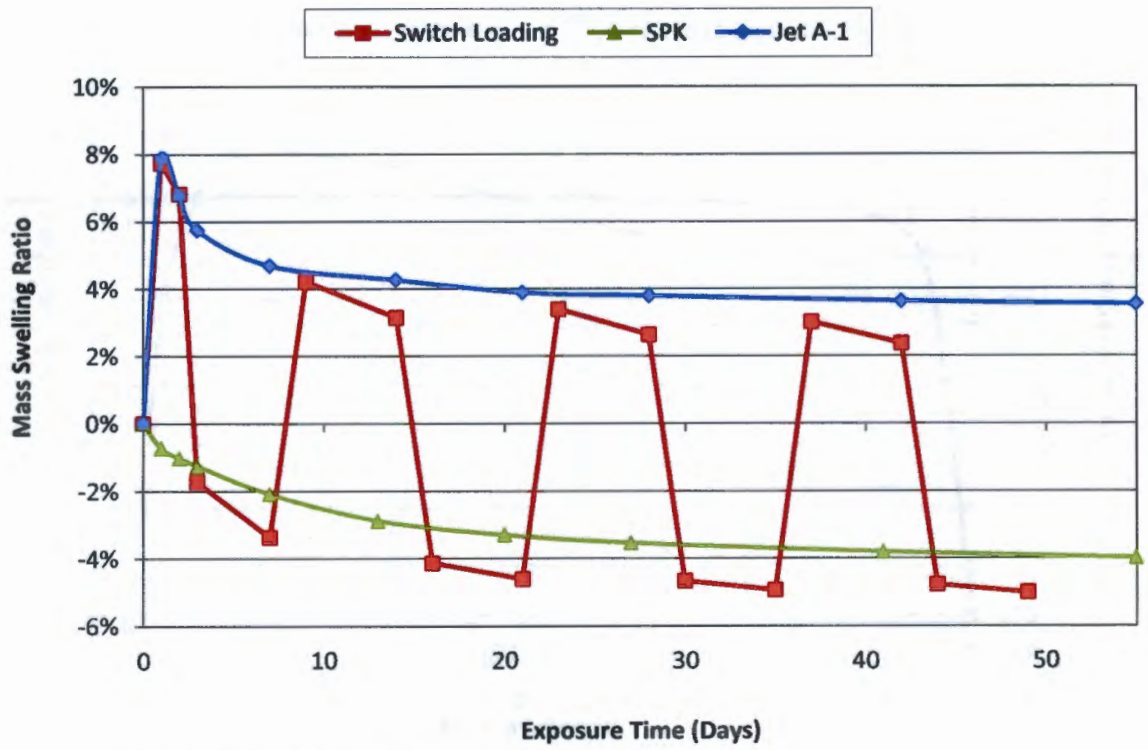

Graphs are plotted as the average of three experiments.

Figure 5.11: Switch loading experiment between Jet A-1 and SPK conducted on "as received" samples. The swelling curves for neat Jet A-1 and SPK are included for comparison.

During the later Jet A-1 cycles of the switch loading experiment, the sample appears not to reach the upper limit of samples in Jet A-1. This is probably because some SPK remains in the sample. When the switch loading experiment solvent was changed to SPK it is observed that the values measured were lower than those for samples exposed to neat SPK. This can be understood by noting that a greater amount of plasticiser would be extracted during the Jet A-1 cycle than would have been extracted by the SPK alone.

Further experiments were performed using deplasticised O-rings. In all subsequent experiments the samples were again exposed to Jet-A1 first. The results can be seen in Figure 5.12.

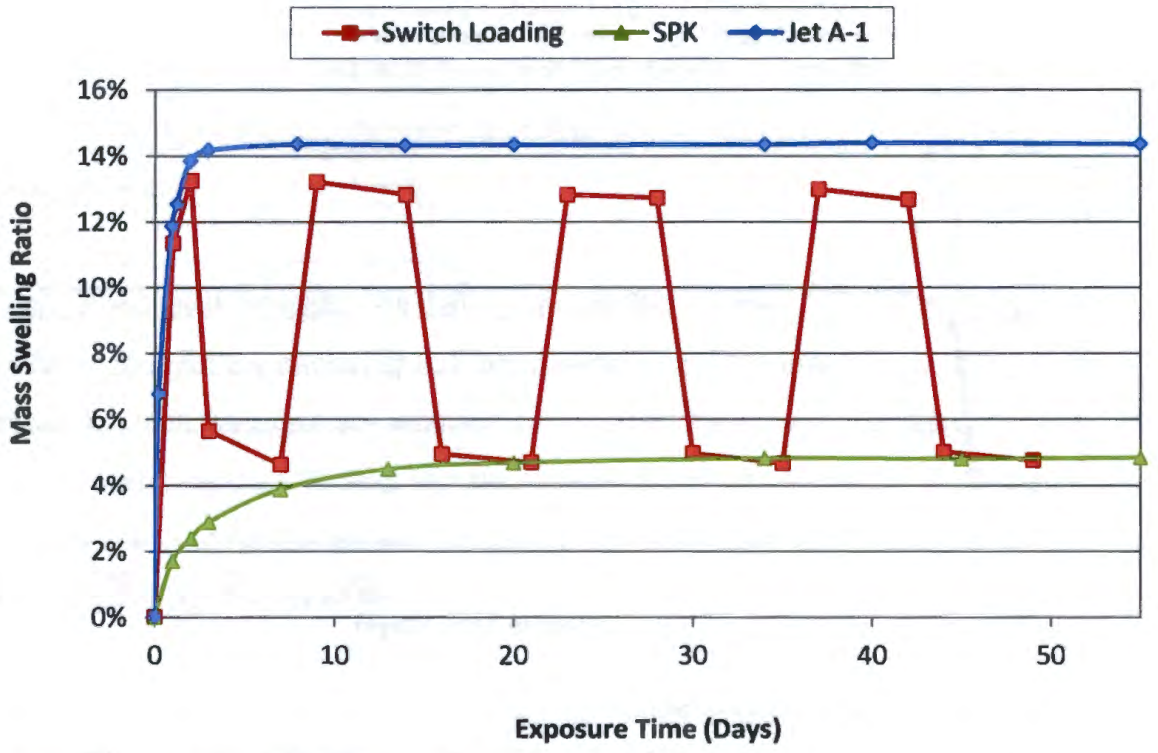

Graphs are plotted as the average of three experiments.

Figure 5.12: Switch loading experiment between Jet A-1 and SPK conducted on deplasticised O-rings. The swelling curves for neat Jet A-1 and SPK are included for comparison.

The swell is contained between upper and lower limits defined by the swell of deplasticised O-rings in the respective solvents when no switching occurs. As before, the maximum swell, during the Jet A-1 cycle did not reach the swell observed for samples treated in neat Jet A-1. The curve does not dip below the neat SPK curve because here plasticiser has been removed prior to the experiment.

The importance of adding blending components to SPKs in order to produce adequate seal swell can be seen when additised blends are considered. Experiments were performed by switching between Jet A-1 and SPK additised with 8% toluene and between Jet A-1 and SPK with 4% dibenzyl ether. The results can be seen in Figure 5.13 and Figure 5.14.

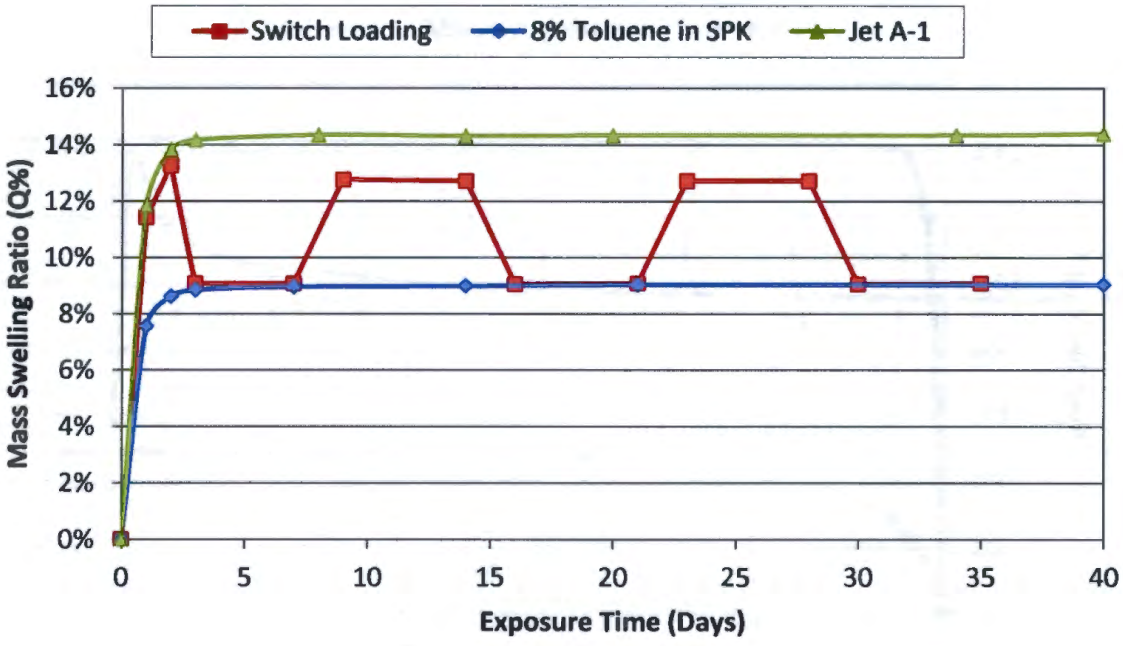

Graphs are plotted as the average of three experiments.

Figure 5.13: Switch loading experiment conducted on deplasticised samples with graphs of O-rings exposed to Jet A-1 and SPK + 8% toluene provided for reference

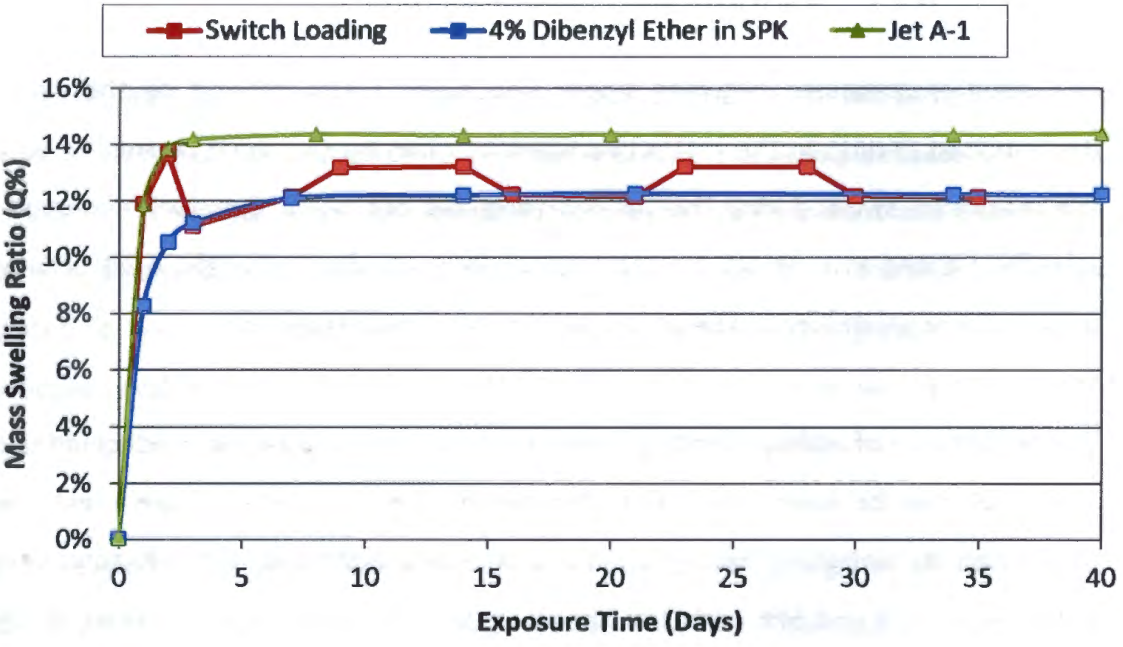

Graphs are plotted as the average of three experiments.

Figure 5.14: Switch loading experiment conducted on deplasticised samples with graphs of O-rings exposed to Jet A-1 and SPK + 4% dibenzyl ether provided as reference

The blend of SPK + 4% dibenzyl ether shows less change than SPK + 8% toluene during switch-loading events. This was expected from previous experiments (Table 5.6 and Table 5.7). At equilibrium the swelling of SPK + 8% toluene is less than that of SPK + 4% dibenzyl ether.

5.4. Blend levels at which the density specification is met

In order to meet the density specification additional components need to be added to the SPKs. Typically these are aromatic compounds since they have higher densities. It can be seen that the GTL SPKs contain more n-paraffins than the CTL SPK in Table 2.4. The Jet A-1 used for comparison contains a significant faction of cycloparaffins. These too increase the density of Jet A-1.

In order to meet the density specification additional components need to be added to the SPKs. Typically these are aromatic compounds since they have higher densities. It can be seen that the GTL SPKs contain more n-paraffins than the CTL SPK in the table. The Jet A-1 used for comparison contains a significant faction of cycloparaffins. These too increase the density of Jet A-1.

The compatibility of synthetic fuels with aviation fuel systems is a particular issue. Strict regulations regarding the levels of aromatics in synthetic jet fuels were introduced in order to prevent potential problems arising from seal swell differences .

Table 2.4 contains a comparison of the properties of Jet A-1 with various synthetic paraffinic kerosenes. The table indicates that pure SPKs would fail to meet the required density specification. By the addition of blend component to the synthetic kerosene, the density can be raised to the minimum density of 0.771 g/cm^3 at 15°C (4). Table 5.9 indicates the volume percentage of the aromatics tested here that

would be required to meet the minimum density specification if they were added to the CTL SPK and GTL SPK used in this study.

Table 5.9: Solvent blend percentage required in order to obtain minimum jet fuel density specification of 0.771 g/cm^3

Solvent	Blend percentage of fuel solvent in CTL SPK at which specification is met (%)	Blend percentage of solvent in GTL SPK at which specification is met (%)
Jet A-1	17.2	55.5
Cumene	6.2	28.4
Tetralin	3.1	15.4
Anisole	2.7	13.9
Benzyl alcohol	2.2	13.6
Dibenzyl ether	2.2	13.6

These calculations show that CTL SPK + 2.2% dibenzyl ether is sufficient to meet the density specification for Jet A-1. It can be seen, however, that in the case of the GTL SPK tested a considerably greater amount of blending components is required to meet the minimum density specification. This is due to the density of this particular GTL SPK being much lower. The GTL SPK blend with cumene which met the density specification would in fact fail the maximum aromatics specification for jet fuel.

5.5. Discussion

The effect that different chemical classes have on seal swell are discussed in the following sections.

5.5.1. Paraffinic Isomers

5.5.1.1. Paraffinic Structure

For a particular carbon number, the equilibrium swell observed for the n- and iso-paraffins were similar. What differed was the rate at which solvent absorption occurred, with n-paraffins absorbing faster than iso-paraffins. The initial increase

observed for the n-paraffins can be attributed to the molar volume being slightly smaller. This leads to the n-isomers reaching equilibrium sooner than the iso-isomers.

Cyclic paraffins swelled NBR to a greater extent than n- or iso-paraffins. This increased swell means that SPKs which contain more cyclic paraffins would require less aromatics to swell sufficiently. The higher density of cyclic paraffins would also mean that less aromatic species would be required to meet the density specification. The greater swell obtained with samples exposed to the cyclic-paraffins can be attributed to both the greater solubility parameter of the cyclic paraffins as well as their lower molar volumes compared to other isomers. A comparison of the n-hexane and cyclooctane data is informative. These two compounds have similar molar volumes (cyclooctane's is slightly higher) yet the mass increase is 5.5% for cyclooctane but -2.4% for n-hexane. This highlights that as soon as cyclic alkanes are included, the effect of the solubility parameter becomes significant.

5.5.1.2. The Influence of Molar Volume

The lower the carbon number, the greater was the swell observed. This was observed for both n- and iso-paraffins. As the carbon chain length increases so does the molar volume and the solubility parameter. However, the influence of the increase in solubility parameter appears not to be significant. This is because n-paraffins have no polar and hydrogen bonding interactions which means that the solubility parameter is dominated by the dispersion term. Although δ_d increases this is solely because the area of contact increases, a natural consequence of the increase in molar volume.

The smaller n-paraffinic molecules display the greatest gravimetric and volumetric increases in swell. Results in the literature support this observation (2). This can be further explained by considering Equation 2.7 which shows the Flory-Rehner polymer-solvent interaction equation (14). The higher χ, the lower is the swell. Thus care needs to be taken when predicting swell purely based on solubility parameters, especially if the interaction is caused only by dispersion forces in systems in which the interaction between the solvent and elastomer is weak to begin with ($\Delta\delta_d > 3.5$).

This has particular implications for the production of synthetic fuels. Synthetic jet fuels typically consist of paraffins in the C9 to C15 range. Lighter synthetic fuels, having a greater fraction of C9s and C10s would display greater swell. Corporan *et al.* (10) in fact observed that synthetic fuels (FT fuels and hydrogenated esters and fatty acids) with lower final boiling points, *i.e.* lighter fuels, swelled slightly more than heavier fuels.

The use of light fuels, however, would mean that the fuels density would be lower, making it harder to meet the specification. Furthermore, light compounds would impact on the flashpoint and distillation gradient of the fuel which are also specified (6).

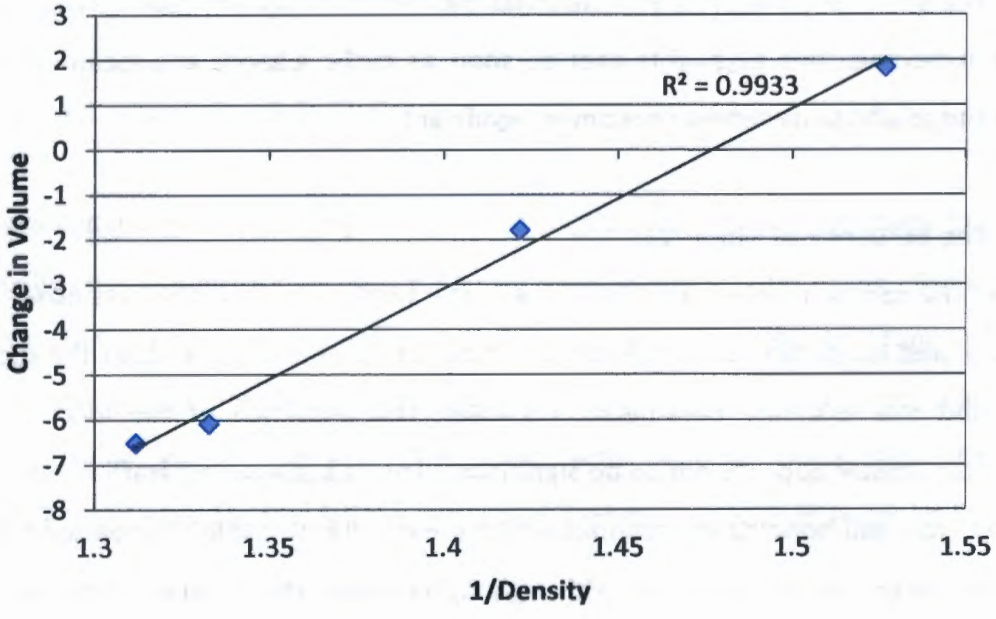

Figure 5.15: Correlation between volume change and the inverse of density caused by the exposure of "as received" O-rings to pure n-paraffins at 50°C

Analysis of the data suggests that a relationship between density and the degree of swell caused by linear paraffins might exist. The correlation between volume change and the inverse of density for the volume swell for "as received" O-rings can be seen in Figure 5.15.

The higher the density the less is the swell observed. The correlation between the inverse of density and volume change has $R^2 = 0.993$. The correlation of molar volume and volume change is less robust ($R^2 = 0.940$).

5.5.2. Blends of SPK and petroleum-derived Jet A-1

The data suggest that swell increases linearly with the content of Jet A-1 present in a blend with SPK. The actual aromatic content of the Jet A-1 used in this study is 18% (17) (66). No obvious interaction behaviour can be observed which would result in swelling behaviour above or below the linear trend. This is not surprising given the n-/iso-paraffinic nature of SPK. The relationship is illustrated in Figure 5.16.

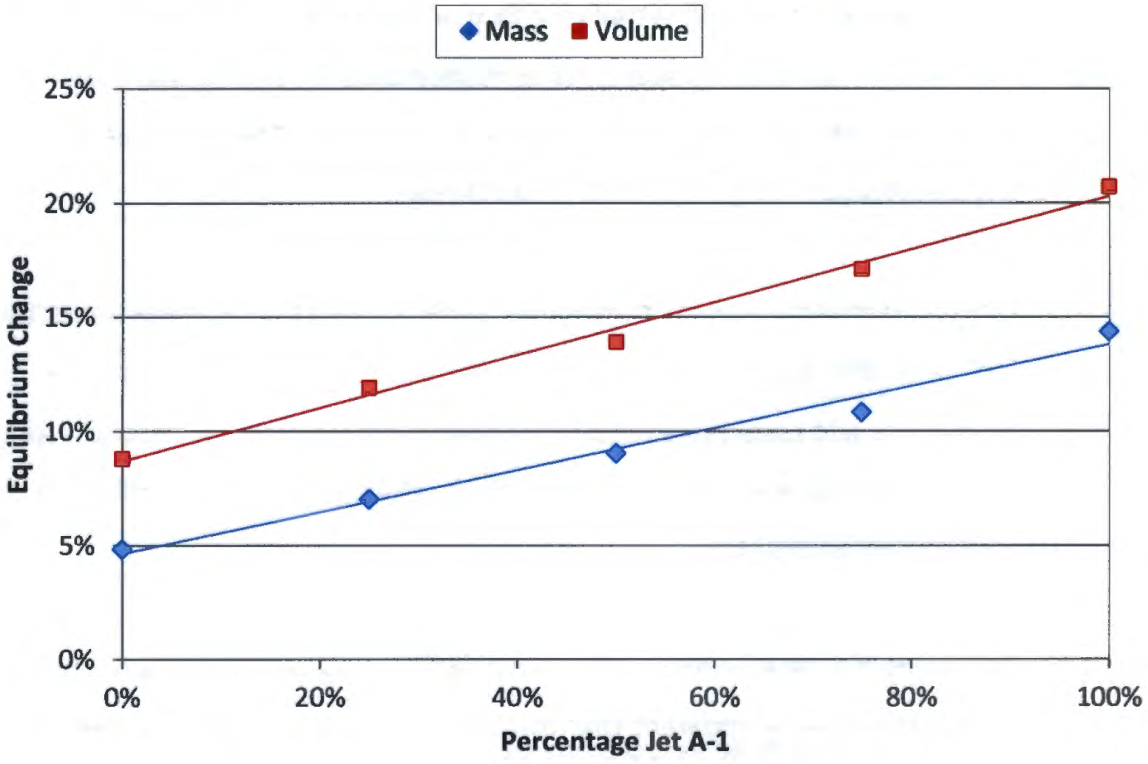

Figure 5.16: The relationship between change in swell at equilibrium and Jet A-1 content in CTL SPK : Jet A-1 blends

5.5.3. Blends of SPK and Aromatic Hydrocarbons

All the blends which contained aromatic hydrocarbons were observed to swell more than SPK (Table 5.6). By comparing the overall volume increase with that when the O-rings were exposed to SPK alone, the volume increase due to the aromatic can be estimated. The calculated volume increase due to the aromatic components (large

O-rings: 3.4-6.2%; small O-rings 3-5-7.4%) compares with that due to the SPK (large O-rings 8.9%; large O-rings 7.7%) which is surprising given that they constituted only 8% or the original blend. This indicates that the aromatic components constitute between 25 and 50% of the solvent/fuel in the O-ring. This is indicative of preferential uptake whereby the aromatic components are concentrated in the O-ring.

The data reveals a strong molar volume effect. The average increase for large O-rings due to the aromatics are 6.2% for the C7 aromatic (toluene), 5.5% for the C8 aromatics, 4.2% for the C9 aromatics and 3.6% for the C10 aromatics (tetralin excluded). The respective values for small O-rings are 7.4%, 5.4%, 4.2%, 3.7%. Of the C10 aromatics, however, tetralin has both a small molar volume and also higher δ_d, δ_p and δ_h. The increase in seal swell with increased δ_p and δ_h and lower molar volume is consistent with the results of Graham *et al* (2). The contribution due to tetralin is 5.9% (large O-rings) and 6.0% (small O-rings).

Within the C8 aromatics o-xylene contributes more to swell than ethylbenzene. This is consistent with the larger δ_h for o-xylene. No significant difference can be seen between cumene and mesitylene despite the former having higher δ_p and δ_h. It should be borne in mind, however, that the estimates for the solubility parameters provided by Hansen contain errors (47).

If one compares the data for these compounds with tetralin which has a similar molar volume, it is immediately apparent that the latter has a much higher degree of swell which can be ascribed to its much greater ability to form polar and hydrogen-bonded interactions. This was also observed by Graham *et al.* (2) for new NBR O-rings but not in fact for deplasticized O-rings. However, Graham *et al.* (2) did not allow their O-rings to reach equilibrium which may account for this anomalous result.

The results indicate that the extent of swell is highly dependent on the type of aromatics being blended with SPK. This has implications for any industrial process used to provide aromatics to be blended to make a FSJF. The results here suggest that monoaromatics with 8 and 9 carbons would provide better swell. However, the

flashpoint of ethylbenzene and xylene are 20 and 25°C respectively. Toluene is 4°C (62). The minimum flash point that Jet A-1 is allowed to have is 38°C which means these compounds are not suitable as blend components (28). The flashpoints of cumene (44) and mesitylene (48) are above the minimum, although below that required by the US Navy. Because of fire risks at sea, the flash point for JP-5 is more stringent at 60°C (28). Furthermore, large volumes of C9 compounds would also not be suitable because more would be required to meet the density specifications (Table 5.9). They would also make it more difficult to meet a distillation slope specification for FSJF.

C10 and heavier compounds would be more suitable for density and flash point reasons although they come at the expense of less swell. Visram in fact noted much less swell than toluene for C12 aromatics (hexyl benzenes) although his results must be treated with caution given the lower diffusivity of C12 aromatics than toluene (17) and the fact that he made measurements after just 2 days. The exceptions are cycloalkyl aromatics such as tetralin. Not only would they swell more, but they have high density, their boiling points are higher (impacting on distillation slope less) and their flash points are higher. That of tetralin is 77°C (62). Because petroleum-derived Jet A-1s may contain more than 5% C11 and higher compounds and significant fractions of C10 (3-4%) aromatics, the seal swell observed for the 50:50 SPK:JetA-1 blend appears higher than expected. However, this is because the JetA-1 used in this study contains cycloalkyl aromatics (5%), polyaromatics (4%) and cyclic paraffins (22-27%).

It can be expected, as is the case where not all SPKs producing the same swell, that among jet fuels those with lower naphthalene and cycloalkyl aromatic content would swell less.

Anderson (3) concluded that the specification where aromatic content is specified should also indicate the ability of an aromatic to be a good "hydrogen bond" donor. Anderson proposed that it may be the combination of aromatics, polar species and heteroaromatics in petroleum-derived fuel that actually lead to the observed swell

and not entirely on the aromatic content. This is consistent with the observation that a higher δ_h, as seen with tetralin, is beneficial for swell. Anderson worked with naphthalene which has a much higher δ_h (5.9) (47). Naphthalene content in Jet A-1, however, is limited to 3% (v/v) because it is known to be a strong soot-producing agent (5).

5.5.4. Blends of SPK and Aromatic Oxygenates

Although aromatic phenols and alcohols have been studied before (17) (27), this study is the first to report on aromatic ethers. It was observed that aromatic oxygenates swell even more than aromatic hydrocarbons and can provide the same swell at lower concentrations. In particular dibenzyl ether and benzyl alcohol were seen to swell significantly for reasons discussed below.

Despite its molar volume which is larger than any of the aromatic hydrocarbons and oxygenates tested, dibenzyl ether swells O-rings significantly. This is driven by its higher solubility parameters (δ_d, δ_p and δ_h) than the aromatic hydrocarbons. Significantly this result and that for tetralin suggest that dispersion interactions (reflected by δ_d) are still significant.

It should be noted (Table 3.1) that the presence of ring structures (aromatic and hydrocarbon) increases the dispersion solubility parameter. Both dibenzyl ether and tetralin have more than one ring which would explain the greater δ_d of these compounds compared to monoaromatic compounds, *e.g.* toluene (δ_d = 18.0). This suggests that the influence of δ_d on the swell induced by aromatic compounds should not be completely ignored when predicting an ideal swelling agent. Graham *et al.* noted the influence of δ_p and δ_h but ignored the influence of δ_d in aromatics. This is may be because of the low variation in δ_d in their experiments (2).

The measurements made here are indicative of preferential uptake whereby compounds in a mixture are absorbed to a greater extent than others. This was observed for both aromatic hydrocarbons and oxygenates. It is suggested that the

aromatic species are being concentrated in the O-rings over the paraffins. Table 5.10 indicates the concentration factor for both the hydrocarbon and oxygenate aromatics. It is calculated as a ratio of the volume fraction of the component in the blend and in the O-ring. The latter is calculated as discussed in Appendix D.

Table 5.10 Concentration factors of aromatic compounds during swelling

Blend component	Molar volume at 20°C (cm^3mol^{-1})	Solubility parameter ($(MPa)^{1/2}$)				Volume % in O-ring – large O-ring	Concentration factor – large O-ring	Volume % in O-ring – small O-ring	Concentration factor – small O-ring
		δ_d	δ_p	δ_h	δ_{Total}				
Toluene	106.3	18.0	1.4	2.0	18.1	41.0	5.1	48.9	6.1
o-Xylene	120.6	17.8	1.0	3.1	18.2	39.4	4.9	42.1	5.3
Ethylbenzene	122.5	17.8	0.6	1.4	17.9	36.6	4.6	39.8	4.9
Mesitylene	139.1	18.0	0.0	0.6	18.0	32.5	4.1	34.7	4.3
Cumene	139.4	18.1	1.2	1.2	18.2	31.7	4.0	35.8	4.5
p-Cymene	156.6	17.6	1.2	1.2	17.7	26.0	3.2	32.8	4.1
n-Butylbenzene	156.1	17.4	0.1	1.1	17.4	29.4	3.7	31.4	3.9
s-Butylbenzene	155.5	17.9	1.2	1.2	18.0	27.6	3.5	33.3	4.2
Tetralin	136.3	19.6	2.0	2.9	19.9	39.9	5.0	43.7	5.5
Anisole	108.7	17.8	4.1	6.7	19.5	58.5	7.3	64.0	8.0
Benzyl methyl ether	128.7	17.9	4.9	4.3	19.1	55.9	7.0		
Dibenzyl ether	190.1	19.6	3.4	5.2	20.6	66.2	8.3	73.2	9.2
Benzyl alcohol*	103.6	18.4	6.3	13.7	23.8	42.1	84.2	38.0	76.0
DIEGME	118.1	16.2	7.8	12.6	22.0	67.3	8.4		

Data for 4% blends may be found in Appendix E. The high concentrating effect can be seen. This is caused by polar and hydrogen bond-like interactions with NBR. The latter are not conventional hydrogen bonds but result from interaction of the nitrile group and the partial positive charges on the hydrogen atoms (67). Interestingly the concentration factor reported for alkyl benzenes over alkanes during swelling of NBR in Jet A-1 that is reported by Graham *et al.* (2) is 3.4 which is of a similar order to that reported here.

These compounds do not have hydrogen atoms which are capable of forming conventional hydrogen bonds with the nitrile group of NBR. Benzyl alcohol, by contrast, is capable of such an interaction and this is reflected in its much higher concentration factor than dibenzyl ether. Interestingly, this is not reflected in the pure compounds where the % volume change after 2 days was 125% and that of benzyl

alcohol was 127%. This suggests that the nitrile groups are swamped at higher concentrations and that this concentration effect would be concentration dependent. DiEGME, which was also included in the test matrix is highly polar. This accounts for the high swell observed although, despite having a hydroxyl group like benzyl alcohol, the concentration effect was similar to the aromatic ethers. This would suggest the hydrogen bond formed by benzyl alcohol with NBR is very strong, in contrast.

The results, observed with aromatic oxygenates, further support Anderson who noted the importance of a solvent being good hydrogen bond donor to improve seal swell ability (3). As noted previously, Anderson proposed that the swell due to Jet A-1 is also influenced by polar species and heteroaromatics in petroleum-derived fuel. Note though that even n-paraffins contribute to swell as demonstrated by SPK swelling deplasticised O-rings.

5.5.5. Effect of Temperature on the Swelling of NBR O-rings

In all cases, where measurements were made, swell was reduced at elevated temperature. This is in contrast to Mostafa *et al.* (43). Note though that Mostafa *et al.* (43) worked with pure compounds and made measurements at 48h before equilibrium had been reached. Importantly, the swell of blends with benzyl alcohol was significantly reduced as the temperature rose, while the decrease for other blends was less. Where studies on the swelling of elastomers by jet fuel do report temperatures, the experiments are at one temperature only which is room temperature (2).

By comparing the swell due to the aromatic species at 23 and 50°C it was found that approximately 6% additional mass swell (absolute terms) was estimated to be the benzyl alcohol at 50°C while this is closer to 11% additional swell at 23°C. The contribution of each % benzyl alcohol to the total swell was thus increased by about 85% in relative terms when the temperature was lowered. By way of comparison the extra contribution to the extent of Jet A-1 of dropping the temperature was only 8% in relative terms (see Figure 2.1). Because of a decrease in density, the magnitude of the

changes would be reduced if determined for volume changes. Nonetheless, the change for Jet A-1 would still be much less than that for benzyl alcohol.

As was observed during the dibenzyl ether investigation, the experiments conducted at 23°C showed a greater degree of swell. The relative change observed for the dibenzyl ether blend was, however, not nearly as large as seen in the exposure experiments with benzyl alcohol. The increase in swelling upon cooling is only 15% in relative terms.

Link *et al.* (27) and Visram (17) noted the potential of benzyl alcohol as a seal swell promoting additive. Visram, however, observed a similar temperature effect when O-rings were exposed to BzOH. He, however, made no comment on these results (17).

Visram showed that at ambient temperature the seal swell of samples exposed to Jet A-1 and SPK + 0.5% BzOH had similar seal swell at 48 hours, of approximately 8%. His results are presented in Figure 5.17.

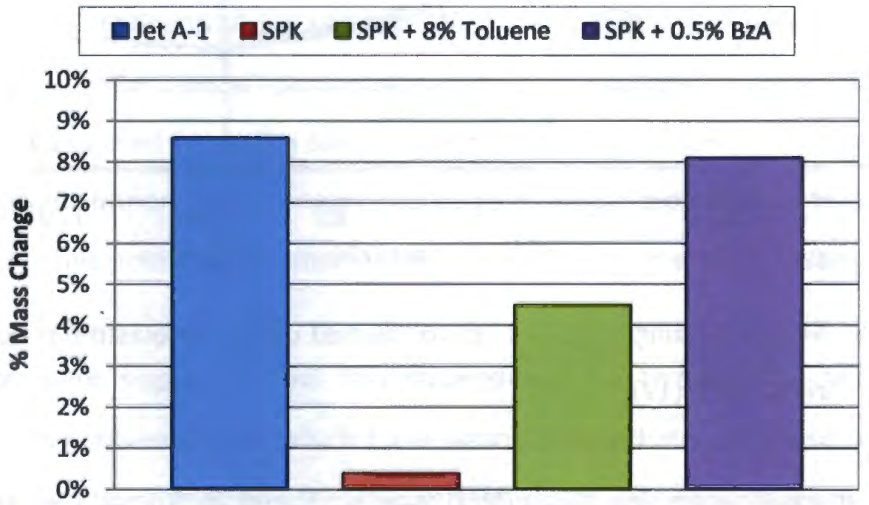

Figure 5.17: Percentage mass change for NBR O-rings exposed to Jet A-1, SPK, SPK + 8% Toluene and SPK + 0.5% BzOH for 48 hours at 23°C (Adapted from Visram (17))

Similar extents of swell were not obtained for samples exposed to SPK + 0.5% BzOH in later switch loading experiments using the elastomer compression rig at 50°C. The results from the switch loading experiment showed a notable decrease in swell once

the fuel was switch from Jet A-1 to SPK + 0.5% BzOH. By contrast a switch from Jet A-1 to fresh Jet A-1 saw the swell unaffected (the light blue curve below). This can be seen in Figure 5.18. The vertical lines indicated the points where fuel was changed. When Jet A-1 was added back the swell rose back to where it was previously. This can be clearly seen in the dark blue curve (a switch from Jet A-1 to Jet A-1 and then to a SPK/ BzOH blend) and the orange curve (a switch from Jet A-1 to an SPK/BzOH blend and back to Jet A-1). Visram (17) also observed the effect when a 1% blend of SPK/BzOH was switched with Jet A-1).

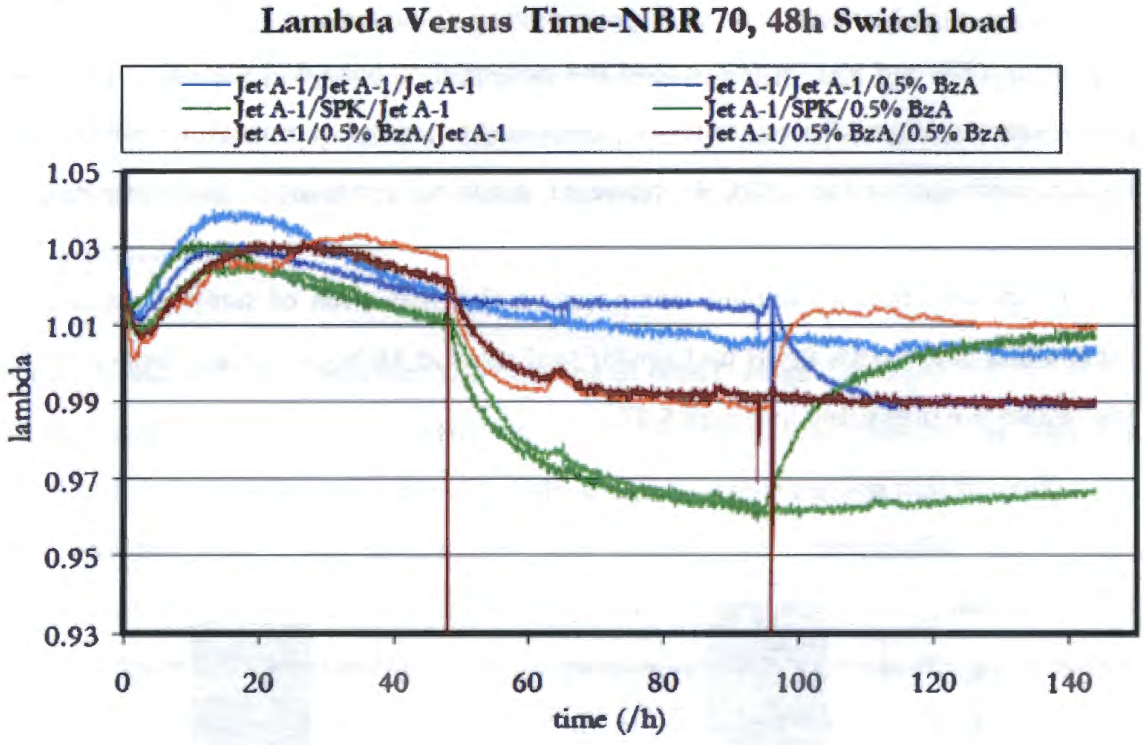

Figure 5.18: Switch loading experiments conducted using the elastomer compression rig at 50°C (17)

A proposed explanation for this effect may be found in Yamada *et al.* (31). As temperature is increased the average force of attraction decreases as molecules move apart; thus at lower temperatures more swell is observed (68). The effect is smaller for Jet A-1 because there are no conventional hydrogen bonds.

As polymeric swell is caused by the mixing of the solvent with the polymer, Gibbs free energy can be used to describe this system. Swelling increases the entropy resulting in a lowering of the free energy which is the driving force for swelling. In typical systems

the enthalpy of mixing is positive (endothermic) or sometimes slightly exothermic. Consistent with the Van't Hoff equation (Equation 2.8), this would imply a greater swell in the endothermic case as temperature rises. The size of ΔH_{mix} is small, however, and the dependence is thus small.

However, in the case of hydrogen bonded systems, the enthalpy of mixing is larger and negative (69). This means that as temperature rises, the equilibrium constant decreases and so less swell is observed. The larger the size of ΔH, the larger would be the temperature dependence. The high increase in concentration of BzOH in the O-ring over the base fuel as indicated by the concentration factor and the predictions of Yamada *et al,* all point to a strong hydrogen bond and consequently exothermic mixing (31). This then explains the strong negative dependence of BzOH swell on temperature.

It is thus suggested that, in addition to the criteria for an ideal fuel additive, *i.e.* that they should produce similar swell as conventional petroleum-derived fuels, be effective at low concentration, not introduce significant environmental or toxicity hazards and not alter fuel properties adversely (27), another be added, *i.e.* that the extent of swell caused by such a component not be strongly temperature dependent. This is especially import for jet engine fuel systems which are exposed to variations in temperature. This points to the importance of elevated temperature testing.

It is furthermore suggested that this dependence on temperature will be more pronounced for solvents/fuels which form strong interactions, *i.e.* those with high δ_p and δ_h. However, confirmation of this hypothesis would require testing with a number of components with δ_h which are not suitable for inclusion in jet fuels, *e.g.* chlorinated compounds and so was deemed beyond the scope of this study.

5.5.6. Switch Loading

The final part of this study was to determine the effects that switch loading has on seal swell with pure and additised synthetic fuels. This illustrates the potential

problem that could occur should fuel be switched in service from a petroleum-derived fuel to pure synthetically derived kerosene. Here, the experiments where the fuel was switched from Jet A-1 to SPK demonstrate an extreme case with a rapid change in seal swell occurring once the fuel was switched to the SPK. This change resulted in a degree mass swell of approximately 8% in 24 hours. Thus, it can be expected that if similar fuel switching were to take place in service, any failure that may follow due to the change in O-ring volume would occur fairly rapidly.

The experiments conducted on "as received" samples showed that the seal swell observed during the SPK cycle was somewhat lower than that of samples solely exposed to SPK. This is due to the greater rate of plasticiser extraction during the Jet A-1 cycles. This shows that the rate of plasticiser extraction is dependent on the solvent being used and is accelerated during the treatment in Jet A-1.

In both "as received" and deplasticised samples undergoing switch loading tests the swell obtained during the Jet A-1 cycles which followed the SPK exposure steps did not reach the expected upper limit, this is presumed to be due to residual SPK remaining in the sample. As SPK has a lower density than Jet A-1 the mass swelling ratio is expected to be less than samples solely exposed to Jet A-1. Similar observations were also made by Lamprecht (70) and Visram (17), the results of whom can be seen in Figure 5.19 below (17).

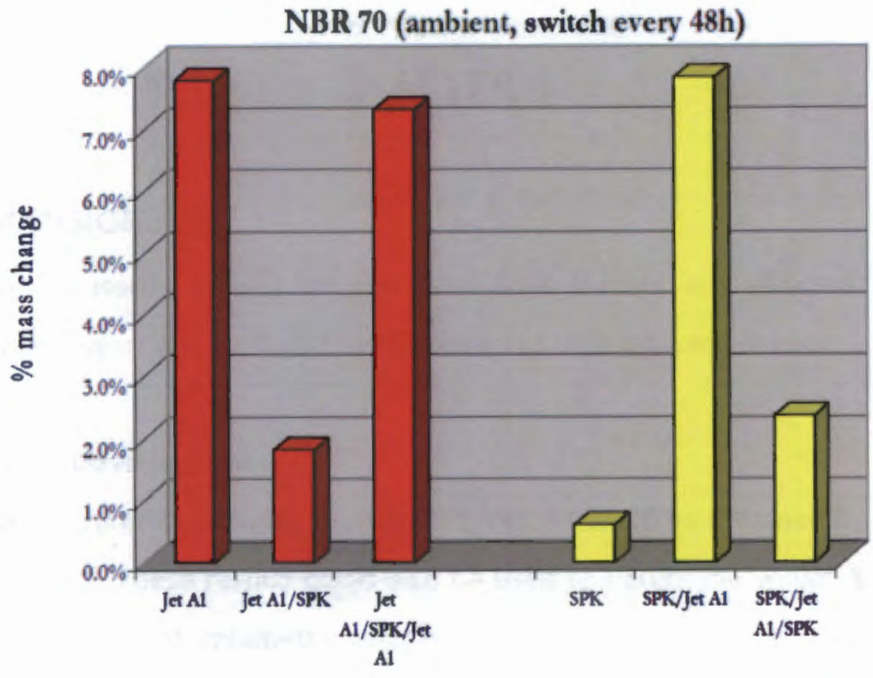

Figure 5.19: Switch loading investigation, switching between Jet A-1 and SPK (17)

CHAPTER 6

6. CONCLUSIONS

This study focused primarily on the how NBR O-rings are affected by various components in synthetic jet fuel. The following conclusions were drawn:

6.1. Method Development

It was demonstrated that highly repeatability results could be obtained by monitoring changes in mass. These results could also be used to determine volumetric changes. The measurements of volumetric changes, however, could not be achieved using methods in the ASTM method D1414 (15). The use of a micrometer was too crude. More success was achieved by changes in volume using a microscope. These changes correlated well with those predicted from the gravimetric measurements. Unfortunately the method of calculating volume changes from dilatometric measurements (Equation 3.2) meant that the uncertainty was cubed. This did not allow the method to discriminate between small differences as was observed during the study on blends of aromatics with SPK. However, the use of small O-rings and the measurement of projected areas reduced the uncertainty, allowing these small differences to be discriminated. The use of area changes rather than cross-sectional diameter changes also greatly speeded up the collection of data.

It was noted that the temperature, duration of the experiment and whether plasticisers were present have a significant effect on the results obtained. By contrast the fuel:rubber ratio had no effect over the range tested.

Typically in the literature, the temperature, experiment duration and O-ring conditioning are not reported which makes the comparison of results difficult. In some cases temperature is not controlled while in many measurements are made early (1 to 2 days) on "as received" O-rings. The latter is most significant because at this time significant plasticiser remains in the O-rings. Furthermore the derivative of the mass

(or volume) vs. time curves are steep which means that making measurements 3h late, for example, can significantly affect the results.

It is suggested, here, that for comparative purposes measurements be made at equilibrium. However, given the long time to reach equilibrium which may be impractical in some cases, data be collected at elevated temperature, *e.g.* 50°C and after at least a week, preferably two. In the case of poorly swelling systems, *e.g.* SPK this might need to be extended. When small O-rings were used, equilibrium was reached sooner (between 4 and 7 times) because of shorter diffusional path lengths.

Furthermore, it is suggested that experiments for the selection of additives/low level blend components be made on deplasticised O-rings. This eliminates interpretation problems caused by the fact that plasticisers extract into different solvents at different rates. A method for preparing deplasticised O-rings using dichloromethane was reported here. Any other solvent that swells NBR rapidly and significantly could also be used, provided it can be easily removed from the rubber, *e.g.* by evaporation, before further experiments are performed.

Caution must, however, be taken when using the results to infer behaviour at other temperatures. This is especially the case for strongly hydrogen bonding additives such as benzyl alcohol. This may have significant implications for real world systems and in such cases, testing at a variety of temperatures is advised. It is suggested that this might also be the case with systems, without conventional hydrogen bonds, but which have high Hansen polar and "hydrogen-bonding" solubility parameters, δ_p and δ_h.

6.2. Effect of Different Chemical Classes on Seal Swell

Neat FT SPKs lead to seal swell that is less than that caused by Jet A-1. In the case of many plasticised seals this may in fact cause seals to shrink, as was observed here, since the uptake of SPK is less than amount the plasticiser leached out. For this reason, low level blending components might be required and the addition of 8% aromatics in SSJF and FSJF is mandated.

It was observed that smaller paraffins swell NBR both faster and to a greater extent. This effect is strongly determined by the molar volume of the solvent and thus its carbon number and depends little on whether the SPK is n or iso-paraffinic. Swelling was observed to be inversely proportional to density. However, in cases where an SPK contains cycloparaffins, these compounds can be expected to contribute towards seal swell. It is consequently predicted that lighter SPK cuts and those containing napthenes will swell more. The effect on densities and flash point are opposite. The former approach will make achieving density specifications harder and more aromatics would have to be blended from another source to meet specification. Cycloparaffins, by contrast, would improve the density of SPKs.

It has been demonstrated that the number of rings as well as the length and number of the aromatic compounds side-chains under investigation is significant where aromatics are concerned. Again lighter aromatics (smaller C numbers), which have smaller molar volumes, lead to greater swell. However, their use as blending components for SPKs is limited by their negative effects on flash point, density and distillation behaviour. C10 and C11 aromatics would be better in this regard.

The results suggest that aromatics with higher δ_h would improve seal swell as was demonstrated by tetralin. Tetralin contains two rings and that also plays a role. The swelling of O-rings in SPK/dibenzyl ether support the importance of when δ_d aromatic compounds are blended.

Given the restrictions on naphthalenes, the most ideal aromatics to target from a seal swell perspective would be cycloalkyl aromatics such as indanes and tetralins which would require cyclisation of C10 and C11 monoaromatics.

It was shown in this study that aromatic oxygenates, such as the phenolic (anisole) and benzyl (benzyl methyl and dibenzyl) ethers, produce even greater swell. This is consistent with the solubility theory of Hansen since these compounds have higher δ_p and δ_h and in the case of dibenzyl ether higher δ_d values which are closer to those for

NBR (47). Aromatic ethers have been shown to be capable of achieving the same swell as Jet A-1 at levels below the level of aromatics in petroleum-derived Jet A-1s and in some cases (dibenzyl ether) below the minimum 8% aromatic specification.

In fact the swell achieved by 50:50 SPK/Jet A-1 blends can be achieved by all aromatic ethers below the 8% level. The 8% level was derived from analysis of Jet A-1s which are hydrocarbon in nature and was not intended for such oxygenated compounds.

All aromatic species and aromatic oxygenates in particular are concentrated in NBR above their level in the base fuel. This is likely also the case with Jet A-1 where the aromatics present would also be more likely to be absorbed. The equipment available did not allow this hypothesis to be tested. In the case of benzyl alcohol, very strong concentrating of the additive occurred in the O-rings tested which likely indicated a strong hydrogen bond between NBR and the alcohol. This strong interaction is also suggested to be the reason why swelling of benzyl alcohol is strongly temperature dependent since the equilibrium constant for such bonding would be temperature dependent.

It has been clearly demonstrated that the nature of the aromatic species plays a large role in determining the extent of swell. The ideal candidate would have as low a molar volume as possible, be a multi-ring structure and a high δ_h (possibly also δ_p) while still allowing all other jet fuels specifications such as flashpoint to be met.

CHAPTER 7

7. RECOMMENDATIONS FOR FUTURE WORK

A number of recommendations are made for future work:

In this study a number of experimental procedures were investigated. It was found that conventional ASTM methods where mass is measured had the greatest repeatability. The mass measurements, however, do not take into account the density effects of the solvent. It is thus recommended that future studies should attempt to obtain volumetric measurements, either by the refinement of the mass to volume calculation or by making more volume measurements, *i.e.* using more samples.

7.1. Equipment Improvements

Gaining accurate volumetric measurements is challenging. Repeatability, even using microscopy, was lower. Cross-sectional diameter measurements are labour intensive compared to mass measurements. A number of equipment and method improvements are recommended.

7.1.1. Continuous Mechanical Measurements of Dilation

The compression rig has the potential to significantly reduce the labour intensive process of static methods as well as reduce issues of repeatability. The rig also has the potential to simulate in-service conditions and be tailored for ageing tests. A number of adjustments, however, would be needed to be made before the existing rig could be used. Possible changes include the replacement of the expanding silicon tubing with an electronically controlled piston with built in displacement and pressure transducers. This should address the level of mechanical noise and reproducibility between experimental runs. It is also recommended the electrical circuits of the rig be redesigned, as electrical noise would appear to be caused by adjacent cylinder readings. Such a rig could also be tailored for ageing tests.

Another option would be to modify an Elastocon, a commercially available instrument. This instrument is used to study the stress relaxation of O-rings in lubricating oils and could be used in a similar fashion (18). The instrument, would provide data from which swelling would have to be inferred. The data is comparable to the compression pressure seen in the SAFL rig. Like the rig, the Elastocon is designed to take multiple samples.

Recently TA Instruments have released compression clamps that allow dynamic mechanical analysis (DMA) measurements to be made in fluids. These could be used to measure changes in the physical properties as a result of swell and could also be used to monitor changes as swelling occurred. However, the instrument can only operate on one sample at a time. Accelerated testing would have to be done at even higher temperatures, *e.g.* 80°C which could also allow the temperature sensitivity of swelling to be analysed.

Alternatively, such an instrument could be used to investigate any changes brought about in the O-rings as a result of swelling. These O-rings would not necessarily have to be swollen in the DMA but this could be done over a number of weeks on the bench before testing. Since the DMA is more sensitive than DSC to the glass transition temperature, Tg, the relationship between this and swelling could be studied.

7.1.2. Optical Measurements

The amount of uncertainty associated with volumetric measurements could be reduced by measuring cross-sectional areas. Since the O-rings are black, high contrast photographs, suitable for digital area measurement, can be easily obtained. This method has been implemented by Graham *et al.* (49) and was used on small O-rings in the later measurements in this study. An improvement, however, would be to make the process automated in such a fashion that just one camera would be required. Furthermore, the calculations of projected areas could be automated using a computer program. This would increase reproducibility and make the process of obtaining measurements less labour intensive. It would further be possible to provide continuous measurements allowing absorption kinetics to be studied.

It is also recommended that some of the experiments where only mass measurements were made could be repeated using smaller O-rings. Volumetric data should be collected.

7.2. Future Experimental Work

7.2.1. Leakage

The mass and dimensional changes in O-rings investigated throughout this research relied on the comparison of samples exposed to Jet A-1. This, however, does not show the point at which leaking will occur. Consequently seal swell experiments are only a proxy for identifying better or worse fuels but gives no indication on whether a fuel with 8% aromatics would be acceptable in reality and guarantee no leaking. This would require the design of a rig which would mimic how real O-rings are used in jet engines. A method would also be required to accelerate the aging of O-rings and need to include hardening as a result of exposure to hot fuel. This study would then be used to relate leakage behaviour to seal swell so that the latter can be used as a predictor with greater confidence.

7.2.2. Seal Swell of Real Jet Fuel

The importance of cycloparaffins and multi-ring compounds for seal swell has been shown. Most seal swell studies focus only on aromatics and primarily on those of monoaromatics. It is recommended that the variation of swell across real Jet A-1 samples from around the world be investigated. These are expected to be highly variable in terms of their naphthenic (cycloalkane) and naphthalene content. Such a study could be used to assist with setting a baseline for acceptable swell.

7.2.3. Temperature Effects on Seal Swell

Since O-rings in service are exposed to elevated temperatures for prolonged periods of time, these O-rings will undergo changes in their structure such as hardening. This behaviour needs to be further investigated as it is expected that the changes in polymeric structure affects the equilibrium ratio obtained.

Low level blending components such as BzOH are highly temperature sensitive. It is recommended that this sensitivity be further investigated, in particular, the hypothesis that solvents with high δ_h (and δ_p) are more sensitive to temperature. This could be tested with other components such as naphthalene or chlorinated aromatics, although the latter could not be used in real jet fuels.

7.2.4. Concentration of Aromatics in NBR

The measurements made in this study suggest that aromatic components are being concentrated in the O-rings because of preferential absorption. Further kinetic experiments should be undertaken in order to determine the implications that this may have in a real world situations. A specific interest in switch loading experiments should be focused on. This could be further studied by performing desorption analysis on the swollen O-rings, *e.g.* desorption GC-MS or TGA-MS to determine what compounds are preferentially absorbed. This would also validate the conclusions of this study. Such a study could also investigate whether such concentration of aromatics occurs with also with Jet A-1 and to what extent.

7.2.5. Polymer Selection

Although this research specifically focused on NBR O-rings, it is also recommended that similar swelling experiments should be conducted on other polymers, typically used in the jet engine fuel systems, such as Viton and fluorosilicone to investigate whether the observations made for NBR are also applicable to such seals.

7.2.6. The Stability of Blends of Aromatic Oxygenates

This study demonstrated the possibility of using aromatic oxygenates such as dibenzyl ether blends in concentration below 8% to produce similar swell to that of samples exposed to Jet A-1. It is, therefore, recommended that further work be carried out using aromatic oxygenates as a blending components to investigate the effect of such additives on thermal stability.

7.2.7. Polymer degradation

The TGA results in this study on conditioned O-rings showed a decrease in mass of 2.1% at 311.5°C. Investigation into the extraction method should be undertaken, to determine whether changes in polymeric chain structure are occurring. Spectroscopic as well as physical property measurement could be used to address this concern.

In this study it was further found that exposing NBR samples to neat dibenzyl ether showed the greatest swell. Concerns over polymer degradation, however, arose. It is thus recommended that further investigation into the degradation mechanism and kinetics be undertaken. In particular, studies should be performed on 8% dibenzyl ether SPK blends so that service life may be estimated.

CHAPTER 8

8. REFERENCES

1 Daggett, D.; Hadaller, O.; Hendricks, R.; Walther, R. Alternative fuels and their potential impact on aviation. ICAS-2006-5.8.2, 25th ICAS Congress, Hamburg, Germany, **2006**.

2 Graham, J.L.; Rahmes, T.F; Kay, M,C.; Belieres, J.; Kinder, J.D.; Millett, S.A.; Ray, J.; Vannice, W.L. Alternative fuels. FAA Office of Environment and Energy, Washington, DC, **2011**.

3 Anderson, D. How low can you go? Aviation fuel needs to reduce its aromatic content – but by how much?. Mini-project summary report, University of Sheffield, Sheffield, UK, **2011**.

4 Moses, C. A. Comparative evaluation of semi-synthetic jet fuels. CRC Project No. AV-2-04a, Alpharetta, GA, **2008**.

5 DEF STAN 91-91, Issue 7, Turbine fuel, aviation kerosene type, Jet A-1. Defence Equipment and Support, UK Defence Standardisation, Glasgow, UK,**2011**.

6 ASTM Standard D7566. Standard specification for aviation turbine fuel containing synthesized hydrocarbons. ASTM International, West Conshohocken, PA, **2008**.

7 Juma, A.A. Flight news on Sasols 100% synthetic Jet A-1 fuel at the Africa aerospace and defence exhibition in Cape Town South Africa. http://www.articlesbase.com/flights-articles/flight-news-on-sasols-100-synthetic-jet-a-1-fuel-at-the-africa-aerospace-and-defence-exhibition-in-cape-town-south-africa-3480968.html. (Accessed on 1 December 2011).

8 Hemighaus, G.; Boval, T.; Bosley, C.; Organ, R.; Lind, J.; Thompson, T. Alternative jet fuels. Chevron Corporation, San Raman, CA, **2006.**

9 Blakey, S.; Rye, L.; Wilson, C.W. Aviation gas turbine alternative fuels: a review. Proceedings of the Combustion Institute, Atlanta, GA, **2011**, *33*, 2863-2865.

10 Corporan, E.; Edwards, T.; Shafer, L.; DeWitt, M. J.; Klingshirn, C.; Zabarnick, S.; West, Z.; Striebich, R.; Graham, J.; Klein, J. Chemical, thermal stability, seal swell, and emissions studies of alternative jet fuels. Energy and Fuels, **2011**, *25*, 955-966.

11 Jager, B.; Espinoza, R. Advances in low temperature Fischer-Tropsch synthesis. Catalysis Today, **1995**. 23, 17-28.

12 de Klerk, A. Hydroprocessing peculiarities of Fischer-Tropsch syncrude. Catalysis Today, **2008**, *130*, 439-445.

13 Moses, C. A.; Stavinoha, L. L.; Roets, P. Qualification of Sasol semi-synthetic Jet A-1 as commercial jet fuel. SwRI-8531,: South West Research Institute, San Antonio, TX, **1997**.

14 DeWitt, M. J.; Corporan, E.; Graham, J.; Minus, D. Effects of aromatic type and concentration in Fischer-Tropsch fuel on emissions production and material compatibility. Energy and Fuels, **2008**, *22*, 2411-2418.

15 ASTM Standard D1414. Standard test method for rubber O-rings. ASTM International, West Conshohocken, PA, **2008.**

16 ASTM Standard D471. Standard test method for rubber property-effects of liquid. ASTM International, West Conshohocken, PA, **2006**.

17 Visram, S. A novel method to evaluate synthetic fuel options for gas turbines in terms of O-ring swelling. M.Sc., University of Cape Town, Cape Town, South Africa, **2009**.

18 Elastocon Testing with Precision. http://www.elastocon.se (Accessed on 1 December 2011).

19 Link, D. D.; Baltrus, J. P.; Zandhuis, P.; Hreha, D. C. Extraction, separation, and identification of polar oxygen species in jet fuel. Energy and Fuels **2005**, *19*, 1693-1698.

20 Gary, J. H.; Handwerk, G. E.; Kaiser, M. J. Petroleum refining: Technology and economics, 5th Edn, CRC Press, Boca Raton, FL, **2010**.

21 Brandt, A. R.; Farrell, A. E. Scraping the bottom of the barrel: greenhouse gas emission consequences of a transition to low-quality and synthetic petroleum resources. Climate Change, **2007**, *84*, 241-263.

22 Dry, M. E. The Fischer-Tropsch process: 1950-2000. Catalysis Today, **2002**, *71*, 227-241.

23 Lamprecht, D.; Dancuart, L. P.; Harrilall, K. Performance synergies between low-temperature and high-temperature Fischer-Tropsch diesel blends. Energy and Fuels, **2007**, *21*, 2846-2852.

24 Steynberg, A.; Dry, M. Fischer-Tropsch technology. Elsevier, Amsterdam, Netherlands, **2004**.

25 Steynberg, A.; Espinoza, R.; Jager, B.; Vosloo, A. High temperature Fischer-Tropsch synthesis in commercial practice. Applied Catalysis, **1999**, 41-54.

26 Sasol, a technology driven alternative fuels and chemicals company. http://sasol.investoreports.com/sasol_sf_2011/images/c17_big.jpg (Accessed on 1 December 2011).

27 Link, D.D.; Gormley, R.J.; Baltrus, J.P.; Anderson, R.R.; Zandhuis, P.H. Additives to promote seal swell in synthetic fuels and their effect on thermal stability. Energy & Fuels, **2008**, *22*, 1115-1120

28 Handbook of Aviation Fuel Properties. CRC report No.635. Coordinating Research Council, Alpharetta, GA, **2004**.

29 ASTM Standard D1655. Standard Specification for Aviation Fuels. ASTM International, West Conshohocken, PA, **2009**.

30 van der Westhuizen, R.; Ajam, M.; de Coning, P.; Beens, J.; de Villiers, A.; Sandra, P. Comprehensive two-dimensional gas chromatography for the analysis of synthetic and crude-derived jet fuels. Journal of Chromatography A, **2011** 4478-4486

31 Yamada, T.; Graham, J.L.; Minus, D.K. Density functional theory investigation of the interaction between nitrile rubber and fuel species. Energy and Fuels, **2009**, 23, 443-450.

32 Flitney, R. Seals and sealing handbook. Butterworth-Heinemann: Oxford, UK, **2007**, 5, 358-381.

33 Cowie, J.M.G.; Arrighi, V. Polymers: Chemistry and physics of modern materials. CRC Press, Los Angeles, CA, **2008.**

34 Muzzell, P.A.; McKay, B.J.; Sattler, E.R; Stavinoha, L.L.; Alvarez, R.A. The effect of switch-loading fuels on fuel-wetted elastomers. U.S. Army RDECOM, **2007**, 12-22.

35 Patil, A.O; Coolbaugh, T.S. Elastomers: a literature review with emphasis on oil resistance. Rubber Chemistry & Technology, **2005**, *78*, 516-535.

36 Sen, A. Nitrile rubber (NBR) coated textiles: Principles and applications. Technomic Publishing Compony, Charlottesville, VA, **2001**

37 Hickman, J. Polymeric Seals and Sealing Technology. Rapra review reports, Burlington, MA, **1997**, 8, 18.

38 Teegarden, D. Additives. Polymer chemsity: Introduction to an indispensable science. National Science Teachers Association Press, Richmond, VA, **2004**, 172.

39 Ohm, R.F. Rubber Handbook. Vanderbilt Company, Hartford, CT. **1990**. 13, 645-711.

40 Garbarczyk, M.; Kuhn, W.; Klinowski, J.; Jurga, S. Characterisation of aged nitrile rubber elastomers by NMR spectroscopy and microimaging. Polymer, **2002**, *43*, 3169-3172.

41 Subramanian, V.; Ganapathy, S. Aging of vulcanisates of formulations for rubber seals. Journal of Applied Polymer Science, **1998**, *70*, 985-994.

42 George, S. C.; Thomas, S. Transport phenomena through polymeric systems. Progress in Polymer Science, **2001**, *26*, 985-1017.

43 Mostafa, A.; Abouel-Kasem, A.; Bayoumi, M. R.; El-Sebaie, M. G. Effect of carbon black loading on the swelling and compression set behavior of SBR and NBR rubber compounds. Materials and Design, **2009**, *30*, 1561-1568.

44 Burnham, R.G. Methods for accelerated seal aging and their effect on seal swell. BSc(Hons) Project, University of Cape Town, Cape Town, South Africa, **2009**.

45 Belmares, M.; Blanco, M.; Goddard, W. A.; Ross, R. B.; Caldwell, G.; Chou, S. H.; Pham, J.; Olofson, P. M.; Thomas, C. Hildebrand and Hansen solubility parameters from molecular dynamics with applications to electronic nose polymer sensors. Journal of Computational Chemistry, **2004**, *25*, 1814-1826.

46 Burke, J. Solubility parameters: Theory and applications. The Book and Paper Group, The American Institute for Conservation, Washington, DC, **1984**, 3.

47 Hansen, C.M. Hansen solubility parameters. A user's handbook. CRC Press, Fort Lauderdale, FA, **2007**,2, 1-19, 347-483.

48 Feller, R.L.; Stolow, N.; Jones, E.H. On picture varishes and their solvents. Washington, DC, **1985**.

49 Graham, J. L.; Striebich, R. C.; Myers, K. J.; Minus, D. K.; Harrison, W. E. Swelling of nitrile rubber by selected aromatics blended in a synthetic jet fuel. Energy and Fuels, **2006**, *20*, 759-765.

50 Teas, J. Standard Hildebrand values from Hansen. Journal of Paint Technology, **1968**, 40, 19-32.

51 Hansen, C.M.; Skaarup, K. The three dimensional solubility parameter – key to paint component affinities III. Journal of Paint Technologies, **1967**, 511-514

52 Hansen, C.M. Painting Testing Manual, Manual 17. Koleske, J.V. (ed), ASTM International, Philadelphia,PA, **1995**.

53 Flory, P.; Rehner, J. Statistical mechanics of cross-linked polymer networks I. Rubberlike Elasticity. Journal of Chemical Physics, **1943**, 512-521.

54 Flory, P.; Rehner, J. Statistical mechanics of cross-linked polymer networks II. Swelling. Journal of Chemical Physics, **1943**, 521-534.

55 Neuburger, N.A.; Eichinger, B.E. Critical experimental test of the Flory-Rehner theory of swelling. University of Washington, Washington, DC, **1988**.

56 Wall, F. T.; Flory P. J. Statistical thermodynamics of rubber elasticity. Chemical Physics, **1951**, 19, 1435-1439.

57 Campoin, R.; Thomson, S.; Harris, J. Elastomers for fluid containment in offshore oil and gas production: Guidelines and review. Health and Safety Executive, **2005**, 1-111.

58 Joseph, A.; Mathai, A. E.; Thomas, S. Sorption and diffusion of methyl substituted benzenes through cross-linked nitrile rubber/poly(ethylene co-vinyl acetate) blend membranes. Journal of Membrane Science, **2003**, *220*, 13-30.

59 Rahman, M.; Brazel, C.S. The plasticiser market: an assessment of traditional plasticisers and research trends to meet new challenges. Progress In Polymeric Science, **2004**, 1223-1248

60 Lide, D.R. Handbook of chemistry and physics. CRC Press, Boca Raton, FA, **2004**.

61 Thermal application note TN-24, TGA temperature calibration using Curie temperature standards. TA Instruments, New Castle, DE, **2004**.

62 Merck chemicals & reagents catalogue, Darmstadt, Germany, **2008-2010**

63 Coefficients of cubical expansion of liquids. The Engineering Toolbox. http://www.engineeringtoolbox.com/cubical-expansion-coefficients-d_1262.html (Accessed on 1 December 2011).

64 Hansen, C. M. 50 Years with solubility parameters - past and future. Progress in Organic Coatings, **2004**, *51*, 77-84.

65 Hoshina, T.; Kakemoto, H.; Tsurumi, T.; Wada, S.; Yashima, M. Size and temperature induced phase transition behaviors of barium titanate nanoparticles. Journal of Applied Physics. **2006**, 99, 311.

66 Moses, C.A.; Roets, P.N.J. Properties, characteristics and combustion performance of Sasol Fully Synthetic Jet Fuel. ASME Turbo Expo. Berlin, Germany, **2008**

67 Levitt, M.; Perutz, M.F. Aromatic rings act as hydrogen bond acceptors. Journal of Molecular Biology. **1988**, 201, 751-754.

68 Tang, X.C.; Pikal, M.J.; Taylor, L.S. The effect of temperature on hydrogen bonding in crystalline and amorphous phases in dihydropyrine calcium channel blockers. Pharmaceutical Research, **2002**, 4, 484-499.

69 Atkins, P.W. Atkins' Physical Chemistry, 7th Edn. Oxford University Press, Oxford, UK, **2005**.

70 Lamprecht, D. Elastomer Compatibliity of blends of biodiesel and Fischer-Tropsch Diesel. SAE International. **2007**, 29-42.

CHAPTER 9

9. APPENDICES

9.1. Appendix A - Risk Assessments

Risk Assessment Form

General Experimental Procedure

Your Name:	Ross Burnham
Your Supervisor:	Dr Chris Woolard and Prof Eric van Steen

Location (where the activity will take place):	Sasol Advanced Fuels Laboratory
Describe the activity:	Static swell experiments: Exposing polymeric samples to various solvents at room and elevated temperatures in sealed Media bottles. This includes making solutions according to general laboratory practice. Use of elastomer compression rig: Exposing polymeric samples to various temperatures at room and elevated temperate in compression rig, which is operated through the use of compressed air.
Names of persons involved in this activity:	Ross Burnham
Describe in detail the risks you (and others) will face during this activity and the potential consequences of your activities:	Solvent exposure risks, hot surfaces, and the use of sharp items such as scalpel blades.
Does this activity involve any equipment / device designed or built by you which is be plugged into mains electricity?	All equipment used in this study is standard laboratory equipment or has been previously used in prior research.

Does your project involve any new equipment / device designed which contain air or gas at pressure?	The TGA equipment used in this study use compressed gases
Describe the personal protective equipment (PPE) required during this activity – specify in detail:	Standard PPE is to be worn. This includes nitrile gloves, lab coat and safety eye ware.

9.2. Appendix B - SAFL Elastomer Compression Rig Operation and Construction

The SAFL compression rig consists of six modules are connected to a compressed air line which provides the needed pressure for the compression cycle. The rig monitors the change in O-ring thickness while being exposed to various solvents. The compression rig is also able to measure sealing pressure which can be related to changes in physical properties of the O-rings.

Measurements of displacement and pressure during these experiments are made using displacement and pressure transducers that are connected to the rig. The displacement transducers used were non-contact differential variable reluctance transducers supplied by MicroStrain (Williston, USA) with a resolution and repeatability of ±0.1% and ±2μm respectively.

A computer system operates the rig through the use of Lab View software. The software monitors the displacement and pressure data as well as regulates the air pressure inside the system through the control of a three-way valve.

Figure 9.1 illustrates the components of one of the six compression modules. Inside each module base an O-ring is placed inside a groove with a depth of 1.9± 0.1mm. The base of the modules also acts as a fuel chamber holding approximately 80mL of fuel, which allows the O-ring to be in contact with fuel throughout the experiments. The temperature of the cylinders is controlled by the bases being submerged in an oil bath.

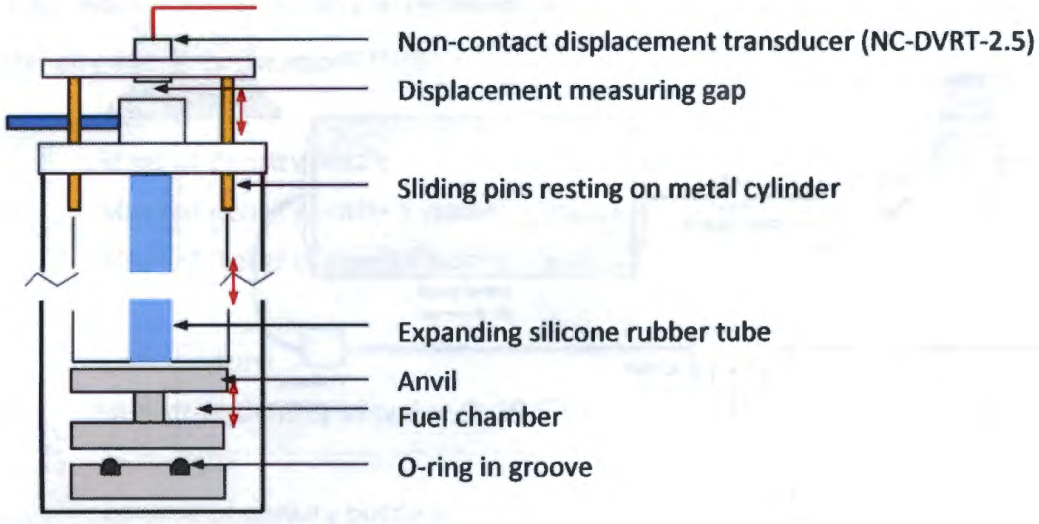

Figure 9.1: Basic compression rig module construction

Measurements are taken when the anvil is compressed to the point of contact with the metal sleeve at which a maximum displacement (X_{max}) is taken. The anvil is then gradually lifted, which results in the O-ring returning to its original dimensions. The point at which the applied pressure reaches zero is captured as the minimum displacement (X_{min}).

Figure 9.2 shows the air flow and control schematic used in order to operate the rig. The computer system, operated through the use of Lab View software, monitors displacement and pressure readings as well as regulating the air pressure inside the system through the control of a three-way valve. Compressed air enters the rig at approximately 7 bar which supplied the pressure needed to compress the O-rings. After a specified holding time at the maximum pressure this valve switches for the evacuation of the compressed air allowing the piston to return to its holding position. This cycle repeats itself for the duration of the experiment thus providing continuous readings of the change in O-rings dimensions in a dynamic environment.

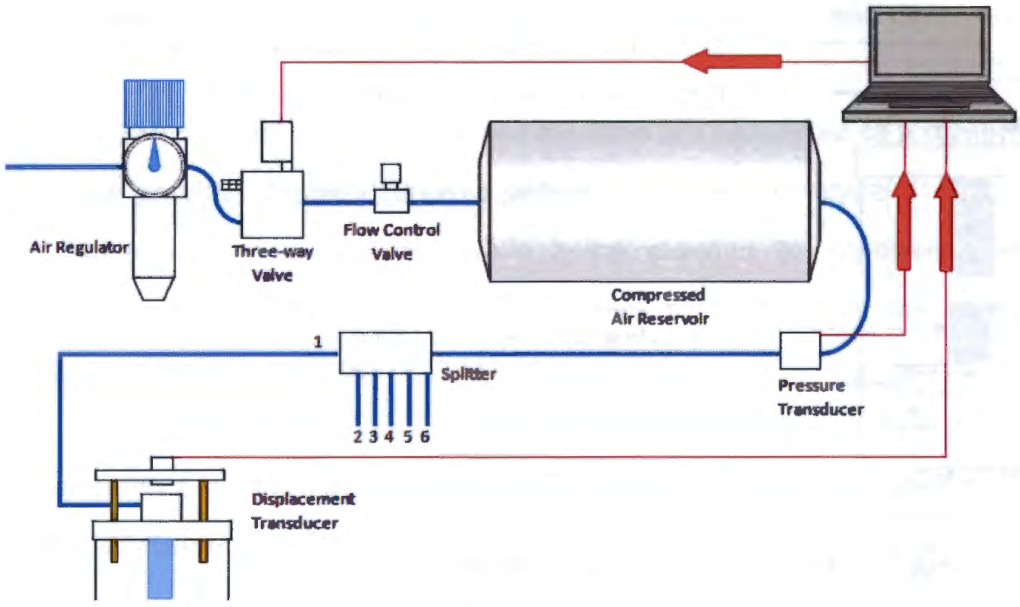

Figure 9.2: Compression rig operation schematic

The hysteresis of the compression and expansion of an O-ring in the compression rig can be seen in Figure 9.3 with specified data capture points illustrated. From this figure the position of X_{min} and X_{max} can be seen, thus providing the change in O-ring diameter to be found.

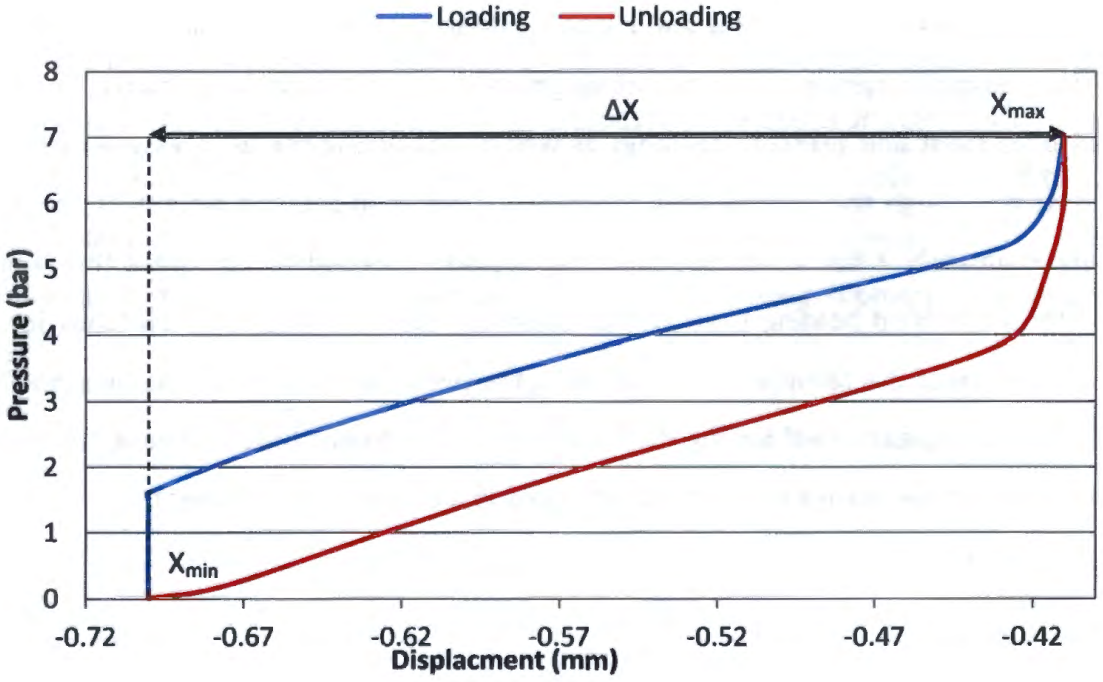

Figure 9.3: Sample compression rig hysteresis curve, indicating data capture points

9.3. Appendix C – Density determinations

Density Bottle Calibration

Mass of density bottle	(m_b)	23.1618g
Mass of density bottle + water	(m_{b+w})	48.2635g
Mass of water in density bottle	(m_L)	25.1017g

Temperature	19.5°C
Literature density of water @ 19.5°C	0.997538g/cm^3

Volume of density bottle =	25.16365 m_L/ρ_L

Density Measurements

"as received" O-rings

	1	2	3	4
Mass of O-ring sample (g)	0.41645	0.42451	0.41990	0.42378
Mass of density bottle + water + sample (g)	48.34284	48.34359	48.34410	48.34288
Mass of water in density bottle (g)	24.76459	24.75728	24.76240	24.7573
Mass of water displaced by sample (g)	0.33711	0.34442	0.3393	0.3444
Volume of water displaced by sample (cm^3)	0.33628	0.34357	0.33846	0.34355
Volume of O-ring sample (cm^3)	0.33628	0.34357	0.33846	0.34355
Density of O-ring sample (g/cm^3)	1.2384	1.2355	1.24061	1.2335

Average density of "as received" O-rings **1.2370 g/cm^3**

Deplasticised O-rings

	1	2	3	4
Mass of O-ring sample (g)	0.37415	0.36541	0.37557	0.36755
Mass of density bottle + water + sample (g)	48.34323	48.34255	48.34532	48.3442
Mass of water in density bottle (g)	24.80728	24.81534	24.80795	24.81485
Mass of water displaced by sample (g)	0.29442	0.28636	0.293745	0.286850
Volume of water displaced by sample (cm^3)	0.295146	0.287066	0.29447	0.287566
Volume of O-ring sample (cm^3)	0.295146	0.287066	0.29447	0.287566
Density of O-ring sample (g/cm^3)	1.2703	1.27291	1.27541	1.27814

Average density of deplasticised O-rings **1.2741 g/cm^3**

9.4. Appendix D – Calculation of volume changes from mass changes

When making measurements, measurements are made at time zero and at intervals thereafter.

These are designated, m_0 and m_t respectively.

In the case of deplasticised O-rings, the mass change due to the solvent may be found as

$$m_s = m_t - m_0$$

For "as received" O-rings, the loss of plasticiser needs to be accounted for and accurate calculations can only be made at equilibrium.

$$m_{depl} = 0.9\, m_0 \quad \text{and} \quad m_s = m_{eq} - m_{depl}$$

The further derivation is for deplasticised O-rings, although it can be adapted by using m_{depl} for m_0 for "as received" O-rings.

The initial volume of the rubber, V_0 is given by

$$V_0 = \frac{m_0}{\rho_r}$$

The density has been determined independently. See Appendix C – Density determinations.

For solvents which are not blends of SPK and aromatics

$$V_s = \frac{m_0}{\rho_s}$$

Thus

$$R\% = \frac{V_s}{V_0}$$

For cases where blends of SPK and aromatics are used, concentration of the aromatics in the NBR occurs. In those cases the volume of SPK needs to be separated from the contribution of the aromatic species.

Based on the observation that the increase in swell for blends of SPK and Jet A-1 is linear, it is assumed that the contribution of the SPK, V_{SPK}, is the same in the blends as for neat SPK. V_{SPK} is thus determined from measurements made when NBR is swollen by neat SPK. This is then converted to $R\%_{SPK}$

So

$$R\%_{arom} = R\%_{overall} - R\%_{SPK}$$

$R\%_{arom}$ is the contribution of the aromatics to overall swell.

The volume fraction of the aromatics in the solvent fraction in the swollen NBR is

$$\phi_{arom} = \frac{R\%_{arom}}{R\%_{overall}}$$

Since the volume fraction of aromatics in the original blend was 0.08 we can obtain the concentration factor as

$$CF = \frac{\phi_{arom}}{0.08}$$

9.5. Appendix E – Volume % changes for 4% blends in SPK

Table 9.1: Solvent properties and experimental summary for the exposure of deplasticised O-rings to blends of aromatic species and SPK at 50°C

Blend component	C No	Molar volume at 20°C (cm^3mol^{-1})	Solubility parameter ($(MPa)^{1/2}$)				Equilibrium mass swelling ratio (%) – small O rings	Calculated volume change due to aromatic (%) – small O-rings
			δ_d	δ_p	δ_h	δ_{Total}		
Toluene	7	106.3	18.0	1.4	2.0	18.1	11.1 (0.6)	3.4
o-Xylene	8	120.6	17.8	1.0	3.1	18.2	10.9 (0.3)	3.2
Ethylbenzene	8	122.5	17.8	0.6	1.4	17.9	10.7 (0.2)	3.0
Mesitylene	9	139.1	18.0	0.0	0.6	18.0	10.4 (0.2)	2.7
Cumene	9	139.4	18.1	1.2	1.2	18.2	9.8 (0.4)	2.1
p-Cymene	9	156.6	17.6	1.2	1.2	17.7	10.4 (0.8)	2.7
n-Butylbenzene	10	156.1	17.4	0.1	1.1	17.4	9.4 (0.3)	1.7
s-Butylbenzene	10	155.5	17.9	1.2	1.2	18.0	9.8 (0.1)	2.1
Tetralin	10	136.3	19.6	2.0	2.9	19.9	10.9 (0.5)	3.2
Anisole		108.7	17.8	4.1	6.7	19.5	14.9 (0.4)	7.2
Dibenzyl ether		190.1	19.6	3.4	5.2	20.6	17.0 (0.3)	9.3

The values in brackets are the standard deviations of the mean. Solubility parameters are for the pure blend component (not the weighted average of the blend).

Table 9.2: Concentration factors of aromatic compounds during swelling

Blend component	Molar volume at 20°C (cm^3mol^{-1})	Solubility parameter ($(MPa)^{1/2}$)				Volume % in O-ring – small O-ring	Concentration factor – small O-ring
		δ_d	δ_p	δ_h	δ_{Total}		
Toluene	106.3	18.0	1.4	2.0	18.1	30.4	3.8
o-Xylene	120.6	17.8	1.0	3.1	18.2	29.1	3.6
Ethylbenzene	122.5	17.8	0.6	1.4	17.9	28.0	3.5
Mesitylene	139.1	18.0	0.0	0.6	18.0	25.9	3.2
Cumene	139.4	18.1	1.2	1.2	18.2	22.1	2.8
p-Cymene	156.6	17.6	1.2	1.2	17.7	25.9	3.2
n-Butylbenzene	156.1	17.4	0.1	1.1	17.4	18.1	2.3
s-Butylbenzene	155.5	17.9	1.2	1.2	18.0	21.2	2.7
Tetralin	136.3	19.6	2.0	2.9	19.9	29.5	3.7
Anisole	108.7	17.8	4.1	6.7	19.5	48.4	6.1
Dibenzyl ether	190.1	19.6	3.4	5.2	20.6	54.6	6.8